Hong Kong Polytechnic University

Jockey Club Rehabilitation Engineering Center

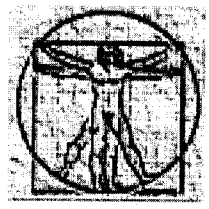

Ultrasonic Assessment of Post-radiotherapy Fibrosis

By Yanping, Huang

A thesis submitted in partial fulfilment of the requirements for the Degree

of Master of Philosophy

6-NOV-2004

CERTIFICATE OF ORIGINALITY

I here by declare that this thesis is my own work and that, to the best of my knowledge and belief, it reproduces no material previously published or written, nor material that has been accepted for the award of any other degree or diploma, except where due acknowledgement has been made in the text.

Yanping Huang

Abstract

Tissue fibrosis is a common late effect of radiotherapy. Clinical assessment of radiation-induced fibrosis is still limited to hand palpation and other subjective grading scales to date, thus making it necessary to develop quantitative and objective methods for this purpose. In the current study, three different ultrasonic approaches were investigated for their potential uses in the assessment of tissue fibrosis.

Firstly, a quasi-linear viscoelastic (QLV) model was adopted to extract the nonlinear mechanical properties of the fibrotic neck tissues from the force-deformation responses obtained with indentation tests using a curve-fitting process. The viscoelastic properties of the patients (n = 105) were compared with those of the normal subjects (n = 8) and also correlated to other measurements of fibrosis. The second part of this study was focused on the assessment of ultrasonic properties in skin fibrosis. Ultrasonic parameters of the dermal tissue *in vivo* were obtained from the echographic radiofrequency (RF) signals. These parameters included the attenuation slope β, the integrated attenuation (IA) and the integrated backscatter (IBS) in the frequency range of 10 to 25 MHz as well as the statistical characteristics of the signal envelope and the skin thickness. Testing sites were selected on the skin of the forearm and the neck. The intra-rater and inter-rater reliability of the measurements of the ultrasonic properties was assessed in 10 normal subjects using tests conducted by two investigators. 20 normal subjects (27 ± 3 yrs of age) and 38 patients (54 ± 11 yrs of age) with a history of radiotherapy in the neck region were recruited for testing. The results were compared between the normal subjects and the patients, and among different patient subgroups which had different palpation scores of fibrosis. Lastly, a high frequency (20-MHz) ultrasonic imaging system was modified to specifically study the skin elasticity. Preliminary tests on phantoms, porcine skins *in vitro* and the human skins *in vivo* were conducted to demonstrate the feasibility of this elasticity measurement system.

Results of the QLV analysis showed that the initial modulus and the nonlinear factor were significantly larger in the patients than in the normal subjects (P < 0.001). Soft tissues with a higher degree of fibrosis were associated with higher elastic parameters. For the viscous properties, significant difference was demonstrated between the patients and the normal subjects (P < 0.007), but not among the patient subgroups (P > 0.05). It was demonstrated that the measurement of the ultrasonic

properties in skin was reliable with an intraclass correlation coefficient (ICC) generally larger than 0.80. In the normal and fibrotic neck skins, β was 0.328 ± 0.029 and 0.303 ± 0.034 dB/mm/MHz, respectively (P = 0.005), and IA was 1.93 ± 1.81 and 2.85 ± 1.93 dB/mm, respectively (P = 0.04). It was found that β and IA were not age-dependent (P > 0.05), while IBS was age-dependent in the palmar forearm skin (P = 0.01). Its relative form of representation, IBS_d, defined as the individual difference between the neck and the palmar forearm was –1.98 ± 2.13 and –4.23 ± 2.59 dB in normal subjects and patients, respectively. In terms of IBS_d, a significant decrease was found in the fibrotic neck skin (P < 0.001). Age-matched comparison among four patient subgroups showed no significant difference for all the ultrasonic parameters (P > 0.05). No significant correlation between the ultrasonic properties and the effective Young's modulus (YM) of the neck soft tissue (P > 0.05) was demonstrated. Furthermore, it was found that the three ultrasonic parameters were correlated with each other (P < 0.01). The statistical parameters of the envelope signal including the mean/standard deviation ratio (MSR), skewness and kurtosis were demonstrated to be age-dependent (P < 0.007). A weakly significant difference was found between the irradiation-affected neck skin and the non-affected forearm skin in the patients (P close to 0.05). When the patients were divided into a total of 2 subgroups (with equivocal and severe fibrosis), the difference was demonstrated to be significant (P < 0.004). The skin thickness of the fibrotic neck skin was significantly larger than that of the normal neck skin (P < 0.01). However, no significant correlation between the skin thickness and the palpation score or the effective YM of the neck tissue was demonstrated. Preliminary results by using the modified elasticity measurement system showed that the difference of the stiffness of the two layers in phantoms or the layers in porcine skins *in vitro* could be discriminated. The deformation of the human skin *in vivo* could also be successfully obtained.

It was concluded that the elastic properties extracted from the QLV model were good representations of severity of fibrosis. For the neck skin, β and IBS were decreased, while IA was increased by the fibrotic process. Ultrasonic and statistical parameters, and skin thickness, were potentially helpful for assessing the skin fibrosis. Our ultrasonic elasticity measurement system has the potential to measure the elasticity of the fibrotic skin with further improvement. However, future study is necessary to confirm some of the current findings.

Keywords: Radiation-induced fibrosis; Palpation; Soft tissue; Ultrasound indentation; Quasi-linear viscoelastic model; Viscoelastic properties; Ultrasonic tissue characterization; Ultrasonic properties; Speed of sound; Attenuation; Backscatter; Skin; Dermis; Reliability; Statistical parameters; Skin thickness; Collagen; Water

Acknowledgements

Given this opportunity, I would like to acknowledge all the help from the people around me. During the two years of study, it was just with their honest help, I could start, keep on and finally finish the work as described in the sections to follow.

First I would like to thank my supervisor, Dr. Zheng Yongping, for helping me so much during the two years. When I began my postgraduate study, I knew little about research. He has taught me a lot of things, such as how to search the literature, to present the research work, and to write academic articles. Among these, a lot are beneficial to me throughout my life. Dr. Zheng is very active in the research and development of applications of ultrasound in medicine and biology and has given me tremendous ideas, suggestions and feedbacks on my research project. Dr. Zheng is very devoted and energetic to his work. His attitude to work has greatly affected me and has become one of the motivations to push me to keep on doing my work. Therefore, my deepest appreciation is especially given to him.

I would like to thank one of my co-supervisors, Dr. Leung Singfai, who is with the Department of Clinical Oncology of the Chinese University of Hong Kong for his suggestions on the design of experimental protocols and the arrangement of clinical tests in Prince of Whales Hospitals. Dr. Leung is the specialist in clinical oncology and his suggestions are very helpful for a correct design of my experiment. His kind arrangement for data collection on patients has made it possible to assess the efficacy of the method I used in the study. I would like to thank the other co-supervisor, Prof. Mak Fuktat Arthur, the head of our department, for his constructive suggestions during the discussion about my research study. He was also the main lecturer of one of my selected subjects “Mechanics of Living Tissues & Systems”. Thanks for his wonderful lectures and sincerely speaking, I learned a lot from this class.

I would also like to thank all the staffs in the Rehabilitation Engineering Center of the Hong Kong Polytechnic University for providing me the help wherever necessary in my work, and the convenience for setting up my experiment.

I would like to thank all the colleagues in REC, especially to those in the Bioinstrumentation Lab. They include Alex, Chenxin, Qinghua, Tracy, Niu haijun, Shijun, Sushil, Wanqing, Grace and Anthony. Some of them have provided great help in carrying out the lab and clinical experiments. Without their assistance, I could not have accomplished the operation. Some discussed with me and gave very precious

suggestions about my project. In addition, I had attended a lot of special activities with them through which I could enjoy myself very well during my spare time.

This thesis is especially dedicated to my family: my parents and my younger brother. Without their support, I could not have concentrated on my work and achieved my goals. Thanks also go to my good friends, Amy, Yanzhong, Wang lei, Zhu youtuan, Ahua and Ha zhang for their kind support during this period.

Finally, I would like to thank the financial support from the Hong Kong Jockey Club Charities Trust, the Research Grant Council of Hong Kong, and the Hong Kong Polytechnic University based on which I could conduct the current project.

Table of Contents

List of Figures

List of Tables

List of Abbreviations

β	Attenuation Slope
CI	Confidence Interval
CT	Computed Tomography
CV	Coefficient of variance
DM	Diabetes Mellitus
ECM	Extracellular Matrix
EORTC	European Organization for Research and Treatment of Cancer
IA	Integrated Attenuation
IBS	Integrated Backscatter
ICC	Intraclass Correlation Coefficient
IVUS	Intravascular Ultrasound
LENT	Late Effect of Normal Tissues
LS	Localized Scleroderma
MNB	Multi-Narrowband
MRC	Medical Research Council
MRI	Magnetic Resonance Imaging
MSR	Mean/Standard Deviation Ratio
NPC	Nasopharyngeal Carcinoma
PVA	Polyvinyl Alcohol
RTOG	Radiation Therapy Oncology Group
QLV	Quasi-Linear Viscoelastic
QOL	Quality of Life
RF	Radio Frequency
RMS	Root Mean Square
ROC	Receiver Operating Characteristic
ROI	Region of Interest
SD	Standard Deviation
SLEB	Subepidermal Low-echogenic Band
SNR	Signal-to-Noise Ratio
SOMA	Subjective Objective Management and Analytic
SS	Systemic Scleroderma
TCM	Tissue Compliance Meter

TUPS	Tissue Ultrasound Palpation System
US	Ultrasound
UTC	Ultrasonic Tissue Characterization
YM	Young’s Modulus

1. Introduction

1.1 Radiation-Induced Fibrosis and Assessment

1.1.1 Fibrosis and Radiotherapy

Fibrosis is a common late effect of radiotherapy, which is one of the three common methods (another two: surgery and chemotherapy) used to treat cancer diseases. Associated with the fast improvement and development of irradiation techniques, the use of radiotherapy has achieved more and more successful outcomes with respect to killing cancer cells and restraining them from proliferating and metastasizing. It is generally recognized that a truly successful therapeutic outcome of radiotherapy requires that the patient be alive, cured, and free of significant treatment-related morbidity (Pedersen et al., 1994). However, fibrosis together with other side effects of the normal tissues surrounding the irradiated part is still of concern in consideration of the quality of life (QOL) of the patients after radiotherapy treatment. The late sequelae significantly affect the QOL of the patients and this issue has been receiving more and more attention when the cure ratio of radiotherapy increases continuously. A balance between more complete cancer eradication and less radiation toxicity to normal tissues should be made for therapy regimens. In order to compare the efficacy of different therapy regimens or anti-fibrotic agents, methods to assess the treatment outcomes are necessary. As for fibrosis, clinically its assessment is still limited to hand palpation and quantitative and objective methods are still lacking to date. This thesis mainly tried to introduce several aspects of using ultrasound indentation, ultrasonic imaging and high frequency ultrasonic tissue characterization (UTC) techniques to assess the cutaneous and subcutaneous soft tissue fibrosis, which is one of the main late effects of radiotherapy in the neck region. Evaluation of the curing effects of cancer and the side effects other than fibrosis are not a keystone of this thesis and thus it is not addressed here.

1.1.2 Clinical Aspects and Pathogenesis of Fibrosis

Radiation-induced fibrosis can be observed in various tissues, including skin, muscle, lung, heart and liver. Fibrosis is generally defined as “an excessive deposition of matrix components that results in a destruction of normal tissue architecture and a compromise in tissue function” (Mutsaers et al., 1997). Because it develops in a pathway similar to that of normal wound healing, it is also described as “a wound that

does not heal" (Martin et al., 2000). Fibrosis differs from the wound healing in that it is chronically progressive, so it is much harder for the fibrosis than the wound to recover from removing the scar tissues. Visually fibrosis involves some additional changes including hyperpigmentation, erythema and dryness of skin. In severe cases it is associated with the retraction of surface contour, which is related to the fibrosis of the dermis and subcutaneous tissues. In extreme cases, it may even result in ulceration and necrosis (O'Sullivan and Levin, 2003). The change of tissue elasticity is a very important clinical reflection of fibrosis. The initiation of fibrosis is clinically associated with a loss of tissue elasticity. As the fibrotic degree increases, the tissue becomes stiffer and stiffer, which may functionally affects the daily activities of the patient and bring much inconvenience to the patient. For example, severe fibrosis can restrict the motion of the neck and joint, or mouth opening and thus activities of these parts in the patient can be significantly limited and reduced. The co-existence of local or regional lymphedema with fibrosis may also contribute to the induration and the compromise of tissue functions (O'Sullivan and Levin, 2003).

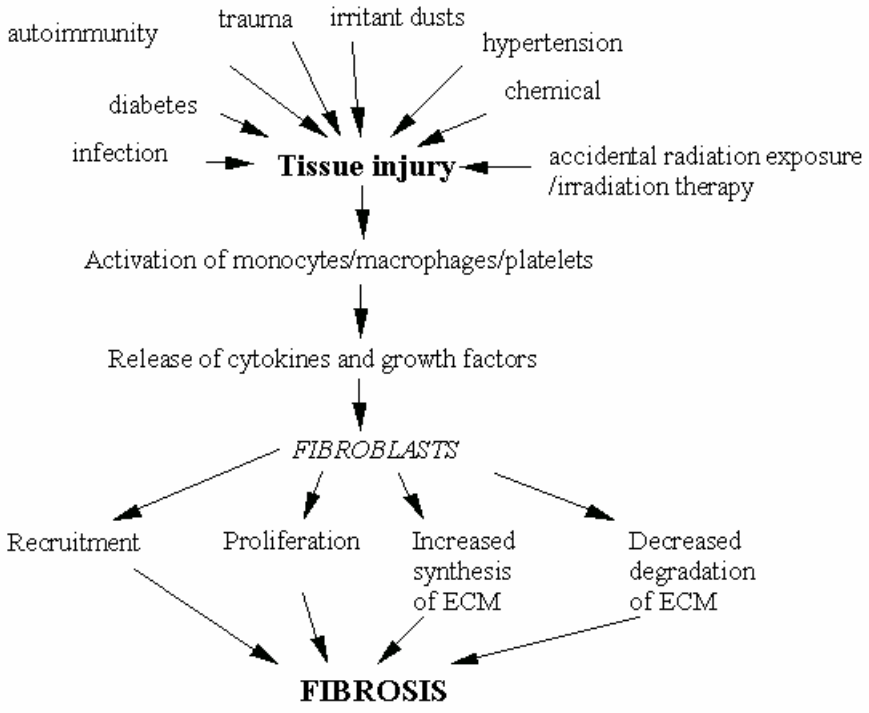

Figure 1-1. Generalised sequence of events leading from tissue injuries (including radiotherapy) to fibrosis (revised from Franklin, 1997).

While there are still a lot of uncertainties with respect to the initiation and chronological progress of fibrosis in various tissues after irradiation, general

manifestations are observed through clinical observations and laboratory experiments in this process. These manifestations are characteristics of fibrosis and therefore they are essential for a specific modality targeting for the diagnosis of fibrosis. Fibrosis is compositionally characterized by “massive deposition of extracellular matrix and excessive fibroblast proliferation” (Martin et al., 2000). Figure 1-1 shows the generalised sequence of events of tissue injuries including irradiation therapy that may lead to tissue fibrosis proposed by Franklin (1997). In irradiated tissue, fibroblasts are constantly recruited, transformed and stimulated, which is very similar to what is observed in the wound healing. Most of these fibroblasts exhibit ultrastructural changes suggesting that they are genically abnormal after exposure of radiation (Denham and Hauer-Jensen, 2002). Excessive abnormal collagen and other extracellular matrix (ECM) in both quality and quantity are deposited due to the existence of the over-produced fibroblasts. In normal wound healing, the production of fibrous matrix is transient before the final equilibrium of production and degradation is achieved. However, in the fibrotic process, regulations to terminate the fibrogenesis are often lacking and the genically abnormal fibroblasts have prolonged life span and capability of faster proliferation, thus making this process chronic and the fibrous matrix overproduced (Martin et al., 1989). Wegrowski et al. (1988) demonstrated in the muscle of a pig model that several times of collagen and noncollagenous proteins were produced and biosynthesized in tissue with fibrosis than without. In addition to the increase of collagen, there is also an increase of other matrix components such as fibronectin and proteoglycans in the fibrotic tissue (Rodemann and Bamberg, 1995). Another factor that can affect the characteristics of the fibrotic tissue under detection utilities such as magnetic resonance imaging (MRI) and ultrasound is the water content. As for the irradiated human skin, it may become dry in the early reactions due to the damage of radiation directly to skin capillaries or indirectly to endothelial cells that may narrow or occlude the capillaries. In the later reactions, on the contrary, the water content may change back and even increase due to the water-bounding capability of the collagen, which is increased in the fibrotic tissue, or due to the oedematous changes or papillary dermal inflammatory lymphocyte infiltration (Warszawski et al., 1997; Nuutinen et al., 1998). The changes of tissue compositions involved in the tissue fibrotic process provide investigators the possibilities to use various medical facilities such as ultrasound, MRI and computed tomography (CT) for its assessment.

The fibrotic tissues have long been described as irreversible dead scar tissues. However, from the time when the field interest was focused on the study of various mediators and growth factors that induce the onset of the chronic fibroblast activation, several therapeutic strategies and anti-fibrotic agents were proposed to reverse the fibrotic process through controlling the proposed intrinsic factors leading to fibrosis and preliminary results seemed to be very encouraging (O'Sullivan and Levin, 2003). With the further development of basic research on the pathogenesis of the formation of fibrosis, together with the objective methods used to precisely assess and document the fibrosis, better therapeutic strategies can be designed in the future and QOL of the patients can be more improved by making them less affected by or free from this late sequela, while still achieving a high curing ratio of cancer diseases.

Table 1-1 MRC rating scale for fibrosis (from Davis et al., 2003)

Grade	*0*	*1*	*2*	*3*
Subcutaneous induration/fibrosis	None	Just palpably increased density	Definitely increased density and firmness	Very marked density, retraction and fixation

Table 1-2 EORTC/RTOG rating scale for fibrosis (from Davis et al., 2003)

Grade	*0*	*1*	*2*	*3*	*4*
Subcutaneous induration/fibrosis	None	Slight induration (fibrosis) and loss of subcutaneous fat	Moderate fibrosis but asymptomatic; slight field contraction; <10% linear reduction	Severe induration and loss of subcutaneous tissue; field contraction >10% linear measurement	Necrosis

Table 1-3 Part of LENT/SOMA subcutaneous tissue scale for fibrosis (revised from Davis et al., 2003)

Grade	*1*	*2*	*3*	*4*
Fibrosis/scar	Present/asymptomatic	Symptomatic	Interferes with function	Total dysfunction

1.1.3 Existing Methods for Assessment of Tissue Fibrosis

To effectively assess the tissue fibrosis is challenging because not only the tissue fibrosis is related to the therapeutic strategies such as single or combined radiotherapy, total radiation dose and fractionation schedule, but also it is a dynamic process, which is progressively developing with the time. Biopsy examination of

tissue samples is a golden method whereas it is invasive and preferred for *in-vitro* study (Yeh et al., 2002) rather than the noninvasive *in-vivo* measurement. Other than the biopsy examination, methods used to assess the soft tissue fibrosis are divided into two kinds: clinician-related grading scales and instrumented quantitative measures (Davis et al., 2003). Several clinician-related measures have already been proposed to measure the late sequelae of fibrosis, among which the three most commonly used ones are the Medical Research Council (MRC) 4-point rating scale; the European Organization for Research and Treatment of Cancer (EORTC)/Radiation Therapy Oncology Group (RTOG) 5-point scale and the Late Effects of Normal Tissue (LENT)/Subjective, Objective, Management and Analytic (SOMA) subcutaneous scale. The details of these criteria are presented in Table 1-1 to Table 1-3 (Davis et al., 2003). It should be noted that Table 1-3 is part of the LENT/SOMA subcutaneous tissue scale.

Table 1-4 Common Toxicity Criteria Version 3.0 (from Davis et al., 2003)

Grade	***1***	***2***	***3***	***4***
Fibrosis: skin and subcutaneous tissue	Increased density on palpation; no interference with ADL	Marked increase in density and firmness, with or without minimal retraction; may or may not impairment of function or interference with ADL	Very marked density with retraction and fixation; may or may not be dysfunction interfering with ADL	Not applicable
Fibrosis: deep connective tissue	Increased density "spongy" feel	Increased density and firmness, tethering	Increased density and firmness, fixation of tissue; may or may not interfere with ADL; surgical intervention my be indicated	Life-threatening; disabling; loss of limb; interfering with vital organ function

NOTE: Subcutaneous tissue is the most superficial layer under the skin, but above the deep connective tissues. Deep connective tissue is the layer below the superficial fat, and it includes muscle, investing fascia and all connective tissue down to bone. ADL-activities of daily life

Because these three scales are problematic when they are specifically used for rating fibrosis with respect to all the components, definitional clarity and uniqueness, a fibrosis working group was formed by Davis et al. (2003) and a revised clinician-related fibrosis measurement has been proposed by this group. The difference between this revised measure and the three original ones is that it divides the fibrosis further into two kinds: subcutaneous and deep fibrosis, which are defined in Table

1-4, respectively. Deep tissue fibrosis can be life-threatening while subcutaneous fibrosis cannot. All the clinician-related fibrosis measures mentioned afore are broadly used to compare the therapeutic strategies (Dische and Saunders, 1999) or to predict the risk factors of fibrosis (Li et al., 1999). Because of its ease in use, minimal time demands and low costs, assessment using various scales is attractive in clinical and research settings. However, for whatever a method used for grading the severity of fibrosis, it should be reliable and valid. From this point of view, using the scale grading is largely based on the experience of the clinicians and oncologists and it suffers from the intrinsic subjectivity. No strong evidence has shown that the reliability of the grading methods is high (Marinus et al., 2000). Thus to achieve high consistent and reproducible results using the clinician-related measurement is problematic.

In addition to the clinician-related measures, variation of organic function induced by fibrosis is occasionally used to describe the severity of fibrosis. At some specific anatomic sites, fibrosis results in the loss of tissue flexibility, and then a cascade effect of symptoms and functional deficits may emerge. A higher level of fibrotic severity may result in an increase in the functional deficits. Thus to measure the limited tissue function can serve as the reflection of fibrotic severity. Shoulder movement, joint range of motion, muscle power and gait are symptoms that are often used for describing the functional deficits caused by fibrosis (Robinson et al., 1991; Stinson et al., 1991; Hojris et al., 2000). In general, the functional deficits can be seen as symptoms of fibrosis and related measures can be used as a simply way assess the severity of fibrosis. However, those functional deficits are indirect reflection of fibrosis and there are potential unseen factors that can also cause the tissue dysfunction. So they are not accurate enough and cannot serve as main parameters alone for describing the severity of fibrosis.

Therefore, in addition to the use of conventional grading scales and functional symptoms for measuring fibrosis, quantitative and objective methods that measure the properties of the soft tissue in the irradiation-affected part are being developed. Although sparsely reported to date, these methods have been attempted to make the assessment of tissue fibrosis more accurate and precise, thus improving the efficacy of therapeutic strategies. Change of stiffness is the most obvious symptom of fibrosis so several instruments that can quantify the change of mechanical properties of soft

tissues have been introduced and have the potential in assessing the fibrosis. Tissue compliance meter (TCM) is one of such devices (Marinus et al., 2000). It is used to measure the tissue compliance, i.e. the relationship between applied force and tissue displacement. The device consists of a rubber disc that slides along the shaft. A force gauge is attached to the shaft so that the applied force can be readable during the operation. When the rubber tip of the shaft is placed onto the skin surface and pressed, the penetration of the shaft can be read from the sliding of the disc. Tissue compliance can be simply expressed by the penetration of the tip under a pre-defined force. Marinus et al. (2000) reported the inter-observer reliability of using the TCM and the palpation to determine the degree of radiation fibrosis. The loss of compliance as measured by TCM was in concordance with the palpation score given by the clinical radiation oncologists, while the inter-observer reliability of the TCM method was superior to that of the palpation method as indicated by a high interclass correlation coefficient (ICC) ranging from 0.85 to 0.95 in breast quadrants for the former and a moderate weighted kappa of 0.65 for the latter. TCM is a device that is small, handheld portable and easy for use. It can reliably measure the change of soft tissue stiffness in a relatively simple way. However, the relatively larger disc in comparison with the rubber tip limits its use in some locations such as the axilla and skinfold at the lower part of the breast. And more, the compliance value given by this device, which depends both on the contact area and the thickness of the underlying tissue, is not an intrinsic material property thus making it improper for comparison of results with standard properties such as Young's modulus measured by other instruments. Another category of devices that have the potential for assessing the fibrotic tissue can measure the mechanical properties of skin through the ways of suction or torsion (Kalis et al., 1990; Diridollou et al., 2000; Balbir-Gurman et al., 2002). Altered skin thickness, collagen metabolism, elastin fiber network and interstitial fluid in the skin which undergoes fibrotic process may all contribute to the change of elasticity, extensibility and viscoelastic properties, thus making it reasonable to use devices that can extract the mechanical properties of skin *in vivo*. To use these specifically designed devices, the skin mechanical properties that can not be easily measured by standard test machine can be estimated in a quantitative way. And it is certainly useful to assess the change of mechanical properties of skin by pathology such as radiotherapy-induced fibrosis. The disadvantage of using these devices is the high demand for controlling the experimental setting, which limits their broad use in clinic

to date. In addition, some of the extracted parameters adopted in the related experiments are not so well standardized, for example, the extensibility in the torsion of skin, which is rather specific for a certain device (Kalis et al., 1990).

In order to quantify the radiation reactions, dielectric method has also been used to measure the dielectric constant of the irradiated skin (Nuutinen et al., 1998). The radiofrequency electromagnetic signals at 300 MHz emitted from an open-ended coaxial probe propagated in the skin and then the dielectric constant of the skin could be obtained by analyzing the reflected waves using a two-layer model for the skin and fat. The constant was regarded to be related to water content in the skin at this frequency. The results showed that during the radiotherapy (about 5 weeks totally) the dielectric constant decreased with time. What's more, a significantly positive correlation of the dielectric constant with the score of subcutaneous fibrosis demonstrated that in the skin with severe fibrosis, the dielectric constant was larger, thus indicating in fibrotic tissue the increase of water content, which might be induced by the increased protein with water-bounding capability. The test showed to measure the dielectric properties might be potential for the use of assessment of skin fibrosis (Nuutinen et al., 1998). Imaging techniques including the CT and MRI have been developing quickly in these decades. CT utilizes material properties of radiation attenuation for imaging (Hounsfield, 1973) and MRI takes advantages of the relaxation characteristics of atoms in materials in the magnetic field for imaging (Lauterbur, 1973). The characteristics shown in these imaging modalities are directly related to tissue physical properties such as density (CT) and water content (MRI), so they are capable of disease diagnosis given the existence of change of corresponding constitutes in these tissue abnormalities. Eich et al. (1999) reported that an increased density indicated by the measure of CT densimetry was associated with the increased fibrotic severity given according to LENT/SOMA scale. It was claimed that the CT densimetry was valuable especially when there was a subclinical or slight change of connective tissue after radiotherapy, due to the quantitative nature of the measure. Johansen et al. (1994) studied the relationship of calculated relaxation values from MRI with the subcutaneous fibrosis. Significantly decreased values were observed in the radiation treated side. While the capability of clinical use of MRI to differentiate the degree of fibrosis is controversial (Johansen et al., 1994; Polgar et al., 1999), there is a broad report of its feasible use in discriminating the tumor recurrence and fibrosis

(Glazer et al., 1985; Gong et al., 1991; Dao et al., 1993). In addition, early reactions of radiation could be detected by MRI before the occurrence of clinical symptoms (Shioya et al., 1997). These studies suggest that CT and MRI are useful tools for non-destructively assessing and monitoring the side effects of radiation. However, drawbacks of these two modalities include a long time for computing, low accessibility and high cost for examination. Due to these reasons, literature that reported the reliability of these expensive measurements for quantifying the soft tissue fibrosis is lacking. In the following part of this section, several aspects that may throw new views on the assessment of soft tissue fibrosis will be introduced in detail.

1.2 Soft Tissues Mechanical Properties for Characterizing Fibrosis

1.2.1 Linear Elastic Properties and Indentation Test

Tissue elasticity is an important parameter in the biomechanical assessment of soft tissues. This is because a lot of diseases shown to be associated with change of tissue elasticity due to compositional abnormalities of the pathologic tissues. Human body soft tissue is composed of connective tissues, which are formed with a fibrous matrix. The fibers of the connective tissue include different types of collagen and elastic fiber, by which the main tissue elasticity such as the tensile or compressive properties is determined (Smith and Karst, 2000). When diseases form and grow, the connective tissues change in their compositional fibers and interstitial fluids so that the mechanical response may alter. From the point of view of the clinical hand palpation, the tissue may be felt softened or hardened. Quantitative elasticity measurement and imaging (elastography) have been recognized as an important method for the detection of early stages of cancers such as in the breasts, livers and prostates.

Material elasticity is defined as the stress-strain relationship, which is complex for different biological tissues. For simplification, it is often assumed to be linear. For bulk soft tissues based on this hypothesis, the measure of elasticity is transformed to obtain the relationship of loading and the corresponding tissue deformation. From the clinical perspective, soft tissue with fibrosis is associated with the observation of induration, which warrants the feasibility of measuring the elasticity for the description of the fibrotic severity.

A clinical method to document soft tissue fibrosis should ideally be noninvasive, reliable, quantitative and objective. Indentation test is potentially such a suitable method. The typical structure of an indentation system consists of two functional units: one is for sensing the force and the other for collecting the deformation (Zheng et al., 2001). The force information is often collected by the load sensor while the deformation information is obtained by facilities in more formats including mechanical devices, linear variable differential transformer, potentiometer, dynamic MRI and ultrasound (Reynolds and Lord, 1992; Zheng and Mak, 1996; Kawchuk and Elliott, 1998; Rome and Webb, 2000; Gefen et al., 2001; Klaesner et al., 2001). The two functional units are synchronized during the data collection process so that the force-deformation curve of the tested material can be drawn and mechanical properties can be extracted. Prototype models of such measurement methods had been investigated to test the mechanical behavior of soft tissues *in vitro*, *in situ* and *in vivo* (Zheng et al., 2001). The test procedure itself is simple, and very much resembles the operation of hand palpation. It has been used by a lot of investigators to extract the mechanical properties of plantar soft tissues for study of foot pathologies (Hsu et al., 1998; Gefen et al., 2001; Rome et al., 2001; Klaesner et al., 2002) and residual limb soft tissues for better fitting of prosthetic sockets (Mak et al., 1994; Vannah and Childress, 1996; Silver-Thorn, 1999). An indentation system, with proper designs, is capable of studying different aspects of soft tissue mechanics. Vannah and Childress (1996) conducted indentation tests to characterize the loading behavior of bulk muscular tissues in posterior lower legs of normal subjects. Hysteresis was consistently observed without preconditioning the tissue. Silver-Thorn (1999) used a rate-controlled indenter to study the lower limb soft tissues in both normal and amputated subjects. Rate-sensitivity was demonstrated and furthermore, it was found that the rate-dependence had different patterns with respect to different testing sites and subject groups (amputated versus non-amputated). Mak et al. (1994) reported that using their mechanically-driven indentation system, the stress relaxation of below-knee limb soft tissues was quite obvious and the relaxation was generally completed within two seconds. Ferguson-Pell et al. (1994) designed a skin indentation system using a pneumatic bellows. A force feedback loop was introduced in the system so it was able to apply a controlled loading sequence to the skin, which was very useful in the study related to pressure sores. With minor revisions, this system could be applied to study the creep behavior of soft tissue. Most of the studies using the indentation

method selected the effective Young's modulus (YM) as the quantitative parameter for the tissue material property. Table 1-5 shows that the main findings of some of the previous investigations that included an indentation test. In most of the studies, effective YM derived from the force-deformation relationship is often used to describe the mechanical properties of soft tissues. The YM is obtained by the relationship of force and deformation plus a theoretical analysis of the indentation model, considering the geometrically nonlinear nature of the indentation process (Zheng et al., 2001).

Zheng et al. (2000b) used a tissue ultrasound palpation system (TUPS) to measure the Young's moduli of neck soft tissue which had fibrosis after radiotherapy due to the existence of nasopharyngeal carcinoma (NPC). Young's modulus is derived from the force-deformation curve and correction factors including the indenter radius, the initial thickness of the soft tissue and Poisson's ratio for the soft tissue. Young's modulus is a standardized material property which makes it possible for the comparison among experiments carried out in different research or clinical settings and for the comparison of results obtained by different instruments. Furthermore, the TUPS device is portably handheld with a small dimension that can be applied to various anatomic body sites (Zheng and Mak, 1996). For tests on the normal subjects, results showed that the mean YM was 12.8 ± 3.9 kPa. Test of the patients with palpable fibrosis showed that the YM varied from 46.4 to 108.3 kPa. The intra-operator and inter-operator repeatability and site-dependence of the parameter were also estimated for this measurement. The results obtained from this device seemed to be highly repeatable with a small variation and it was thus practical to use this device to assess the fibrosis in clinical environment. A subsequent study (Leung et al., 2002) including 105 patients who underwent radiotherapy correlated the YM with the fibrotic degree given by hand palpation from clinical oncologists and nurse specialist and other symptoms of fibrosis including neck rotation range, history of discomfort and restrict movement in the neck. Figure 1-2 shows the relationship between the effective YM and the palpation grade. The results demonstrated a significant correlation of stiffness and palpation grade, neck rotation range, history of discomfort and restricted movement. Furthermore, on the boosted side of the neck, the tissue was associated with increased stiffness. Therefore, the results obtained by the TUPS were

encouraging and had the potential use together with other methods for the improved assessment of tissue fibrosis.

Table 1-5 Literature of indentation test related to the study of the mechanical properties of soft tissues in normal or pathologic states

References	*Tissue studied*	*Description of indentation system*	*Analysis method*
Ziegert and Lewis, 1978	Soft tissues covering the anterior-medial tibia of normal human subjects	A reference frame is fixed firmly and the indentor is placed on the soft tissue through the reference frame. A LVDT is used for measuring the displacement and a Kistler Model 912 force transducer is used. The simultaneous motion of bone is measured by an accelerometer	Curve of force and deformation
	Main findings: Without preloading, the force-deformation relationship was nonlinear and time-dependent. With certain preloading, the force-deformation relationship became linear and time-independent; For quasi-static test, the measured variation of stiffness was 20% percent for identical conditions, 70% for 3 positions along the tibia of the same subject and 300% for the same positions of 12 individuals. For dynamic test on one subject, the stiffness was higher than the quasi-static one.		
Mak et al., 1994	Soft tissues of the lower extremity around the proximal tibia	A series load cell is connected to the indentor and a linear actuator is used to control the indentation	Young's modulus through the force-deformation relationship
	Main findings: Stress relaxation was noted and 90% of the relaxation was finished with 2 s, thus making initial-state YM larger than the steady-state YM; The stiffness of the senior amputees was generally less than that of the non-amputated young normal subjects; The increase of stiffness due to co-contractions of the underlying muscles was less in the senior amputees than in the normal subjects; After the patient was discharged from the hospital with a temporary prosthesis, the residual limb soft tissue increased.		
Vannah and Childress, 1996	Bulk muscular tissues of posterior lower legs of normal human subjects	A load cell and an LVDT are used, with different length indentor tips	Finite element method to reconstruct the material parameters from the force-deformation curve and modelling of the tested geometry
	Main findings: The typical force-deformation response was smoothly varying, nonlinear, and consistently exhibited hysteresis. Preconditioning is not obvious. Stress relaxation is small and was completed mostly within 1 s of the end of the indentation. The stiffness varied by a factor of three across the subjects; The tissue exhibited large non-linearity especially under large loading. The homogeneous material assumption had significant limitations.		
Silver-Thorn, 1999	Soft tissues of residual limbs of five amputees and the right calf of five normal subjects	A linear actuator is used to control the indentation rate. A load cell measures the reaction force. Output can be either force-deformation curve after cyclic loadings or force-time curve after ramp indentation (Pathak et al., 1998)	Force-deformation relationship
	Main findings: The bulk soft tissue response to compressive load was nonlinear, site- and rate-dependent; The force relaxation could be substantial (approximately 55%-95%) with the equilibrium in about 60 s. Most of the relaxation occurred in 5 s.		

Hsu et al., 2000	Heal pad soft tissues of patients with diabetes mellitus (DM) with forefoot ulceration, without forefoot ulceration and age-matched healthy subjects	Ultrasound B-mode image to measure the change of stiffness during indentation and a push-pull scale for measuring the force	Elastic modulus and energy dissipation ratio from the loading force-deformation curve
	Main findings: There was no significant difference of stiffness among patients with DM with forefoot ulceration, without forefoot ulceration and normal healthy subjects. Energy dissipation ratio was increased respectively from normal subjects to patients with DM without forefoot ulceration, and then to patients with DM with forefoot ulceration.		
Zheng et al., 2000a	Soft tissues at the first and second metatarsal head, big toe and heel of the right foot of diabetic patients and normal subjects	A handheld indentation system with an ultrasound indenter for collecting A-mode signal and a load cell in series (Zheng and Mak, 1996)	Effective Young's modulus based on indentation model
	Main findings: Soft tissue stiffness was larger in diabetic patients than in normal subjects; The largest value of soft tissue stiffness was in the first metatarsal head in patients; while in normal subjects no site-dependence was found; Posture affected the stiffness in normal subjects but not in patients.		
Gefen et al., 2001	Plantar soft tissue of normal and diabetic feet	Real time MRI imaging is used to measure the deformation while the contact force is calculated with the contact pressure display technique	Young's modulus through the force and indentation relationship
	Main findings: Plantar soft tissue in diabetic foot was stiffer than that of normal foot; and site-dependence of stiffness among different metatarsal heads was found.		
Rome et al., 2001	Heel pad soft tissues in runners with and without plantar heel pain	A cylindrical flat-ended indenter is attached to the force gauge unit which is also connected to a LVDT to measure the displacement (Rome and Webb, 2000)	Parameters of exponential equation from force-deformation curve
	Main findings: Heel pad less stiff in runners with plantar heed pain than without.		
Klaesner et al., 2002	Plantar soft tissues of patients with diabetes mellitus, peripheral neuropathy and a history of ulcers and age-matched normal subjects	A 3-D measurement device used to locate the indentation deformation and a load cell to sense the force. Whole system can be secured to a sturdy surface.	Force-deformation relationship is transformed to parameters of the 3-element viscoelastic mechanical model
	Main findings: The plantar tissue was stiffer in patients with diabetes mellitus, peripheral neuropathy and a history of ulcers.		

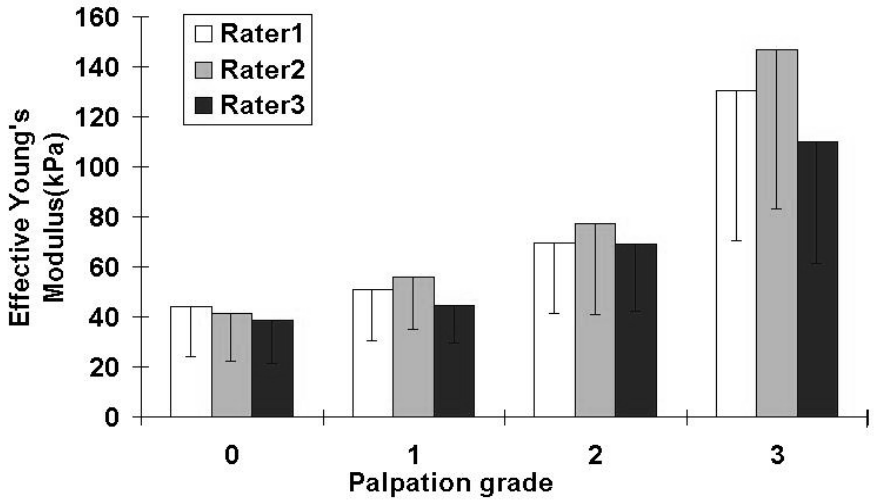

Figure 1-2. Palpation grade from three raters and measured effective Young's modulus (from Leung et al., 2002).

1.2.2 Nonlinear Viscoelastic Properties

It is not only the use of various types of indenters (cylindrical, spherical) and geometry of the indented materials, but also the intrinsic nonlinear properties of the tested materials that bring a complex nature to the indentation test. Therefore, if the latter factor plays a significant role in the test, a simple assumption of material properties is not enough. Klaesner et al. (2001) used an indenter with a radius of 7.9 mm to deflect the plantar soft tissue over the metatarsal heads and on the heel in normal subjects. Based on an indentation model of Hayes et al. (1972), which had already corrected the effect of geometric nonlinearity, they calculated the effective YM under different force ranges. Their results showed that the effective YM at all the testing sites increased as the force range increased, indicating that a pure elastic modulus was not enough to describe the tissue elasticity when larger indentation was applied. In fact, the nonlinear elastic and time-dependent characteristics (viscosity) of soft tissue mechanics have been noticed in some of the previous studies (Ziegert and Lewis, 1978; Mak et al., 1994; Vannah and Childress, 1996; Silver-Thorn, 1999; Rome et al., 2001), but most did not provide quantitative information on them due to a lack of proper models to describe this phenomena. To neglect the nonlinear and viscoelastic behavior of soft tissue is not appropriate since it is well known that the stress-strain relationship of biological tissues is inherently nonlinear and time-dependent, especially where large strains occur. Even though the effective elasticity can discriminate the fibrotic tissue from normal tissues, it should be noted that the

mechanical properties of fibrotic soft tissues are also nonlinear and time-dependent. Therefore, it is particular of interest to know the viscoelastic properties of the fibrotic soft tissues and the study of the viscoelastic properties may open new views to investigate the structural changes of the soft tissues during the formation and progress of radiation fibrosis.

Rome et al. (2001) used an exponential form $F = b_0^{b_1 d}$ to express the relationship between force (F) and deformation (d) of the soft tissue. The nonlinear mechanical properties are described by the two material constants b_0 and b_1. No standardized material parameters were extracted. Gefen et al. (2001) reported that the formula in the power format $F = b_1 + b_2 d^{b_0}$ could describe the relation of force (F) and deformation (d) with a correlation coefficient of $r = 0.995$. Although standard effective elastic modulus was also obtained, it was extracted from the linear part with a relatively small deformation. Alternative methods, such as finite element analysis were used previously to model the indentation test and estimate the nonlinear elastic properties of soft tissue (Vannah and Childress, 1996; Tonuk and Silver-Thorn, 2003). Finite element analysis is a better choice in case of more complicated geometry and boundary conditions. Vannah and Childress (1996) reported that the stiffness of bulk muscular tissue at the calf area increased significantly under the indentation. It was also demonstrated that a homogenous material assumption had significant limitations even when the local and global geometries of the deformation were modelled separately in detail. Tonuk and Silver-Thorn (2003) used finite element analysis plus a James-Green-Simpson strain energy density function to simulate the indentation response of bulk residual limb tissue at different testing sites of different subjects with different indentation rates. Three material coefficients which were incorporated into the finite element analysis could describe the nonlinear elastic properties of the test tissues with a small error. However, the results showed that the three material coefficients varied a lot within subjects, test locations and different indentation rates. It appeared that the results were not so easy to be extrapolated to other situations due to the large variations. In addition, finite element analysis is a complex method in mechanical engineering and lots of experience and time are necessary to apply such a method to solve specific problems. For clinical use, nonlinear viscoelastic properties that are extracted in a more simple, effective and understandable way is more preferred.

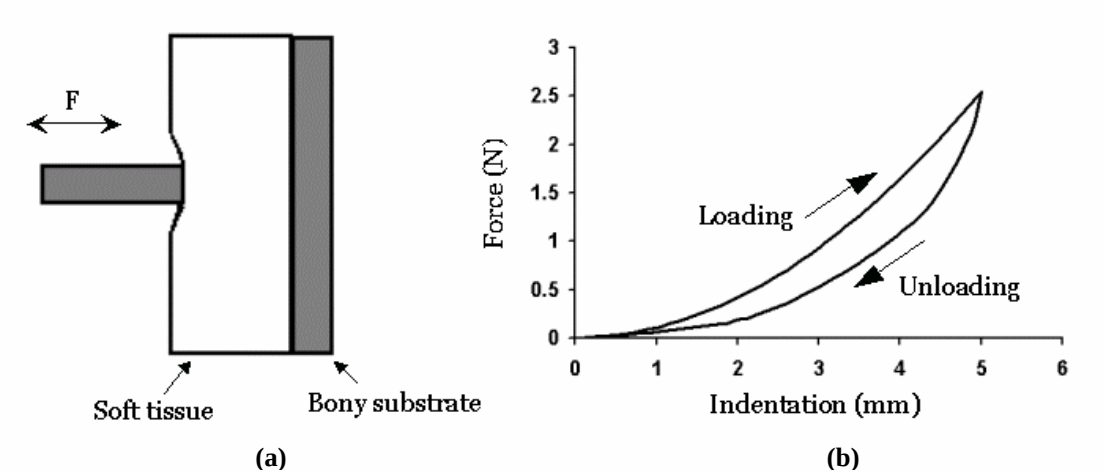

Figure 1-3. (a) Indentation of soft tissues; (b) The relationship of typical indentation and force response during a cycle of loading and unloading.

An extension of the linear elastic indentation solution including a quasi-linear viscoelastic (QLV) model (Fung, 1981) was earlier proposed to extract the viscoelastic properties of the lower limb soft tissue using data collected from a manual indentation experiment (Zheng and Mak, 1999a). QLV model is one of the most successful phenomenological models for soft tissue, such as articular cartilage (Woo et al., 1980), passive cardiac and skeletal muscle (Pinto and Patitucci, 1980; Best et al., 1994), ligaments and tendons (Johnson et al., 1994; Funk et al., 2000). Instead of using a constitutive equation for the nonlinear viscoelastic material, the QLV model assumes that the stress at any time can be superposed by responses of small instantaneous strains before that time. For the case of indentation, the QLV model can be introduced to reconstruct the force response by using the indentation history. If the nonlinear elastic and viscous parameters are included in the two functions of the QLV model, such a model is also capable of studying the viscoelastic behavior of soft tissues. It was hypothesized that the QLV model integrated with the indentation solution of Hayes et al. (1972) could quantitatively describe the nonlinear and viscoelastic behavior of the fibrotic tissue under cyclic loadings (Figure 1-3). Accordingly, one objective of the current study is to obtain and analyze the nonlinear and viscoelastic properties from the indentation data collected previously in a clinical environment (Leung et al., 2002) and correlate them with clinical symptoms of fibrosis.

1.3 Ultrasound Tissue Characterization for Skin Fibrosis

1.3.1 Ultrasound in Dermatology

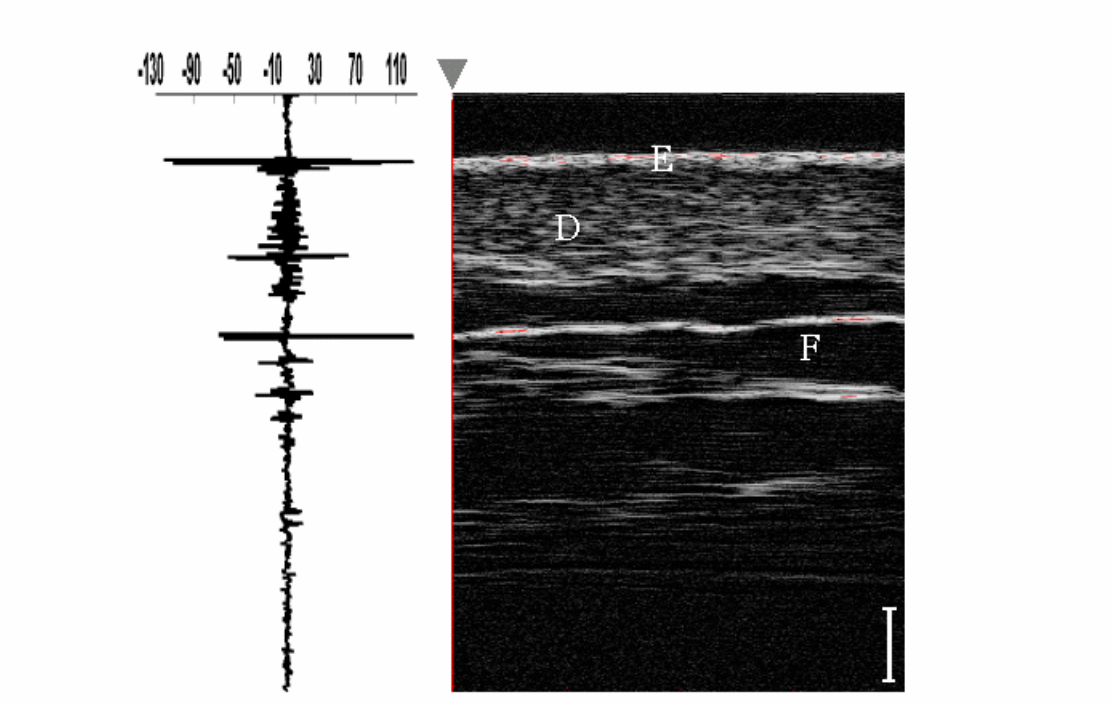

(a) **(b)**

Figure 1-4. (a) RF signal from skin and (b) B-mode ultrasonic skin image. The arrow indicates where the RF signal is obtained. E: epidermal entry echo, D: dermis, and F: subcutaneous fat. The white bar in the image indicates a scale of 1 mm.

Resolution characteristics of ultrasonic imaging systems are mainly determined by the frequency of the signals transmitted by the transducer and whether a transducer is focused or not. With the advance of transducer technologies, the frequency used in ultrasound is raised to be higher and higher which makes it possible to study tissues with fine structures. Application of ultrasound in dermatology is such an example (Altmeyer et al., 1992a). Compared to other techniques such as the X-ray, CT and MRI, the major advantages of using ultrasound are its noninvasive, non-ionizing nature of examination and its relatively low cost. Since the time of late 1970's, A-mode pulsed ultrasound has been introduced to measure the full skin thickness due to the existence of a dermis-subcutis echo (Alexander and Miller, 1979; Tan et al., 1982). The accuracy of this measurement was validated by other methods of proven accuracy such as the radiography and it was later rapidly applied to evaluate the skin diseases or lesions induced by exogenous traumas, operation, burn and medicines (Cole et al., 1981; Tan et al., 1981). Ultrasound two-dimensional B-mode image is

constructed from an array of A-mode lines and based on this kind of imaging the cross-sectional image of tissues such as the skin can be obtained. In the high frequency ultrasound, the array of A-mode lines is normally obtained by translating a single focused transducer due to the lack of the high frequency transducer array. Although the three-dimensional imaging of ultrasound in clinical dermatology seems to have more potential applications (Stiller et al., 1993), it is hampered by the limited resolution of the systems available and the relative high expenditure of time for a measurement, thus keeping this utility still at the experimental stage. Ultrasonic B-mode imaging can provide more information than the pulsed A-mode ultrasound from the point of view of structural visibility and skin thickness measurement, so it can be less abstract and more reliable (Jemec and Gniadecka, 2000).

Quantitative use of the ultrasonic imaging in dermatology, since its birth, mainly consists of two aspects: thickness measurement and echogenicity analysis. Echogenicity is defined as the mean echo level derived from the pixel brightness value in the image in the analyzed region of interest. The typical skin image under ultrasound contains the following layers: an epidermal entrance echo, the hyper-echogenic dermis and the low or non-echogenic subcutaneous fat (Figure 1-4). The subcutaneous fat is not totally echo-poor but with some echo-rich lines or spots due to existence of connective tissue bundles or septa. The distinct visual characteristics of the superficial tissues facilitate the measure of skin thickness and thus the monitoring of dermal processes where the skin thickness undergoes possible variations. The echogenicity of the skin in different depths is also of value to investigate different skin problems. In contrast to a specific pattern of echogenicity observed in the normal skin, certain diseases or reactions affect the distribution of echogenicity in some specific ways. Therefore, it has potential to perform the analysis of echogenicity for detecting and monitoring of certain skin processes. The use of ultrasonic imaging for skin application is almost from the same time with the use of pulsed ultrasound. However, its application is far broader than the pulsed ultrasound, and it has been attempted and applied to study the phenomena observed not only in normal skins but also in skin undergoing various pathological or chronological changes (Dines et al., 1984; Tikjob et al., 1984; Brink et al., 1986; De Rigal et al., 1989; Fornage et al., 1993; Seidenari et al., 1994). Echographic ultrasonic image of skin is very useful for detecting and monitoring various kinds of skin problems.

Given the characteristics of progressive changes observed in a fibrotic process, the high frequency ultrasound may sense some of these changes and this method may be potential for the quantitative assessment of fibrosis. Collagen is the major structural protein and it composes 70-80% of the dry weight of the skin. So modulation of collagen metabolism induced by therapeutic radiation is clinically important for the fibrotic process. Gottlober et al. (1997) examined the cutaneous and subcutaneous tissue by using the 20-MHz sonography in patients who suffered from late effects of exposure of accidental radiation. Increased thickness as well as density was observed in the patient with cutaneous and subcutaneous fibrosis. In extreme cases, skin could be as twice thick as that of the contralateral non-affected side. Subsequently they used the variation of ultrasound-measured skin thickness as the indicator of cutaneous fibrosis to assess the treatment of anti-fibrotic medicine and the late effects of cutaneous damage due to radiation (Gottlober et al., 2001; Steinert et al., 2003). Although not directly related to fibrosis, Riekki et al. (2000) found significant increase of thickness measured by a 20 MHz ultrasound scanner in irradiated human breast skin which was naturally potential to develop late cutaneous fibrosis compared to that of non-treated skin. Local collagen synthesis and accumulation of connective tissue also increased in the irradiated skin by histological biopsy examination, which might contribute to the increase of skin thickness. There were investigators who attempted to measure the echogenicity of the ultrasonic image of the skin to quantify the early and late reactions of therapeutic radiation. Warszawski et al. (1997) tried to quantify the change of breast skin with and without radiation using several ultrasonic parameters of the image including entry echo, thickness of the corium, the signal intensity of the upper and lower corium, the texture of the upper and lower corium and the structure of the border between the corium and subcutis. Changes of parameters were divided into two parts in two periods: early (< 3 months after completion of radiation) and later reactions (> 3 months postirradiation). They reported no significant change of the entry echo. The skin thickness increased impressively in the early reactions and then it decreased slightly in the later reactions. However, although not significantly different from that in the early reactions, the skin thickness in the later reactions was still significantly larger than that of the non-irradiated side. For the signal intensity, the upper and lower corium showed a slightly different pattern of change. They both decreased in the early reactions and increased in the later reactions, and both reactions produced significantly less echogenic skin

images compared to the non-irradiated skin. However, in the lower corium the echogenicity in later reactions was significantly larger than that in the early reactions while in the upper corium, no significant difference of echogenicity was found between the early and late reactions. Although the margin between the corium and the subcutis became less unsharp in both early and late reactions, the difference had not reached a significant level. The changes of echogenicity observed in the early reactions of skin after radiation were similar to those observed in some inflammatory diseases, which might be caused by oedematous water and lymph infiltration (Seidenari et al., 1991). With additional measurement during the radiotherapy treatment and comparison with visible skin reactions described by examining physicians, this study had demonstrated that 20 MHz ultrasound imaging was a reproducible, objective and quantitative tool to assess the time course of skin reactions during and after radiotherapy. However, there was not any report concerning radiation-induced fibrosis as the late reaction in this study.

In diseases such as scleroderma where there is an associated increase of collagen content, the skin may exhibit some similar variation as observed in fibrosis. Thus the study of an ultrasonic examination of these diseases is referential to the ultrasonic assessment of fibrosis. Serup et al. (1984) used 15 MHz pulsed ultrasound to measure the thickness of morphoea plaque thickness. Significantly thicker skin was found in plaques of patients with clinically ‘advanced’ scleroderma than plaques of ‘slight’ scleroderma. Ihn et al. (1995) confirmed the increase of skin thickness in patients with sclerosis. In addition, they demonstrated that the ‘uninvolved’ skin in systemic sclerosis was actually pathologic rather than normal as indicated by the increased thickness. Echogenic analysis also found variations in patients with sclerosis such as in the lower corium with enhanced reflexes (Hoffmann et al., 1991). Cosnes et al. (2003) found by a 13 MHz probe for imaging of dermis and hypodermis that the localized scleroderma had characteristics including undulations of the dermis, disorganization, loss of thickness, thickened hyperechoic bands in the hypodermis and two typical “V” shapes formed around the cutis-subcutis interface. Seidenari et al. (1996) used quantitative parameters to describe the characteristics of systemic sclerosis based on B-scanning ultrasound images. Significant difference was found between patients and control subjects. All these studies showed that measurement based on high frequency ultrasound imaging was a potentially suitable *in-vivo* tool for

use of diagnosis of scleroderma. There is clear evidence that the increase of thickness is associated with an increase in collagen content in sclerosis (Rodnan et al., 1979) and also there is no reason to neglect the contribution of the significant change of collagen to the variation of texture in the skin image. The main characteristics of collagen that affect the dermal ultrasonic reflectivity are generally recognized to be collagen content, collagen type, collagen fiber orientation and collagen bundle size because these factors determine the collagen-matrix interfaces which microscopically scatter the ultrasound (Rallan and Harland, 2003). In addition to collagen, water distribution has been reported to have an effect on the skin thickness and echogenicity (Gniadecka and Quistorff, 1996; Eisenbeiss et al., 2001). In contrast to the hyperechoic collagen fiber, water is poorly reflective and dermal water content reduces the echogenicity. Therefore, pathologic changes existing in fibrotic skin such as collagen metabolism and interstitial fluid merit a further investigation of high frequency ultrasound for the evaluation of radiation-induced cutaneous fibrosis.

1.3.2 Ultrasonic Characterization of Skin

The discussion of the applications of ultrasound in dermatology has been confined so far to the use of either the peak information reflected from the cutis-subcutis interface and the amplitude in the pulsed A-mode or the brightness of pixels in a B-mode image. These applications are often based on the demodulated ultrasound signals processed from the originally backscattered radio frequency (RF) signals. However, the RF signals backscattered from the tested tissues carry more information than the demodulated and log-transformed signals in a B-mode image and researchers have made the effort to extract ultrasonic characteristics directly from these raw signals. These methods used for tissue differentiation or diagnosis of pathologic diseases are more frequently called as “ultrasonic tissue characterization” (UTC) methods (Chivers, 1981; Feleppa and Yaremko, 1987; Taylor and Wells, 1989; Thijssen, 1989). Tissue characterization, from a broad point of view, can be defined as “the identification of one or more physical parameters of a small volume of tissue that are sufficiently well correlated with the type or condition of the tissue that the measurement of these physical parameters may alone be used as an effective index of the type or condition of that volume of tissue” (Chivers, 1981).

The tissue characteristics of ultrasound that are broadly used include single parameters from bulk tissue: speed, attenuation, backscatter, and parameter-based

imaging and the image texture that is formed specifically due to existence of large structural scatterers (Thijssen, 1989). Through some of these parameters, the microstructure of the scattering tissue such as the scatterer size and concentration may also be characterized (Lizzi et al., 1986). Ultrasound is usually assumed to be spreading at a constant speed when it propagates in soft tissues *in vivo* (e.g. 1540 m/s), so the task of characterization is focused on the extraction of another two parameters, i.e. attenuation and scattering. Attenuation and scattering are phenomena that naturally exist when tissue is insonified so that they are intensively studied by investigators. Ultrasound interacts with the tissue structures during its propagation and quantitative parameters extracted from the received signals can be regarded as quantitative reflection of the tissue state. To extract ultrasonic properties from the collected RF signals is complex, especially for the test on *in-vivo* tissues where only echographic mode is allowed. Effects of factors that are involved in the process of signal collection are necessary to be corrected prior to the extraction of tissue parameters. These factors include the inhomogeneity of the ultrasound beam (called as “the diffraction phenomenon”), the data acquisition system and the local structural variations observed in the region of interest of living biological tissues (Fink and Cardoso, 1984; Huisman and Thijssen, 1996). After correction, the diffraction effect such as the near and far field beam characteristics can be minimized. Hence, system-independent parameters can be compared among different setups of measurement (Madsen et al., 1999). In experiments using *in-vitro* specimens, attenuation is often measured using the continuous-wave transmission or pulse-echo reflection methods. These studies put another receiver transducer or a plane reflector in some distance away from the transmitter transducer and compare signals collected with and without the specimens in between. However, for *in-vivo* experiments, it is not possible to make such conditions available and the echographic mode is the only choice for data collection. A proper method that is commonly used in this case is called the “substitution” method (Lizzi et al., 1983; Fink and Cardoso, 1984). In deriving the frequency-dependent ultrasonic properties, spectral analysis is necessary. In the substitution method, the spectrum of the signal obtained from a complete plane reflector located in a water tank at the corresponding distance is used to normalize the spectrum of the received signal and subsequent analysis is based-on the normalized spectrum. There are generally two methods to calculate the frequency-dependence of attenuation (called attenuation slope) in biological tissues *in vivo*. The first one

utilizes the fact that the spectral center (centroid) of the pulsed signal shifts towards a lower frequency with the increase of the propagation depth (Fink et al., 1983; Fink and Cardoso, 1984; Baldeweck et al., 1995). The second method is called the short-time Fourier multi-narrowband (MNB) algorithm which takes advantage of the spectral reduction at each frequency in the bandwidth of the pulsed signal (Kuc and Schwartz, 1979; Huisman and Thijssen, 1996; Roberjot et al., 1996). In centroid shift techniques, a linear frequency-dependence of the attenuation coefficient is assumed and the attenuation slope is directly affected by the spectral variance, a parameter describing the frequency content of the incident ultrasound pulse. However, in MNB method, a linear relationship between the attenuation coefficient and frequency is not necessary to be secured and the knowledge of the spectral variance is not required.

In addition to the deterministic analysis to obtain physical ultrasonic parameters, statistical information of the ultrasound signals scattered from biological tissues is also useful for tissue characterization. The rationality comes from the fact that mammalian tissue is spontaneously constructed to be very complicate in its geometry, composition and function. Structural inhomogeneity and anisotropy commonly exist in a specific tissue. Therefore, the signal scattered from a living biological tissue can be regarded to be absolutely stochastic. A well-known example is the Rayleigh scattering where there are large numbers of uniformly spatially distributed scatterers in a resolution cell so that the signal-envelope has a probability density function of Rayleigh distribution (Wagner et al., 1987). Although this simplest case is not enough to characterize more complicated scattering where number and size of internal scatterers vary drastically, it best explains the valuable use of statistical analysis. Based on other statistical models of scattering, characteristics of detected tissues such as the effective density of scatterers can be obtained (Ossant et al., 1998; Lebertre et al., 2002) and pathology-induced variation of scattering structure can be detected.

UTC methods have been introduced to detect the abnormalities of various tissues and organs in the human body, although most of them are still in the experimental stage. These applications include the involvement of ultrasound in the research of diseases in liver, lung, kidney, prostate, heart, bone, brain, blood and vessel, cartilage, breast, and in the related investigations in ophthalmology, gynecology and obstetrics, dermatology and venerology. Some promising applications of UTC methods include the detection of diseases in bone such as osteoporosis using the measurement of

attenuation and the speed of sound (Laugier et al., 1996); in heart using the cyclic variations of myocardial integrated backscatter (Perez and Miller, 1991); in liver such as diffuse and focal diseases (Huisman et al., 1998); and in vessel such as the atherosclerosis with high frequency of intravascular ultrasound (Bridal et al., 1997).

An evident difference of the application of UTC methods in dermatology compared to in other large tissues is the high frequency needed thus the high resolution provided by the transducer. Early experiment in skin is only limited to *in-vitro* study in the transmission mode using transducer with low center frequencies, thus making the measurement confined to the speed of sound and attenuation, but without backscatter (refer to the tabulation of ultrasonic properties of skin by Goss et al., 1978, 1980). Due to the difficulty in fabricating ultrasonic transducers with high frequencies, UTC of skin was not reported until the late 1980's (Riederer-Henderson et al., 1988; Steiger et al., 1988). In this study, attenuation of canine skin at the frequencies of 25 and 100 MHz evaluated by the backscattering acoustic technique and the scanning laser acoustic microscope separately was quantified and compared with the value obtained in early experiment with a frequency range of 1-10 MHz. Stronger frequency dependence was found than that tested at lower frequencies. Since then, several groups of researchers have significantly contributed to this field up to now (Olerud et al., 1990; Moran et al., 1995; Pan et al., 1998; Guittet et al., 1999a, 1999b; Fournier et al., 2001; Raju and Srinivasan, 2001; Lebertre et al., 2002; Raju and Srinivasan, 2002; Fournier et al., 2003; Raju et al., 2003). The ultrasonic parameters generally used in skin characterization were the same as those used in other tissues including the speed of sound, attenuation and backscatter coefficients. The technique has also advanced from the early *in-vitro* study (Olerud et al., 1990) to the recent *in-vivo* study (Guittet et al., 1999a). Different aspects that will be encountered in a practical detection have been intensively studied. The ultimate objective of ultrasonic characterization of skin is to extract ultrasonic properties or to further map the distribution of ultrasonic parameters within this very thin tissue so that skin aging or modifications by specific skin disorders can be quantitatively, objectively and noninvasively assessed by this noninvasive modality.

Acquisition of skin ultrasonic properties is potentially affected by two main factors. One is the tissue essential status (such as the gender, race, aging, compositions, density, structure homogeneity, environment and interior temperature,

external loading, internal stress and diseases) and the other is related to the detection technique. Several of these issues have already been addressed in the existent literature. Table 1-6 summarizes the various aspects studied in the skin by some of the existing literature. Bhagat et al. (1980) used an *in-vitro* mouse model to study the effects of aging on the ultrasonic velocity and attenuation coefficient. Lower values of these two parameters were reported in the aged skins than in young ones. Discrepant results of the *in-vivo* effects of aging on the attenuation slope have been reported in human skins. Guittet et al. (1999a, 1999b) demonstrated in a large population of 150 healthy subjects with an age from 14 to 85 years that the attenuation slope decreased with the advancing age. Elderly subjects with the age of 60-85 had a significant higher attenuation slope than the younger subjects with the age of 15-30. Alternatively, Fournier et al. (2001, 2003) measured the dermal ultrasonic properties in 29 healthy volunteers aging from 24 to 76 and showed that attenuation slope was not correlated

Table 1-6 A summary of the literature on the ultrasonic characterization of skin

No.	*Reference*	*Preparation method, species, age*	*Testing site*	*US frequency (MHz)*	*Detection technique*	*Parameters*	*Emphasis*
1	Bhagat et al., 1980	In vitro, skin tissue, young and aged mice	-	2.25-10	Reflection	US speed and attenuation	Change of ultrasonic properties with aging
2	Olerud et al., 1987	In vitro, mature dog, normal skin and wound	Back	100	SLAM*	US speed and attenuation	Correlation of ultrasonic properties and collagen content, water content and tensile strength
	Riederer-Henderson et al., 1988	In vitro, mature dog, normal	Back	100 10-40	SLAM and echographic mode	US Speed and attenuation	Frequency dependence of attenuation
	Steiger et al., 1988	In vitro, mature dog, normal skin and wound	Back	100	SLAM	US Speed and attenuation	Measurement uncertainty
	Forster et al., 1990	In vitro, mature dog, normal skin and wound	Back	10-40	Echographic	Attenuation	Wound healing process
	Olerud et al., 1990	In vitro, mature dog, normal skin and wound	Back	100	SLAM	US Speed and attenuation	Correlation between tissue constituents and acoustic properties

3	Moran et al., 1995	In vitro, epidermis and dermis, two cadavers, age: 45 and 68	Back, chest and abdomen	20-30	Reflection and echographic mode	US speed, attenuation coefficient and backscatter coefficient	Ultrasonic properties of excised skin and correlation with protein and fat content
4	Pan et al., 1998	In vitro, skin tissue, rabbit and human	Breast in human	15-40	Reflection and echographic mode	Echogeneity, US speed, attenuation and backscatter	Variation of viscoelastic and ultrasonic properties of skin under transverse stress
5	Guittet et al., 1999a	In vivo, dermis and hypodermis, human subject, age: 14-85	Forearm	40	Echographic with axial translation	Attenuation slope	Correlation of attenuation slope and gender, age
	Guittet et al., 1999b	In vitro, dermis and hypodermis, human	Abdomen	40	Echographic with axial translation	Attenuation slope	Attenuation slope, reproducibility, and correlation with gender and age
		In vivo, dermis and hypodermis, human, age: 14-85	Forearm				
6	Lebertre et al., 2002	In vitro, dermis, female subjects, age: 46.5 ± 12.2	Abdomen	22-45	Echographic	Attenuation slope, integrated attenuation and integrated backscatter	Spatial variation of ultrasonic parameters
7	Fournier et al., 2001	In vivo, dermis, human subjects, age: 24- 76	Forearm	12.5-25	Echographic	Integrated backscatter and its frequency dependence	Reproducibility of backscattered spectra, and observations in normal skin with respect to age, gender, pressure and temperature
	Fournier et al., 2003	In vivo, dermis, human subjects, Age: 24-76	Forearm	11-27	Echographic	Attenuation slope Integrated attenuation	Effectiveness of different algorithms and observations in normal skins with respect to age, gender, pressure and temperature
8	Raju and Srinivasan, 2001	In vivo, dermis and subcutaneous fat, young human subjects, age: 19-36	Forearm and fingertip	14-50	Echographic with axial translation	Attenuation slope and backscatter coefficients	Ultrasonic properties of different skin layers and their anatomical dependence
	Raju and Srinivasan, 2002	In vivo, dermis and subcutaneous fat, young human subject, age: 20-36, median: 26	Forearm and fingertip	28	Echographic with axial translation	Parameters of statistical models	Statistical information of the signal envelope from different skin layers and anatomic sites
	Raju et al., 2003	In vivo, human dermis with and without contact dermatitis, human subjects, age: 25-66, median: 41	Forearm	33	Echographic with correction spectra collected from normal subjects	Skin thickness, echogenicity, attenuation slope, statistical parameters	Capability of ultrasonic characterization for skin lesions

***: SLAM – scanning laser acoustic microscope**

with the subject age significantly. Possible reasons for the discrepancy of the age effect on the attenuation slope might be the differences between the two studies such as the population size, detection frequency bandwidth, and effect of the diffraction. In contrast, a significantly positive correlation with the age in most of the studied depths beneath the skin was demonstrated for the integrated attenuation and integrated backscatter. Furthermore, it was found that ultrasonic parameters were sensitive to the probe pressure and the temperature, thus suggesting that those factors should be well controlled during data collection. The integrated backscatter was also found to increase with depth, which might be caused by the fact that the collagen fibers are oriented more perpendicular to the ultrasonic beam in the deep region (Urmacher, 1990). Gender differences of ultrasonic parameters were also demonstrated and this was most probably attributed to the difference of collagen content between male and female. Ultrasonic properties were also sensitive to the transverse tensile stress in the skin, which was demonstrated by Pan et al. (1998) in well-controlled *in-vitro* experimental conditions. The increase of transverse stress significantly decreased the attenuation while only minor variation of backscatter coefficient was induced. These changes led to the observation in an ultrasound B-mode image that the brightness and penetration significantly increased with the increased stress. Skin is naturally with transverse tension in the direction along the Lange's lines (Alexander and Cook, 1977) so that the chronological change of skin in tension may also be a factor contributing to the age effect on ultrasonic properties. Intrinsically, interaction between ultrasound and skin is related to the skin compositions and structures. The dermis of skin is mainly organized as combinations of collagen and elastin fiber network, water embedded in the extracellular matrix, blood and lymph vessels, nerves and various appendages. Among them, collagen and water have been regarded as two compositions that play a significantly important role in determining the ultrasonic properties (Olerud et al., 1990; Moran et al., 1995). In a dog model, Olerud et al. (1990) demonstrated a significant correlation of the attenuation with the collagen and water contents in the dermis. It was reported that the collagen made an increase in the attenuation while the water decreased the attenuation. Moran et al. (1995) confirmed the correlation between the attenuation and the collagenous protein in the human dermis *in vitro*. While the role of the collagen and water contents in determining the ultrasonic properties has been already studied, reports on the effects induced by skin appendages, collagen fiber configurations such as type, size, orientation and cross-

linking are still lacking. In other tissues such as the tendon, insonification perpendicular to the collagen-rich fibers orientation produces much larger backscatter than the parallel direction (Hoffmeister et al., 1995). Thus this is a very important research interest for further investigation on more details of the role played by the collagen fiber in skin. While the effects of various factors on the ultrasonic properties have become clearer and clearer through the previous studies, new experiments are still necessary to be conducted and new models are necessary to be proposed in the future to clarify the relationship between ultrasonic features and skin characteristics.

Detection techniques of ultrasound usually include two modes: the insertion loss method that is often used *in vitro* and the echographic mode. Although generally the insertion loss method is more accurate, skin can be analyzed noninvasively only with the echographic mode *in vivo* where the insertion loss mode is inaccessible (Guittet et al., 1999b). With a good technique to correct the diffraction effect, the accuracy of the echographic mode can be improved to the similar level as that of the insertion loss mode. Axial translation ensures the beam being focused at the center of a region of interest at each step of movement, thus being a proper choice for correcting diffraction (Ophir and Mehta, 1988). In a phantom test, it was showed that the attenuation slope obtained from the echographic method with use of the axial translation technique was very similar to that obtained using the double-transmission method (Guittet et al., 1999b). However, such a technique is somewhat time-consuming, which limits its use in real clinical trials. The lateral scanning technique and tissue preparation are also considerations in data collection for UTC. Lebertre et al. (2002) studied the variation of ultrasonic parameters with respect to the surface area scanned and demonstrated that more consistent and representative estimations would be obtained when a larger area was used for computation. The spatial variation comes mostly from the acoustic heterogeneity of the skin due to its complex structure. Although a homogeneous volume is assumed in analyzing the ultrasonic properties, such an assumption cannot be approximately matched until a large area for data collection is under consideration. However, it should also be noted that a too large area is not necessarily a better choice due to the possible existence of inhomogeneous interface such as large vessel in normal skin or the limited affected area in a skin disease. For *in-vitro* experiment, one should take care to the specimen preparation process because the dead skin does not have internal stress and blood and lymph

supply compared to *in-vivo* skin and it changes progressively with time after excision. It was demonstrated that the preparation technique had a significant effect on the measured ultrasonic properties (Bamber et al., 1977). Thus if any, standard techniques of preparing the sample are preferred for better comparison. As for tissue characterization by using ultrasonic systems, inter-lab comparison appears to be a little difficult due to the different devices and detection techniques used. Therefore, it is difficult to transfer the measurement precision of one system to another and it is very important to assess the reliability of a specific measurement technique before its clinical practice. Steiger et al. (1988) measured the uncertainty of ultrasonic measurement using a 100 MHz scanning laser acoustic microscopy and reported a precision of 16% for the attenuation coefficient in the heterogeneous canine tissue *in vitro*. Guittet et al. (1999b) reported a reproducibility of attenuation slope with a value of 12% in terms of the coefficient of variation (CV). Fournier et al. (2001, 2003) reported the reproducibility of backscatter spectra and attenuation parameters with a value of less than 20% using the standardized CV. However, it is uncertain whether it is proper to use a coefficient of variance for describing measurement reliability. On the other hand, whether the reliability of measurement is acceptable for a clinical practice depends on the order of variation provoked by the skin process to be detected. For example, Raju et al. (2003) demonstrated that the *in-vivo* measurement of the attenuation slope was capable of differentiating the normal healthy skin from the skin having contact dermatitis induced by the patch test. It is expected that with a proper measurement, different skin modifications can be detected by high frequency UTC.

Investigators have attempted to use the ultrasonic properties to characterize fibrotic process in other tissues such as the liver and myocardium (Lin et al., 1988; Bridal et al., 1997; Saijo et al., 1998). Lin et al. (1988) found an increased attenuation slope at 5 MHz for the liver with fibrosis in comparison with the normal liver without fibrosis. In addition, they found a nonlinear increase of this parameter with the fibrosis grade assessed by biopsic examination. In studying vascular tissues with atherosclerosis, Saijo et al. (1998) demonstrated that an evident increase of attenuation slope was associated with the fibrous part of the arteries, while Bridal et al. (1997) reported an only slight increase of attenuation and no increase of attenuation slope in the collagen-rich region. It should be noted that between them the former used a scanning acoustic microscope operation in the frequency range of 100

to 200 MHz, while the later utilized the frequency from 30 to 50 MHz. Despite the discrepancies, it appears that the fibrotic process in these two tissues really causes the change of their ultrasonic propagation properties. Komiyama et al. (2000) studied the statistical information of the backscattered signals from the atherosclerotic plaque and found a significant correlation between the statistical parameters and histology. Thus to study the statistical aspects of the signals from fibrotic tissues is also potentially useful. For skin tissues, though sparse, use of ultrasonic characterization methods for characterizing different pathologies has been reported. Forster et al. (1990) used ultrasonic properties to monitor the healing process of surgical wounds. The attenuation was observed to increase in most but not in the late part of the period studied, while collagen content increased continuously during the studying period. They claimed that other factors might also influence the attenuation during a healing process. Raju et al. (2003) tried to characterize the contact dermatitis induced by the patch test using the measurement of ultrasonic properties. The skin thickness, echogeneity and attenuation slope were found to be different in subjects receiving patch test. The contact dermatitis is mainly expressed as an inflammatory skin condition with the infiltration of extra water content. The ultrasonic measurement seemed to be sensitive to the variation of water content in the skin. There are clear evidences in the literature that the collagen fibril structure has been altered after treatment of irradiation (Leontiou et al., 1993; Riekki et al., 2000). Related studies also demonstrated a change of water content measured by dielectric method in human skin as early and late reactions of the radiotherapy (Nuutinen et al., 1998). Therefore, it was hypothesized that the related change of skin compositions would also influence its ultrasonic properties. Accordingly, the second objective, also the main part of this study, is to introduce high frequency ultrasonic characterization method into the field of assessment of skin fibrosis. Reliability of our measurement with respect to intra- and inter-rater operation was assessed. Then measurement protocol was established in normal subjects and also applied to patients in clinical trials. Clinical symptoms of fibrosis were also measured and correlated to the ultrasonic properties.

1.4 Elastography for Skin Application

As the echogenicity and the stiffness of tissue are generally uncorrelated, elastography is emerging as an important method to measure the soft tissue mechanical properties and to detect some pathologies in their early stage (Ophir et al.,

1991, 1999). The general method to form an elastogram is to conduct a quasi-static, transient or dynamic perturbation to the detected tissue and then to record the tissue mechanical response by using imaging modalities including ultrasound, MRI, optical coherence tomography, etc. Compared with MRI, ultrasonic elastography is cheaper, more portable and less time-consuming so researchers seem to have put more effects on using the ultrasound than MRI in the past 15 years and all the current discussion is based on using ultrasound as the imaging modality. In a quasi-static operation mode, pre- and post-compression information is obtained and then internal strain is extracted using algorithms such as the cross-correlation technique. If associated with a stress analysis, the distribution of the tissue elasticity can also be reconstructed. The contrast of the elastic properties within the tissue induced by certain pathology would be revealed in the elastography because lower strain would be induced in harder tissue and vice versa. The quasi-static elastography is easy to be understood because usually the directly measured stain information will be displayed in the image. However, the use of static elastography is limited by its high sensitivity to boundary conditions that would certainly induce artifacts in the so-called elastograms when controlled standardized compressions are not possible for some tissues *in vivo* such as the liver. The dynamic (or transient) elastography is to record the tissue response after low frequency periodic (or pulsed) vibrations are generated on the tissue. In such cases, the amplitude of the internal vibration or the shear wave velocity is measured by Doppler or pulsed ultrasound. The directly measured parameters or elastic parameters extracted based on them will be displayed in the elastograms and those elastic abnormalities, which are always not visible in the pure B-mode images, will be more visualized. In addition to external vibrations, physiological stimuli, such as pulsation of the cardiac system, can also be used as excitations in the elastographic operations. Dynamic elastography is especially appropriate for those non-static tissues which are easy to be affected if quasi-static compression is used. But compared with quasi-static elastography, the dynamic or transient elastography needs higher system requirements such as fast image acquisition ability, and it also suffers from some particular problems such as the diffraction phenomenon.

Clinical trials of elastography have been carried out in breast tissues and it was shown to be helpful in discriminating benign and malignant masses and in cases where the shadowing is present in the sonogram (Garra et al., 1997). The elastography

has also been applied to tissues with fine structures for which high frequency ultrasound is the most suitable noninvasive tool to detect pathologic changes, such as vessel plaques (De Korte and Van der Steen, 2002) and cartilage degeneration (Zheng et al., 2004). Associated with intravascular ultrasound (IVUS) imaging method, the use of intravascular elastography enhances the differentiation between different plaque types such as fatty and normal components and can identify the high strain regions under blood pressure (De Korte and Van der Steen, 2002). Identification of these components and regions are important to identify the potential vulnerability of the plaque and to make better clinical decision for treatment. The skin is a thin tissue which has a similar scale of thickness with the artery and the similar frequency of ultrasound is often used for detection in these two types of tissues. For example, in human skin 20 MHz imaging system is most generally accepted for use (Seidenari et al., 1996; Warszawski et al., 1997; Fournier et al., 2003), while IVUS with this frequency range is also introduced to imaging the elasticity of arterial plaques both in animal and human models (De Korte et al., 2000, 2002). Thus it will also be helpful to apply the principles of elastography to skin tissues. To obtain the elastogram of skin is more beneficial for the detection of local diseases than diffuse diseases because only tissues with inhomogeneous distribution of mechanical properties can show a contrast pattern in elastography. Therefore such a technique is very potential to the diagnosis and quantification of volume of skin tumors. On the other hand, compared to that of intravascular elastography, the difficulty in applying such a technique to skin may be that uniform pressure cannot be easily conducted on the skin due to a small contact area of the currently available probe. Furthermore, due to the existence of the softer subcutaneous fat beneath the dermis, most of the deformation caused by the external pressure may occur in the fat rather than in the skin, thus making the strain in the dermis relatively small and difficult to be detected. However, the progressive advances of techniques and signal processing methods developed in ultrasonic elastography have opened a broad field for its applications in a number of tissues including the skin.

We have introduced a 20 MHz ultrasonic imaging system to study the acoustic properties of fibrotic tissues. We are also trying to measure the distribution of mechanical properties in the skin by incorporating this system with other pressure-sensing device. Although in the current stage, it is not possible for us to obtain the

elastogram and analyze the fibrosis using the elastogram from the human skin, it is feasible as the first step to study the elastic property of the whole layer of fibrotic skin by investigating the relationship between force and deformation which is measured from the ultrasonic high resolution system. It is hypothesized that not only the mechanical properties of the bulk soft tissue, which can be measured using the TUPS, but also the mechanical behaviour of the thin skin tissue, change in the patients with the post-radiotherapy sequelae of fibrosis. If the skin stiffness can be measured with our modified ultrasonic imaging system, it can be potentially used to assess the skin fibrosis, as well as to correlation with other clinical symptoms. Accordingly, the third objective of this study is to develop a modified ultrasonic elasticity measurement system that can measure the overall stiffness of skin *in vivo*. The feasibility of this system using test on phantoms and porcine skin *in vitro* and human skin *in vivo* was demonstrated.

1.5 Objectives of This Study

The objectives of this study included:

1. To study the viscoelastic properties of the irradiation neck soft tissues using the quasi-linear viscoelastic model plus the indentation test and to assess the capability of the four model parameters to differentiate the severity of fibrosis;
2. To introduce high frequency ultrasound for characterizing the skin fibrosis and to evaluate its capability to differentiate the severity of fibrosis;
3. To conduct some preliminary studies for the purpose of developing an ultrasonic system which could measure the skin elasticity *in vivo*

2. QLV Properties of Fibrotic Soft Tissues

2.1 Methodology

2.1.1 Description of Indentation System

The system used was based on a manually-driven ultrasound indentation system, which was previously developed to assess the mechanical properties of soft tissues *in vivo* (Zheng and Mak, 1996). Figure 2-1 shows the diagrammatic representation of this system. A real prototype of the indentation system used for this part of the study is shown in Figure 2-2. The system is mainly comprised of a hand-held indentation probe, an ultrasound pulser/receiver and a personal computer to display and process the collected data. The probe has an unfocused ultrasound transducer of 5 MHz at its tip, and an in-series 10 N strain gauge load cell. The ultrasound transducer has a cylindrically flat end with a diameter of 9 mm and serves as an ultrasound emitter, receiver, and indenter at the same time. The initial thickness of the soft tissue and the indentation are calculated from the signal between the time of pulse transmitting and the time of pulse receiving from the reflection of a soft tissue-bone interface assuming a constant speed of sound 1540 m/s in soft tissues (Goss et al., 1980). The force response during the indentation is simultaneously sensed by the load cell. Signals of force and ultrasound are saved in the hard disk and used for the subsequent analysis. The sampling rate for the force response and the indentation, which is extracted from the ultrasound signals using a cross-correlation algorithm, is approximately 12.5 Hz.

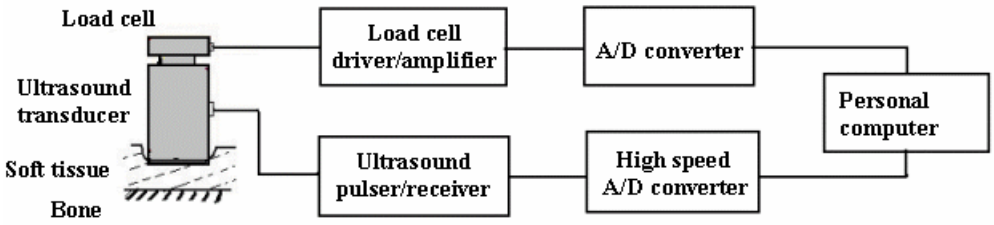

Figure 2-1. The schematic diagram of the indentation system.

2.1.2 Subjects and Indentation Procedure

It should be noted that the recruitment of normal and patients subjects and experimental data collection for this part of study was conducted previously (Zheng et al., 2000b; Leung et al., 2002). They were briefly described here and details can be found in the literature. 105 patients (age: 51 ± 11 years) who had received

radiotherapy to the full length of both sides of the neck were recruited in the present study. The patients had been followed for at least two years after radiotherapy and had no evidence of cancer recurrence at the time of recruitment for the biomechanical indentation tests. The whole study was completed within a 12-month period in the oncology follow-up clinic. All the patients had been treated for the same type of cancer (nasopharyngeal cancer) by uniform radiotherapy protocols. In order to compare the viscoelastic properties between irradiated patients and normal subjects, the indentation tests were also conducted on a group of 8 normal healthy but younger subjects (age: 25 ± 2 years) using the same protocols.

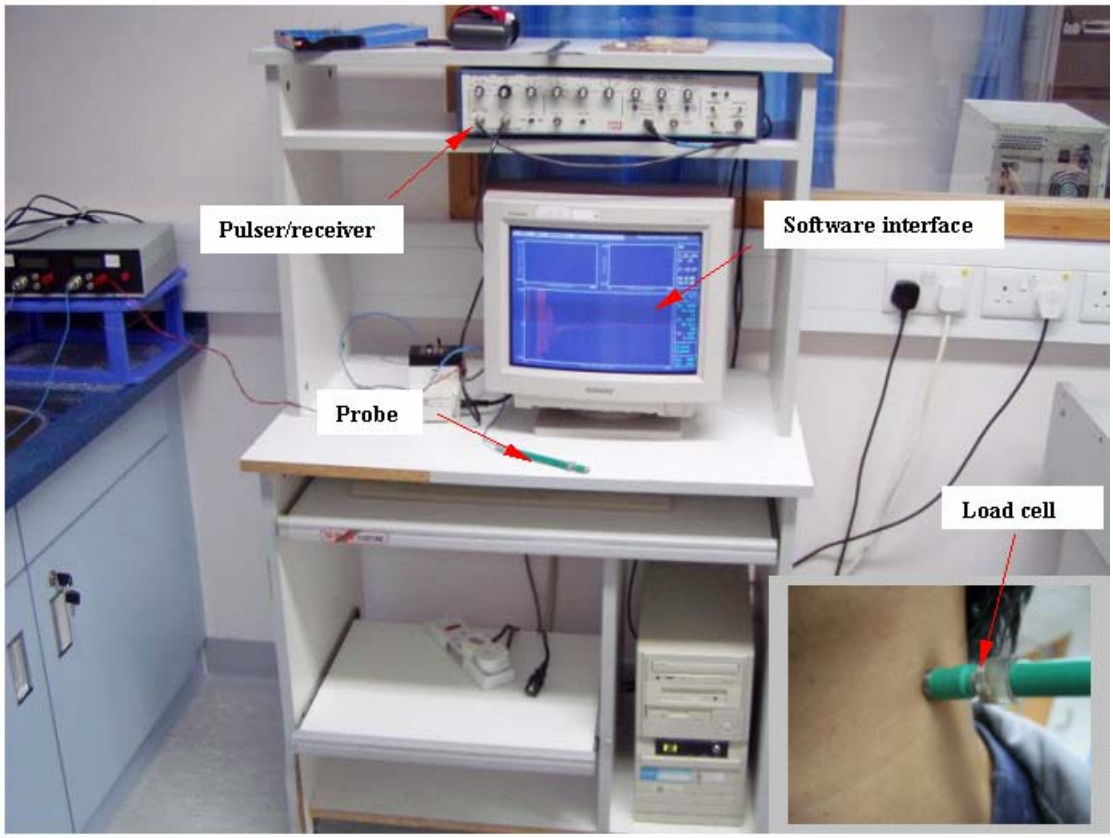

Figure 2-2. A prototype of the indentation system and the operation of the probe on the neck soft tissues (the right bottom corner).

The indentation tests were conducted at two standard reference sites on each side of the neck. These two sites were located 3 cm and 7 cm inferior to the mastoid bone, which is a readily palpable reference landmark (the small image in Figure 2-2). These two sites were chosen because they overlie the cervical spine which provides an interface for consistent reflection of ultrasound signals. The site-dependence, inter- and intra-observer variations of an effective stiffness indicator viz. the Young's

modulus at these testing sites in normal and irradiated subjects had been investigated and reported in a feasibility study (Zheng et al., 2000b). It was demonstrated that the two points selected were effective to distinguish the stiffness between the two populations. During the test, the subject sat on a chair, with the neck neither extended nor flexed and with the eyes looking forward. The neck was kept in a natural position because it had been demonstrated that the state of muscle contraction did affect the tissue stiffness (Mak et al., 1994; Vannah and Childress, 1996; Zheng et al., 1999). After the subject was properly seated, the ultrasound probe was placed on the defined site and oriented to obtain a maximum reflection peak from the bony interface. Before the actual measurement, several cycles of loading and unloading with a gentle pressure were performed to precondition the tissue (Mak et al., 1994; Silver-Thorn, 1999; Klaesner et al., 2001) and to ensure a repeatable behaviour of the soft tissue. It was also adjusted to ensure that a stable ultrasound reflection signal could be obtained and then a consistent shift could be obtained from the moving of the reflection. After a preload of less than 0.5 N was applied on the skin, a load of 5 N or less if the indentation had reached 30% of the original tissue thickness was applied. Applying such an extent of indentation never or minimally caused discomfort to the patients. For each indentation trial, it typically included three cycles of loading and unloading, which were completed within approximately 10 seconds. The indentation rate was manually controlled in the range of 0.5 mm/s to 7.5 mm/s, in which a stable manual indentation could be imposed (Zheng et al., 1999). Care was taken during the indentation in order not to cause the sliding of the probe. Figure 2-3 shows a typical force and indentation curve from one site of subject #1. For each site, totally 3 trials were conducted and the 3 sets of the extracted material parameters were averaged to give the viscoelasticity parameters for the testing site.

2.1.3 Two Clinical Measurements of Tissue Fibrosis

The first measurement was the scoring by hand palpation. Each side of the neck of the patient was palpated by at least one of 3 independent raters and given a palpation score from 0 to 3. The scoring criteria were as follows: Grade 0, nil or equivocal presence of fibrosis; Grade 1, unequivocal presence of fibrosis of mild degree; Grade 2, moderately severe fibrosis change; and Grade 3, severe fibrosis. According to the palpation score, the patients were divided into four subgroups: Group 0, Group 1, Group 2, and Group 3 for the subsequent data analysis. The raters

were blind to the ultrasound measurement results and did not communicate about their experience of palpation rating throughout the study period. The average score of the 3 raters on each side of the neck was used in the subsequent analysis. The second clinical measurement of tissue fibrosis was about the neck rotation range. This was performed using a protractor positioned horizontally above the patient's head. During the measurement, shoulder movements were attentively avoided to secure the accuracy. The range of rotation to the left side was taken to reflect the severity of fibrosis of the right neck in the analysis, and vice versa. A small neck rotation range is regarded as a severe degree of neck fibrosis. The two clinical parameters of fibrosis (palpation score and neck rotation range) were then correlated to the viscoelastic properties obtained from the indentation test.

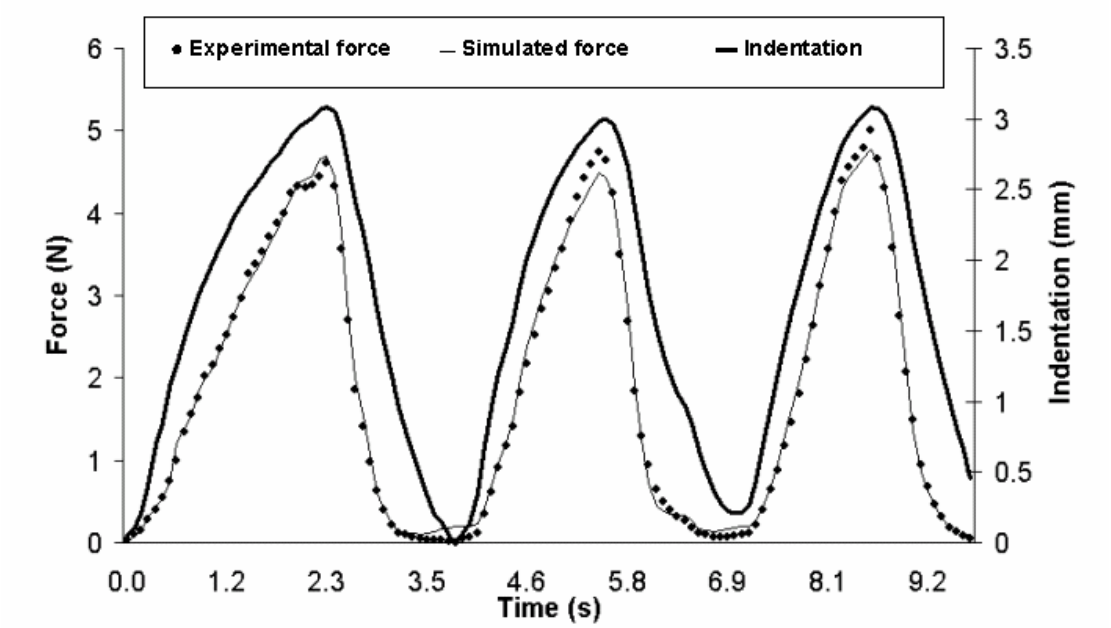

Figure 2-3. A typical indentation showing the corresponding force and indentation and its curve fitting results for Subject #1 (Group 3). The original tissue thickness is 22.5 mm. The maximum indentation is 14.1% of the original tissue thickness. The QLV parameters obtained from the simulation are E_0 = 59 kPa, E_1 = 1278 kPa, τ = 0.13 s, α = 0.577. The Pearson correlation between the simulated and experimental force was 0.998 with a percentage RMS simulation error of 0.045.

2.1.4 Extraction of Quasi-Linear Viscoelastic Parameters

The data reduction method used was similar to the one described previously (Zheng and Mak, 1999a), but with an improved modification to include the effect of large indentation in the model. Instead of a detailed explanation, it was just briefly

described as follows. The indentation value is written in the form of the relative indentation with respect to the original thickness:

$$u = w / h \tag{2-1}$$

where w is the applied indentation and h is the original tissue thickness. If viscosity of the test tissue is considered, an instantaneous Young's modulus in the quasi-linear viscoelastic (QLV) form as proposed by Fung (1981) is written as follows:

$$E(u,t) = E^{(e)}(u) \cdot G(t), \; G(0) = 1 \tag{2-2}$$

where $E^{(e)}(u)$, assumed to be a function of u alone, is called the unrelaxed elastic modulus, and $G(t)$, a normalized function of time, is called as the reduced relaxation function. In the current study, the two functions are further simplified to be in the following forms:

$$E^{(e)}(u) = E_0 + E_1 u \tag{2-3}$$

$$G(t) = 1 - \alpha + \alpha e^{-t/\tau} \tag{2-4}$$

where E_0 is called the initial modulus, E_1 the nonlinear factor, τ the time constant, and α a viscosity-related constant. The two elastic parameters have different mechanical meanings. E_0 is the YM which is meaningful at zero or an infinitesimal indentation ratio of the soft tissues, while E_1 is the parameter showing the level of the indentation-related increase of YM. The two viscous parameters also show different time-dependent properties where τ reflects the speed of the stress relaxation and α shows the extent of relaxation at the equilibrated state. According to the data processing described previously by the investigators (Zheng and Mak, 1999a), the force response at any time t can be reconstructed from the indentation history $u(\xi)$ $(0 < \xi < t)$ as:

$$P(t) = \frac{2rh}{1-\nu^2}[\kappa(u(t))[E_0 u(t) + E_1 u^2(t)] - \frac{\alpha}{\tau}\int_0^t \kappa(u(t-\xi))[E_0 u(t-\xi) + E_1 u^2(t-\xi)]e^{-\xi/\tau} d\xi] \tag{2-5}$$

where ν is the Poisson's ratio of soft tissue, assigned to be a constant of 0.45 in this study assuming the tissue is almost incompressible, r is the radius of the indenter and

κ is a scaling factor that only depends on the indentation ratio u for a certain indentation test at a specific site. The force response $P(t)$ in Eq. (2-5) can be written in a discrete form:

$$P(i) = \frac{2rh}{1-\nu^2}[\kappa(u(i))[E_0 u(i) + E_1 u^2(i)] - \frac{\alpha}{\tau}\sum_{j=1}^{i}\kappa(u(i-j))[E_0 u(i-j) + E_1 u^2(i-j)]e^{-j\cdot\Delta t/\tau}\Delta t] \quad (2\text{-}6)$$

where Δt is the time interval between two adjacent data points. The scaling factor $\kappa(u(i))$ for an arbitrary $u(i)$ can be interpolated from the indentation-dependent values provided by Zhang et al. (1997). In the previous study by the investigators (Zheng and Mak, 1999a), the scaling factor κ was assumed to be constant for a different indentation depth and the effect of a large indentation was compensated by changing the initial tissue thickness for each step of indentation. This approach could only be used when the indentation was relatively small where the boundary conditions were not significantly changed between two steps. In comparison, the current approach could better compensate the effect induced by a large indentation because the geometrical nonlinearity was considered in the compensation. The effect of friction was neglected in the analysis because the ultrasound coupling gel applied between the transducer and skin surface was regarded to serve as a lubricant.

To obtain the material constants from the force and indentation data collected experimentally, an optimization process was used. This method utilizes the principles of maximum likelihood estimation and has been broadly adopted to obtain mechanical properties of soft tissues especially in finite element analyses (Vannah and Childress, 1996; Tonuk and Silver-Thorn, 2003). The material constants were selected according to an error indicator defined as follows:

$$S_{err} = \sqrt{\sum_i (P_s(i) - P_e(i))^2} \Big/ \sqrt{\sum_i (P_e(i))^2} \quad (2\text{-}7)$$

where S_{err} is the simulation error, named as percentage root mean squared (RMS) error, $P_e(i)$ is the experimentally measured force sequence, and $P_s(i)$ is the numerically simulated force sequence. A Matlab (MathWorks, Natick MA, USA) program was custom-designed to search the optimal material constants using the

transient force deformation response of the tested soft tissues. Instead of automatically being searched by the Matlab function (*fminsearch*), the time constant τ was deliberately increased in a loop in the optimization process to avoid reaching a local minimum value because this constant was in the exponential form and might induce a complex pattern of simulation error. The increment was nonlinear with an increased interval when τ was increased. The values of the other 3 parameters, i.e., E_0, E_1 and α were optimized by the Matlab function *fminsearch(*)*. A previous study showed that these parameters extracted from lower limb soft tissues were repeatable (Zheng and Mak, 1999a).

2.1.5 Statistical Analysis

Results were presented in the form of mean ± standard deviation (SD). After the QLV parameters were extracted from the three repeated indentation trials on each testing site, the values of the two testing sites on the same side of neck were averaged and the mean values were used to represent the viscoelastic properties of the neck tissue on that side. The QLV parameters were grouped into four subgroups according to the hand palpation scores of 0, 1, 2 and 3. One-way *ANOVA* was used to test the difference of the viscoelastic parameters among the four patient subgroups. Post-hoc t-test was used to further test for the cases where the difference existed if a significant difference was found in the *ANOVA* analysis. The viscoelasticity parameters were also correlated to the neck rotation range and the effective Young's modulus using a Spearman correlation. Spearman correlation was considered because we had noted the non-normal distribution of some viscoelastic parameters and the Spearman rank correlation was more proper in this case than the Pearson correlation. The effective Young's modulus has been previously defined as the average Young's modulus extracted from the overall load-indentation relationship neglecting the nonlinear and time-dependent properties (Zheng et al., 2000b). The Viscoelastic results obtained from the patients were also compared with those from the 8 normal subjects. Commercial statistical analysis software SPSS (SPSS, Chicago IL, USA) was used for the statistical analysis and in all cases $P < 0.05$ was used as a level of significant difference.

2.2 Results

2.2.1 General Observations and Test Repeatability

Figure 2-3 shows the typical indentation response at one site of Subject #1. The optimized simulation results using the QLV model are also shown in this figure. In this case, the extracted QLV parameters well predicted the force response which was reconstructed from the indentation history. For this typical indentation, the percentage RMS thus derived was 0.045. It was 0.096 ± 0.029 for all the tests. It was demonstrated that the QLV model was effective to analyze the experimentally obtained indentation data. Figure 2-4 shows the comparison of force-indentation responses obtained from two patient subjects with different degrees of fibrosis. In Figure 2-4, the phases of loading and unloading can be well differentiated, which shows the typical "hysteresis" phenomenon involved in the viscoelastic behavior of soft tissues. Through the hysteresis, partial energy was dissipated. Although not obviously visible in the figure, the time dependent creep and stress relaxation phenomena did exist in the indentation cycles. The force responses were significantly different in two cases. The same force applied on the tissues with more severe fibrosis induced smaller indentations. This observation, from the perspective of an experienced palpation rater, would be transferred as a feeling to him/her that the palpated tissue was stiffer so that a higher score indicating more severe fibrosis would be given. The mean indentation rate for all the tests in this study was 3.3 ± 3.0 mm/s, indicating it was well controlled in the range as previously suggested in the indentation study of lower limb soft tissues (Zheng et al., 1999).

Repeatability of the test was assessed by three typical experiments performed separately but repeatedly on a site of a patient. E_0 and E_1 were calculated to be 23 ± 4 kPa and 362 ± 67 kPa, respectively. So the variation of E_0 and E_1 was 16% and 18%, respectively. τ and α of the three tests were 1.03 ± 0.08 s and 0.357 ± 0.018, respectively. So the variation of τ and α was 8% and 5%, respectively. The test repeatability was comparable to a previous study (Zheng and Mak, 1999a) and therefore, the test was thought to be reliable in terms of clinical conditions.

2.2.2 Elastic Parameters E_0 and E_1

The mean initial modulus E_0 of the irradiated, fibrotic neck soft tissues in the 105 patients was 26 ± 22 kPa, ranging from 3 kPa (for a patient in Group 0) to 134 kPa (for a patient in Group 3). The mean nonlinear factor E_1 in all patients was 507 ± 683 kPa, ranging from 19 kPa (for a patient in Group 0) to 4058 kPa (for a patient in Group 3). Figure 2-5 shows a comparison of the initial modulus E_0 and the nonlinear factor E_1 in all patient subgroups with different palpation scores. Although there were overlaps of the elastic parameters between different patient subgroups, the minimum and maximum values of E_0 and E_1 in each subgroup generally increased with the increase of the palpation score. Table 2-1 shows the mean E_0 and E_1 in different patient subgroups. One-way *ANOVA* showed that there was a significant difference of E_0 and E_1 among patient subgroups ($P < 0.001$). Post-hoc *t*-test showed that E_0 and E_1 were significantly larger in patients with a higher palpation score, except between Group 0 and Group 1 for E_0 (Table 2-2). There were often outliers in each subgroup, which might be caused by the inconsistent nature of a hand palpation, even for an experienced rater, provided the elastic parameters measured from the indentation test rightly represented the mechanical properties of the bulk soft tissue.

Figure 2-6 shows the results of correlation of E_0 and E_1 with the neck rotation range. A significantly negative Spearman correlation of E_0 (r = -0.40, $P < 0.001$) and E_1 (r = -0.48, $P < 0.001$) with the neck rotation range was found. Figure 2-7 shows the correlation of E_0 and E_1 with the effective YM as derived in the previous study (Leung et al., 2002). A significantly positive Spearman correlation of E_0 (r = 0.65, $P < 0.001$) and E_1 (r = 0.84, $P < 0.001$) with the effective YM was demonstrated. The correlation coefficient was higher than that of the two parameters with the neck rotation range. The high correlation of E_0 and E_1 with the effective YM appeared to indicate that measuring the effective YM was as "effective" as measuring the E_0 and E_1. As expected, the slope of the regression line between E_0 and effective YM was smaller than one. Thus the effective YM appeared to be the elastic modulus obtained at a certain level of indentation. However, from the point of

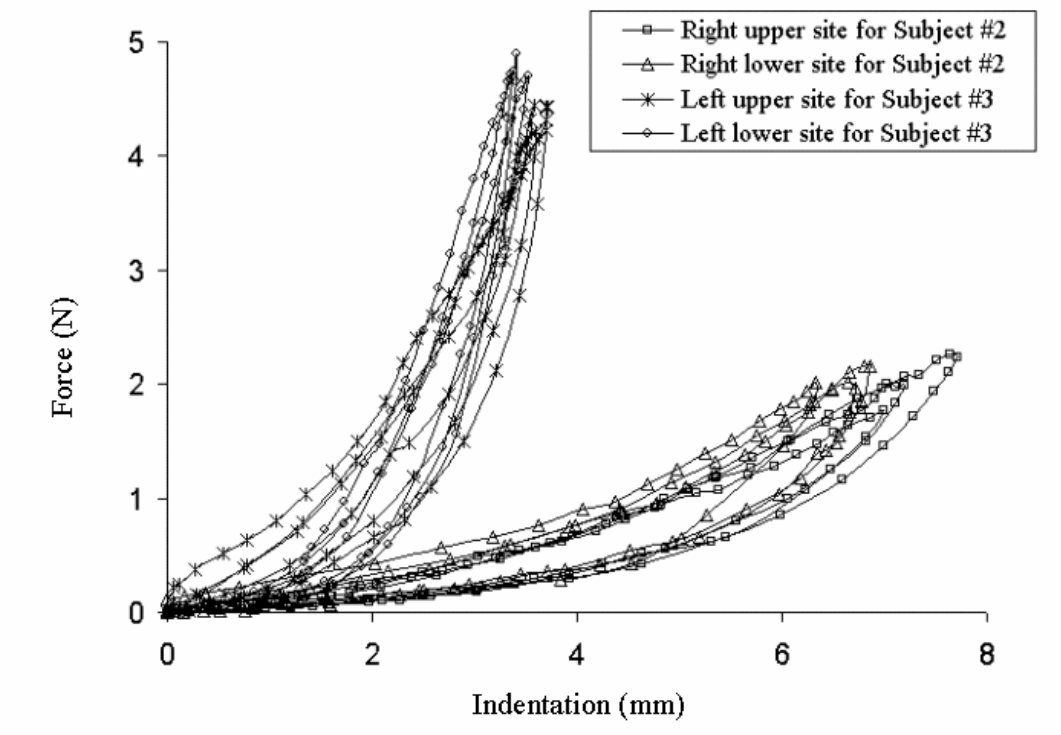

Figure 2-4. Force-indentation responses of two testing sites in two patients having different palpation scores. Subject #2 was in Group 0 and subject #3 was in Group 3.

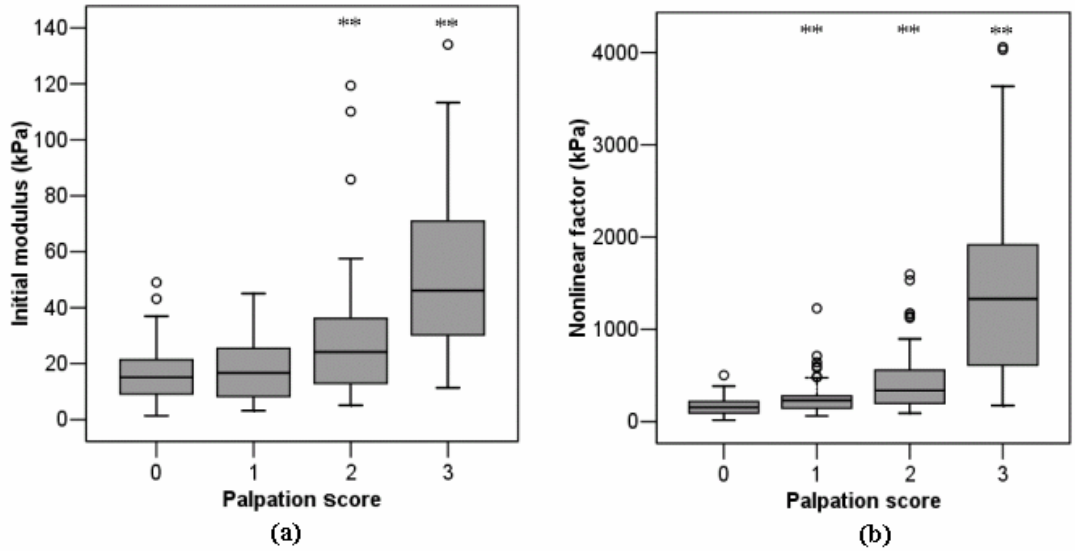

Figure 2-5. Boxplot of (a) the initial modulus E_0 and (b) the nonlinear factor E_1 in different patient subgroups. The box represents the inter-quartile range. The upper and lower limits of the box indicate the 75th and 25th percentile. The horizontal line in the box represents the median. The box and the whiskers together indicate the area in which all observations are found, unless outliers (○) are present. Outlier is defined as a value which is located more than 1.5 times the inter-quartile range below the lower quartile or above the upper quartile. "" represents a significant difference ($P < 0.04$) in comparison with the patient subgroups with a lower palpation score.**

view of the mechanics, the intrinsic meanings of the two QLV elastic parameters are different from that of the effective YM. Comparatively, QLV parameters can more accurately delineate the mechanical response of the soft tissues under indentation. More details about this issue are discussed in the Discussion section.

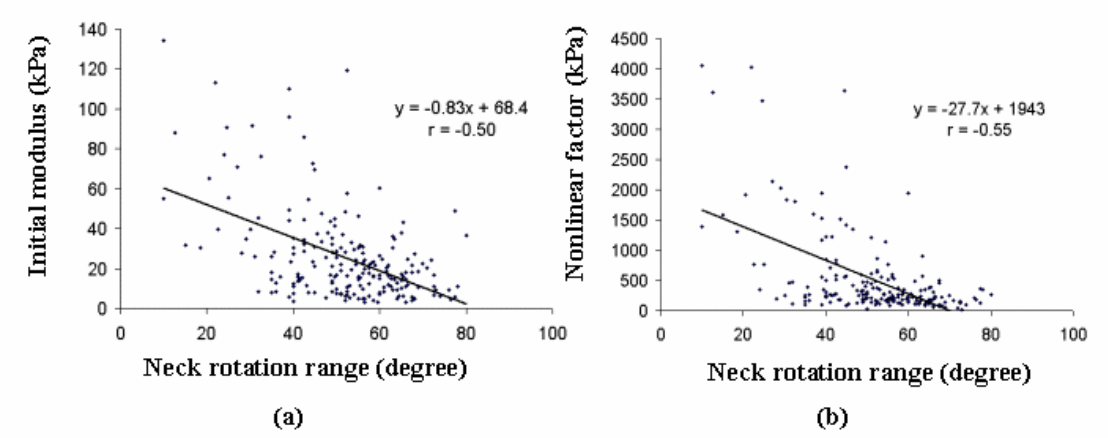

Figure 2-6. Correlation of (a) the initial modulus E_0 and (b) the nonlinear factor E_1 with the neck rotation range. Note that the correlation shown in the figure was Pearson correlation but not Spearman correlation.

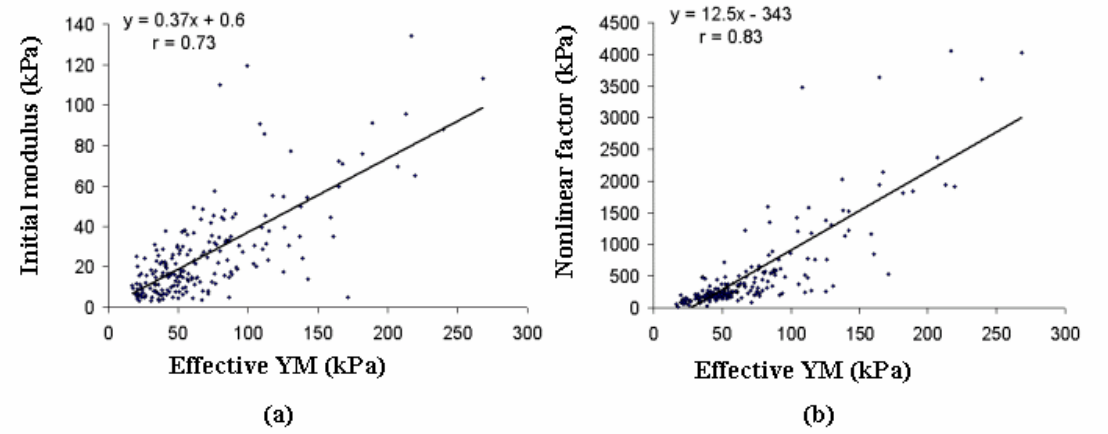

Figure 2-7. Correlation of (a) the initial modulus E_0 and (b) the nonlinear factor E_1 with the effective Young's modulus. Note that the correlation shown in the figure was Pearson correlation but not Spearman correlation.

2.2.3 Viscous Parameters τ and α

The mean time constant τ in the patients was 1.34 ± 1.10 s, ranging from 0.12 s (for a patient in Group 3) to 6.99 s (for a patient in Group 1). The mean parameter α of the irradiated tissues in the patients was 0.421 ± 0.119, ranging from 0.209 (for a patient in Group 2) to 0.693 (for a patient in Group 0). Table 2-1 shows τ and α measured in different patient subgroups. A large standard deviation was observed in

these two parameters. There was no significant difference of τ across patient subgroups (P > 0.05, one-way *ANOVA*). For the parameter α, it increased from 0.399 for Group 0 to 0.458 for Group 3, but still the increase was not significant among the patient subgroups (P > 0.05, one-way *ANOVA*). No significant correlation was found between either τ or α and the neck rotation range or the effective Young's modulus (P > 0.05).

Table 2-1 The QLV parameters of the four patient subgroups

Patient subgroups		*Score 0 (n* = 24)*	*Score 1 (n = 35)*	*Score 2 (n = 28)*	*Score 3 (n = 18)*	*Overall mean*
E_0 *(kPa)*	*Mean*	*16*	*19*	*28*	*50*	*26*
	SD	*11*	*11*	*23*	*31*	*22*
E_1 *(kPa)*	*Mean*	*181*	*266*	*450*	*1501*	*507*
	SD	*108*	*187*	*355*	*1117*	*683*
τ *(s)*	*Mean*	*1.35*	*1.52*	*1.17*	*1.24*	*1.34*
	SD	*0.90*	*1.32*	*0.95*	*1.08*	*1.10*
α	*Mean*	*0.399*	*0.418*	*0.419*	*0.458*	*0.421*
	SD	*0.109*	*0.118*	*0.118*	*0.131*	*0.119*

***: *n* represents the number of patients in each subgroup.**

Table 2-2 The *P* values of *t*-test of E_0 (upper left part) and E_1 (lower right part) among different patient subgroups

Patient groups	*Group 0*	*Group 1*	*Group 2*	*Group 3*
Group 0	-	*0.15*	*0.001*	*< 0.001*
Group 1	*0.02*	-	*0.002*	*< 0.001*
Group 2	*< 0.001*	*< 0.001*	-	*< 0.001*
Group 3	*< 0.001*	*< 0.001*	*< 0.001*	-

2.2.4 Comparison between Patients and Normal Subjects

For the 8 normal subjects, E_0 and E_1 were 6 ± 1 kPa and 56 ± 22 kPa, respectively. They were significantly smaller than those of the patient group (P < 0.001). The time constant τ was 0.24 ± 0.05 s in the normal subjects, which was significantly smaller than that for the patient group (1.34 ± 1.10 s) (P = 0.003), indicating that the irradiated tissues required a longer time than the soft tissues of

normal subjects to recover to the equilibrium state after an indentation. For the parameter α, it was 0.526 ± 0.084 for normal subjects, which was slightly but significantly larger than that for the patient group (0.421 ± 0.119) (P = 0.007), indicating that the irradiated tissues of the patients relaxed to a lesser extent than that for the normal subjects after a step indentation.

2.3 Discussion

A linear elastic indentation solution was extended to include a quasi-linear viscoelastic model to simulate the mechanical behavior and to assess the nonlinear elastic and viscous properties of the bulk fibrotic soft tissues in the neck region of the post-radiotherapy patients. The QLV parameters were obtained from a curve fitting process using the force and indentation data collected by a manually-driven hand-held ultrasound indentation probe. The results showed that the QLV indentation model could well describe the mechanical properties of the fibrotic tissues through the indentation test. It was also demonstrated that this method was more sensitive in discriminating the nonlinear elastic properties of fibrotic tissues than in discriminating the viscous properties among the patient subgroups with different degrees of clinical tissue fibrosis.

2.3.1 Elastic Properties

To the best of my knowledge, quantitative results on the study of mechanical properties of the irradiated soft tissues in the neck region are scarce. Factors that affect the measured results in the previous studies included the geometry and structure of the tissues tested, the clinical background (for example, amputated or non-amputated status, with or without diabetes), posture, state of muscle contraction and preloading, i.e. the initial strain level as well. Most of the previous studies have focused on the soft tissues in other regions and generally chosen the effective Young's modulus or the effective stiffness as the parameter. The effective Young's modulus obtained in such a way was in the range of 43 to 118 kPa (Zheng et al., 2000a), 27 to 162 kPa (Gefen et al., 2001) in the plantar soft tissues; 53 to 141 kPa (Malinauskas et al., 1989), 27 to 106 kPa (Torres-Moreno, 1991), 50 to 145 kPa (Reynolds and Lord, 1992), 21 to 194 kPa (Mak et al., 1994), 2 to 600 kPa (Vannah and Childress, 1996), 10 to 89 kPa (Zheng and Mak, 1999b) in the soft tissues of lower limbs; 14 to 59 kPa (Zheng et al., 1999) in the soft tissues of forearms. However, the extraction of the

effective stiffness was based on a linear force-indentation relationship, while it was demonstrated that soft tissues expressed distinguished nonlinear and viscoelastic behaviour under the indentation test. Klaesner et al. (2001) used an indenter of 7.9 mm to deflect the plantar soft tissue over the metatarsal heads and on the heel in normal subjects. They used a similar indentation solution as adopted by Zheng et al. (1999) and calculated the effective Young's modulus in the different force ranges. Their results showed the effective Young's modulus at all the testing sites increased as the force range increased, indicating that a sole effective elastic modulus was not enough to describe the tissue elasticity, especially when there was a large indentation applied. Hence, a model that can better describe the force-indentation relationship in soft tissues other than the linear one is preferred, because it can characterize the mechanical behavior more accurately and intrinsically. The current method introduced the nonlinear elasticity in a simplified form of an initial modulus plus a nonlinear factor in the QLV model, where the geometrically nonlinear nature of the indentation procedure was compensated by an indentation-dependent scaling factor κ. The initial modulus is a parameter representing the stiffness when no or infinitesimal strain is applied. The nonlinear factor is a parameter indicating the rate of increase of stiffness when the indentation ratio increases. However, it should be noted that the two elastic parameters were obtained assuming a not too large indentation ratio (less than 30%). With too large indentation, higher order of nonlinearity could be generated and the structural elements within the tissue might be broken and the response might be more complicated. Compared with the effective Young's modulus derived based on the assumption of linear elasticity, the initial modulus and nonlinear factor used in this study were extracted using the QLV model in which the effects of viscosity were also considered so that they could more accurately describe the nonlinear elastic properties of the irradiated tissue.

Figure 2-8 shows the results of our present study in the indentation ratio of 0% to 30%. The comparative data, i.e., the effective YM of the patient subgroups and the elastic properties of the normal limb soft tissue, were also plotted in the figure. The effective YM for each subgroup appeared to be the YM calculated at a certain indentation ratio according to the initial modulus and the nonlinear factor. The Young's modulus with the indentation range of 30% of the irradiated tissue in Group 0 was similar to that of the normal limb soft tissue obtained previously using a similar

method (Zheng and Mak, 1999a), but in Group 3 it was much larger than that of the normal limb soft tissue (Figure 2-8). The tissue with a more severe degree of clinical fibrosis was found to be stiffer initially and the stiffness increased faster under the indentation loading. The mean difference of YM was 33.4 kPa at the indentation ratio 0% between Group 0 and Group 3, but that increased to 429.2 kPa at the indentation ratio 30%. According to these findings, the initial Young's modulus and the nonlinear factor extracted using QLV model could provide more information than using the effective Young's modulus alone. The results also suggest that it is important to document the initial and the maximum deformation and/or indentation load when the effective Young's modulus is reported alone, as the results significantly depend on these conditions. This issue is particularly important in the comparison of the results reported by different research groups.

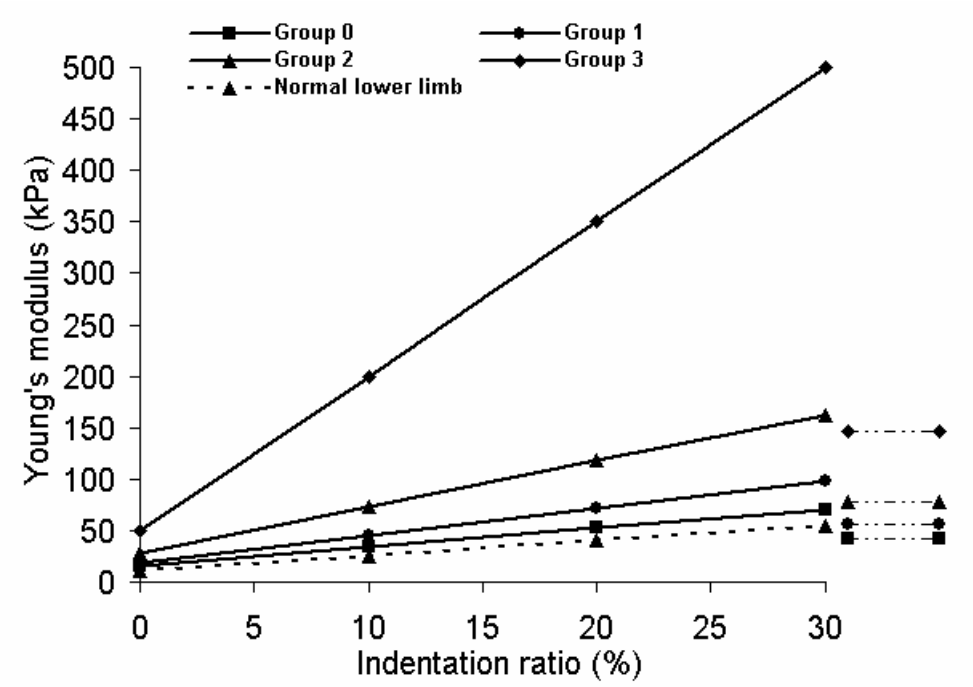

Figure 2-8. Comparison of the elasticity of the neck soft tissues obtained by analyses of the QLV model (left increasing lines) and the previous linear indentation solution (right horizontal lines). The elasticity of the lower limb soft tissues obtained using the QLV analysis (Zheng and Mak, 1999a) is also shown.

Alternative method, such as finite element analysis was used previously to model the indentation test and estimate the nonlinear elastic properties of soft tissue (Vannah and Childress, 1996; Tonuk and Silver-Thorn, 2003). Vannah and Childress (1996) used a materially and geometrically nonlinear, large-strain finite element formulation

to study the bulk muscular tissues at the calf area. The global and local geometries of the deformation were modelled in detail by incorporating more concentrated meshes at the various indentation locations into the global leg model constructed from the CT scanning. They reported that the stiffness of bulk tissues increased from the initial value of 2 kPa without load to 600 kPa at a load level of 7 N using an indenter with a diameter of 8 mm. It was also demonstrated in their study that a linear and homogeneous material model was not enough to explain the experimental difference of stiffness tested at various testing ports. Nonlinear tissue parameters calculated by using the James-Green-Simpson strain energy formulation were also computed for two testing ports. Tonuk and Silver-Thorn (2003) recently used a finite element analysis plus the James-Green-Simpson strain energy density function to simulate the indentation response of bulk residual limb tissues at various sites and indentation rates. It was demonstrated that the three material coefficients they adopted could represent the nonlinear elastic properties of the test tissues. But the results showed that the three material coefficients varied a lot within subjects, test locations and different indentation rates, thus making it difficult to be extrapolated to other sites, individuals or testing made at different times. Direct comparison between their coefficients and our parameters appeared to be difficult due to the different models and test regions used in the studies. Other forms of elasticity as indicated by more complex stress-strain relationships could also be taken into account in the QLV model in future studies.

2.3.2 Viscous Properties

The time constant of the irradiated tissue extracted in this study (1.34 s), which characterizes the length of time required to relax to an equilibrium state after step indentation, was generally smaller than that of the lower limb tissues measured previously (4.69 s) (Zheng and Mak, 1999a). The difference of the time constant across the different patient subgroups was not established in the current study. But when compared with that of the 8 normal subjects (0.24 s), the time constant of the patients was significantly larger. The larger time constant indicated that the patient needed a longer time for the soft tissue to recover after it was indented, which was a general phenomenon consistently observed by the investigators during the indentation tests on patients. Another QLV parameter α, referring to the level of relaxation at the equilibrium state, was 0.421 for the patients. Although there was a slight increase of

α with respect to the increase of fibrotic severity, the increase had not reached a statistical significance. Compared with the limb soft tissues studied previously (α = 0.132), the neck soft tissue of patients relaxed to an equilibrium state with a significantly smaller force response after a step indentation. But compared with the results of the 8 normal subjects (α = 0.526), it relaxed to slightly larger force equilibrium after the step indentation. An indentation study on the residual limb soft tissue by Silver-Thorn (1999) showed that the stress relaxation in 2 minutes could be 50.6% (i.e. approximate equivalent to α = 0.506 in our model) at a mean step indentation ratio of 23% in one patient with amputation. Their value was very similar to that of our normal subjects. It should be noted that the viscous parameters reported by Silver-Thorn (1999) were extracted directly from the force-relaxation tests but the current parameter was extracted indirectly from the QLV analysis of the cyclic indentation test. The difference of the viscous parameters for the neck soft tissues tested in this study and those for the lower limb soft tissues might be induced by factors such as the difference of geometrical structure, muscle distribution and contraction state and the intrinsic differences of tissue viscoelastic elements. In fact, an increase of the time constant with muscle contraction was demonstrated in a previous study (Zheng and Mak, 1999a). Thus the biomechanical and biological reasons for the behaviors of viscous parameters deserve to be further investigated. In the present study, the difference in mean age between the patients and control groups may introduce the bias in the comparison. To address this problem, a correlation analysis was made between the age of the patients in the range of 29 to 75 and the viscous parameters, but no significant correlation was found between the time constant and age (P = 0.45) and between the parameter α and age (P = 0.48). Even though no significant correlation was demonstrated between the clinical palpation score and the viscous parameters, extracting them was important to improve the reliability for the measurement of the elastic properties, with which the effect of viscosity could be reduced in the extraction of the effective Young's modulus.

2.3.3 Current Findings and Limitations of the QLV Analysis

The mechanical properties of irradiated tissue may be affected not only by the tissue fibrosis, but also by other late side effects of radiotherapy such as the lymphedema, fat necrosis and vascular injury (Padhani et al., 2002; O'Sullivan and Levin, 2003), though these problems are uncommon in the irradiated neck. These

factors that may potentially have effects on the mechanical properties of the irradiated tissues should be taken into account in further investigations. The significant correlation of E_0 and E_1 with the clinical parameters of hand palpation score and the neck rotation range, and with the effective Young's modulus, suggests that the QLV parameters are addressing clinically meaningful properties of the irradiated tissues. In the present study, both the elastic and viscous parameters of the patients were demonstrated to be different from those of the normal subjects. The main components involved in determining the mechanical properties of the connective tissues are the type, quantity, structure and cross-linking of collagen fibers (Culav et al., 1999; Ottani et al., 2001). It is proposed that the consistent changes of the nonlinear elasticity parameters are due to the consistent change of syntheses and deposition levels of extracellular matrix components such as the collagen and noncollagenous proteins in the skin and subcutaneous tissues (Wegrowski et al., 1988; Remy et al., 1991; O'Sullivan and Levin, 2003). While for the viscous properties in soft tissues, they are tended to be more affected by factors such as the water concentration around the essentially viscoelastic collagen fibers. The change in concentration and rigidity of the water content of the irradiated neck tissues might develop in a rather random manner instead of being closely in parallel with other changes of components in fibrosis, so a consistent change of viscous parameters among the patient subgroups could not be established. Exact reasons on these changes need further investigations. Based on the current findings, the QLV parameters represented a significant advance over the effective Young's modulus in the characterization of radiation-induced fibrosis and could be potentially introduced as a quantitative tool to assess the tissue fibrosis. Further use includes incorporating the measurement of the viscoelastic properties into the assessment and monitoring of the fibrotic process in clinical trials.

With regard to the model used in this study, several issues are worth addressing and paying attention to. The linear indentation solution of Hayes et al. (1972) assumed the tissue layer to be homogeneous, isotropic, linear elastic and the layer was bonded to an infinite rigid foundation. In our case, the difference of geometry and structure of the neck tissues was not considered individually in the simulation. The friction of the contact areas between the indenter and the skin surface could be neglected due to the use of the ultrasound coupling gel, but significant curvature of the neck surface, the nonuniform tissue thickness and the finite dimension of the bony substrate under the

indentation region might affect the accuracy of the extracted material properties. To select a smaller indenter might reduce these effects. However, too small an indenter might pick up variations due to epidermal surface characteristics and tend to cause discomfort to the subjects more easily due to the relatively large stress caused by the small contact area. Numerical and experimental study should be conducted to examine the effect of surface curvature of soft tissue and the underlying bone as well as dimension of the indenter. A recent study using the finite element analysis demonstrated that the bony curvature could significantly affect the extracted Young's modulus, particularly when the tissue thickness and the bony curvature were comparable to the indenter diameter (Lu and Zheng, 2004). The tissue thickness was much larger than the indentor diameter in this study so that the effects of the bone curvature can be avoided. As for the assumed elastic layer for the soft tissue, a constant Poisson's ratio of 0.45 was assigned, assuming the nearly incompressible characteristics under a fast enough loading rate. Mak et al. (1994) had demonstrated that selecting different Poisson's ratios did affect the effective Young's modulus. For some specific cases, such as confined configuration, the Poisson's ratio might greatly affect the tissue biomechanics (Vannah and Childress, 1993). Although a constant Poisson's ratio in the range of 0.30 to 0.50 was commonly used by investigators to study the elastic properties of soft tissues (Mak et al., 1994; Vannah and Childress, 1996; Zheng and Mak, 1999b; Klaesner et al., 2001), cautions are needed to be taken when this assumption was applied on different body sites, in patients with different degrees of pathological conditions, in elderly and young subjects, because the Poisson's ratio might vary from individual to individual and from site to site. To measure the Poisson's ratio *in vivo* is an important and challenging issue for researchers in the mechanical test of biological tissues. In addition, the viscoelastic properties of biological soft tissues are strain rate dependent. In our test, the indentation rate was generally controlled in a small range so that it was assumed that the effect was neglectable and it would not play an important role in determining the extracted parameters. Based on a previous study on the limb soft tissue and the repeatability test of this study, the results obtained by the current method were demonstrated to be reproducible and were unique using the defined protocol (Zheng and Mak, 1999a). The QLV analysis was capable of simulating the whole indentation response and could be used to extract viscoelastic properties from the indentation tests. However, the current QLV model is a phenomenological model that

approximates the macro-mechanical viscoelastic behavior and ignores the microstructure and mechanisms that contribute to the observed viscoelasticity. The phenomenological nature of this method may result in the same parameters extracted but neglecting the difference of physiology and pathology that make such an observation. Investigation using other models such as the biphasic model (Mak et al., 1987) is deserved to extract intrinsic material properties from the indentation test for the irradiated soft tissue in future studies.

Receiver operating characteristic (ROC) analysis is an effective way, independent on prevalence of the disease to describe the accuracy of a new method for disease diagnosis (Obuchowski, 2003). It defines the relationship between sensitivity and false positive rate when different cut points are used. While in this study, ROC analysis was lacking because hand palpation was far away from a gold standard for grading fibrosis. In a test where gold standard did not exist, such an analysis was not too meaningful as test sensitivity and specificity were not accurately estimated. We think in future study a tissue biopsy examination may make such a ROC analysis possible and more meaningful.

3. Ultrasonic Properties of Fibrotic Skin Tissues

3.1 Methodology

3.1.1 High Frequency Ultrasonic Imaging System

The system used for data collection was a high frequency (20-MHz) commercial ultrasonic imaging system developed for skin assessment (Ultrasons Technologies, Tours, France) (Figure 3-1). The system can provide dual imaging modes: the RF-signal based image in addition to the conventional B-mode (envelope signal-based). The system is mainly comprised of an ultrasonic unit, a personal computer with installed data acquisition cards and software to collect data and display images, and a cylindrical probe inside which there is a focused monoelement transducer. Two pneumatic switches are used in this system to switch between RF/echo modes and to start/freeze the image collection. A gain adjustor is available during the data collection to modify the amplitude as well as the brightness of the image in order to achieve a proper signal-to-noise ratio (SNR). The controllable gain is in the range of 0 to 40 dB and this value is easy to be read out from the saved file. The transducer works in the way of linear mechanical scanning and has a nominal center frequency of 20 MHz. According to the measurement of the reflection signals from a planar steel plate immersed in water, the center frequency was 15 MHz with a -3 dB frequency bandwidth approximately between 10 and 25 MHz. The transducer is sealed through a cover at the tip of the probe and immersed in the coupling medium when it works. Distilled water was used as the coupling medium in all the current experiments. When the probe is manually held and put on the testing site, the ultrasound is transmitted from the surface of transducer through the coupling medium, then a membrane as thin as 15 μm of the cover, then the coupling medium again and finally into the tested tissue. According to the measure of the signals reflected from a plane plate in the water, it was found that the beam of the transducer focuses at the distance of approximately 2 mm from the surface of the tip of the probe. The dimension of the contact area is 11×19 mm^2 and the effective width of the image in the direction parallel to skin surface is approximately 6 mm, providing a set of 256 RF signal lines with 1024 points in each line sampling at 100 MHz in the RF mode. The maximum penetration depth provided by the 1024 points of each line is equivalent to 8 mm in the soft tissue assuming a constant speed of sound of 1.58 mm/μs in the skin (Serup, 1992). The lateral resolution of transducer is about 0.2 mm, thus producing

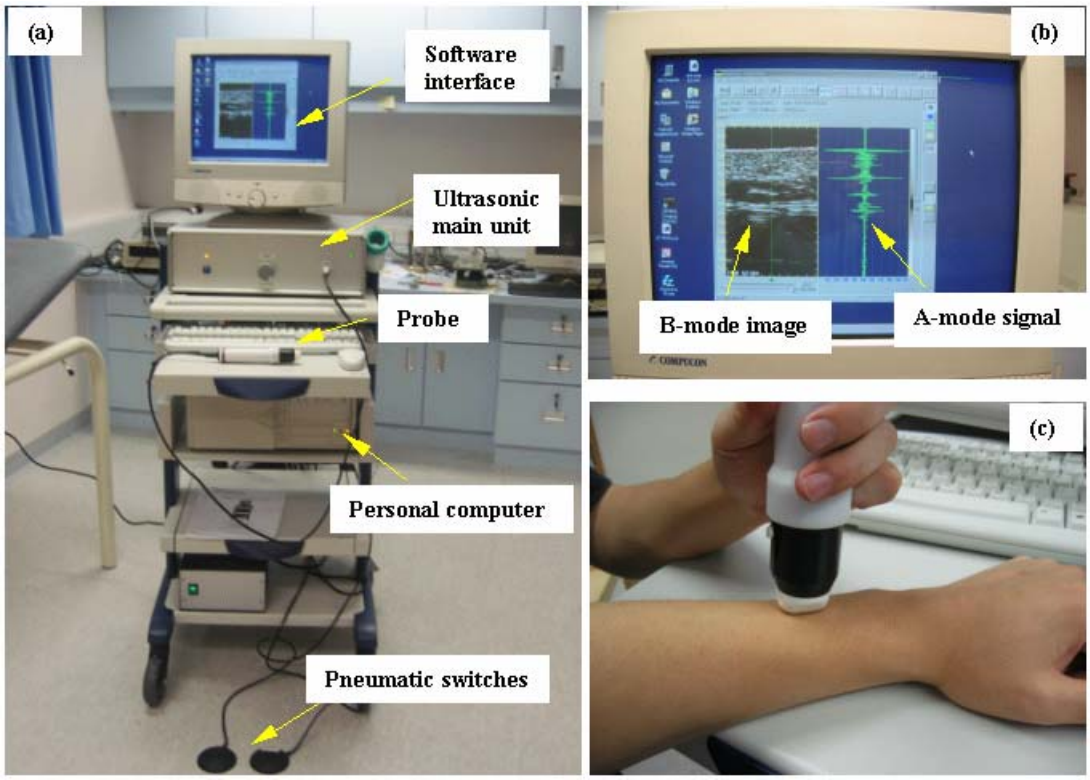

Figure 3-1. (a) The high frequency (20 MHz) ultrasonic imaging system; (b) The zoomed software interface; (c) Operation of the ultrasonic probe.

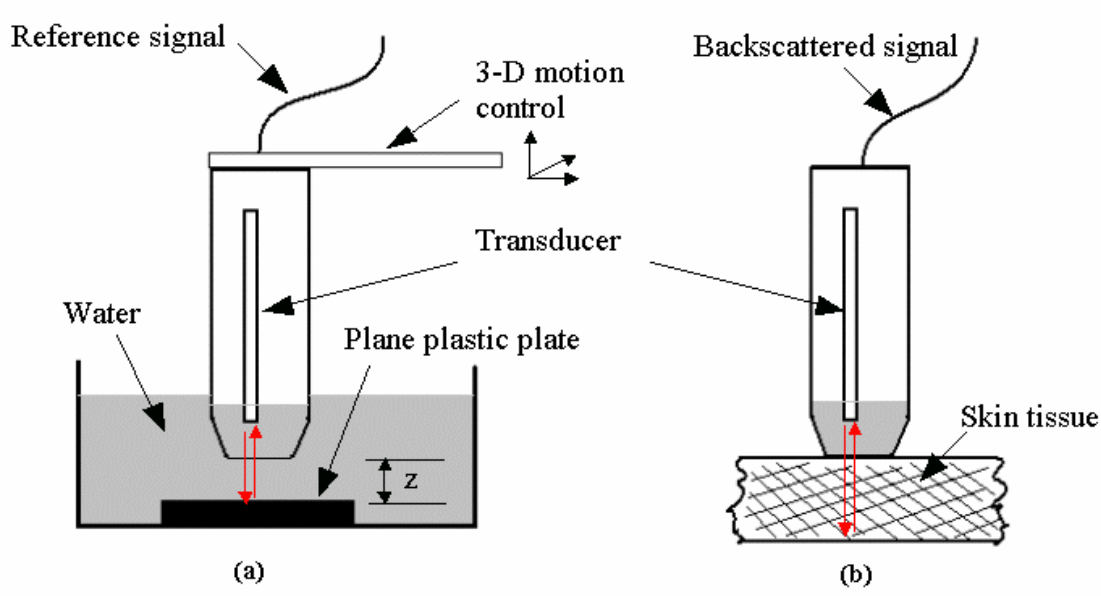

Figure 3-2. A schematic of the substitution method. (a) Reference signals reflected from a plane plastic plate; (b) Signals backscattered from the skin tissue.

approximately 28 independent lines for each set of 256 lines per image. The average correlation coefficient for two adjacent lines among the 28 lines in the studied region

of interest (from 0.3 to 1.3 mm) tested in the forearm skin of 5 normal subjects was estimated to be 0.24 ± 0.04, indicating a large independence between the selected lines.

3.1.2 Extraction of Parameters

3.1.2.1 Ultrasonic Properties

In this study, skin was generally assumed to be composed of hypodermis and dermis with a total thickness of generally larger than 1.3 mm in the tested region (forearm and neck), while the thickness of the epidermis was in the range of less than 100 μm (Hopewell, 1990). The speed of sound was assumed to be constantly 1.58 mm/μs throughout the whole skin (Serup, 1992). One of the advantages to use ultrasound for detecting skin problems is that the ultrasonic wave is not or just minimally influenced by the intermediate medium between skin and transducer. Spectral analysis of the RF signals was employed using a custom-designed Matlab program. To extract the ultrasonic propagation parameters, spatially independent RF signals from the region of interest (ROI) were averaged firstly in order to reduce the variation of the signal spectra. A substitution method and a multi-narrowband algorithm were introduced in the current analysis with the setup shown in Figure 3-2. Reference signals from a planar steel plate at different axial distances z were collected prior to the data collection in real tissues in order to compensate the system-dependent effects (Fournier et al., 2003). It was found even with the minimum gain, the peak of the reflection signal from the plane steel plate was saturated using the data acquisition card in this system. Hence, the steel plate was changed to be a plastic one (Fournier et al., 2001). The spectra of the signals reflected from these two plates obtained using another broadband ultrasonic system with a transducer centered at 20-MHz and with a larger linearly adjustable range of gain demonstrated that there was no spectral difference in the range of 10 to 25 MHz but just a constant mean difference of 7.99 dB (Figure 3-3). As for the spectral analysis, the ultrasonic signal backscattered from the ROI was gated by a Hamming window, then Fourier transformed using FFT (512 points) and squared to get the power spectral density. The signals reflected from the plastic plate were also processed in a similar way and used as reference spectra. The power spectra obtained from the tissues were spatially

averaged in the lateral range of 6 mm using the 28 independent lines of each image. The calibrated power spectra could be written as:

$$\langle S_{cal}(f,z)\rangle = \frac{\langle S_T(f,z)\rangle}{S_R(f,z)} \tag{2-8}$$

where z is the axial distance of the window center, $S(f,z)$ is the power spectrum at z. The subscript "*cal*" stands for the calibrated power spectrum, "T" for from "*Tissue*", "R" for from "*Reference*", and "$\langle ... \rangle$" for the spatial averaging over the 28 independent lines for each image.

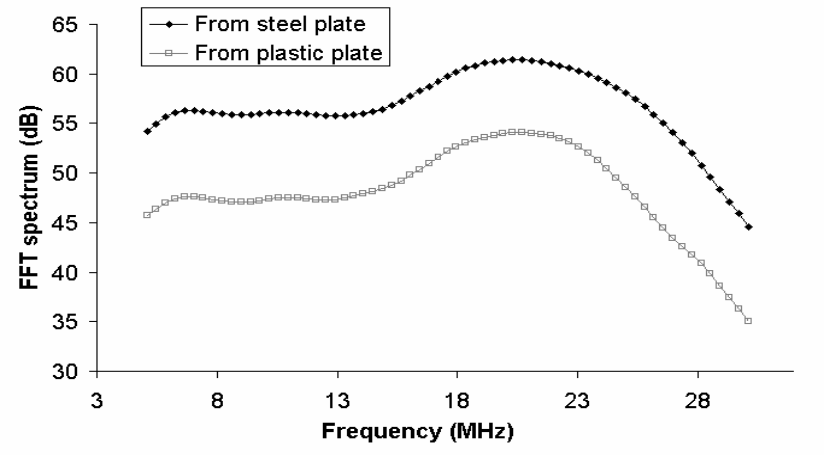

Figure 3-3. Spectral comparison of pulsed signals reflected by the steel and platic plates. The difference of the two spectra is 7.99 ± 0.56 dB computed at 40 frequencies in the range of 10 to 25 MHz.

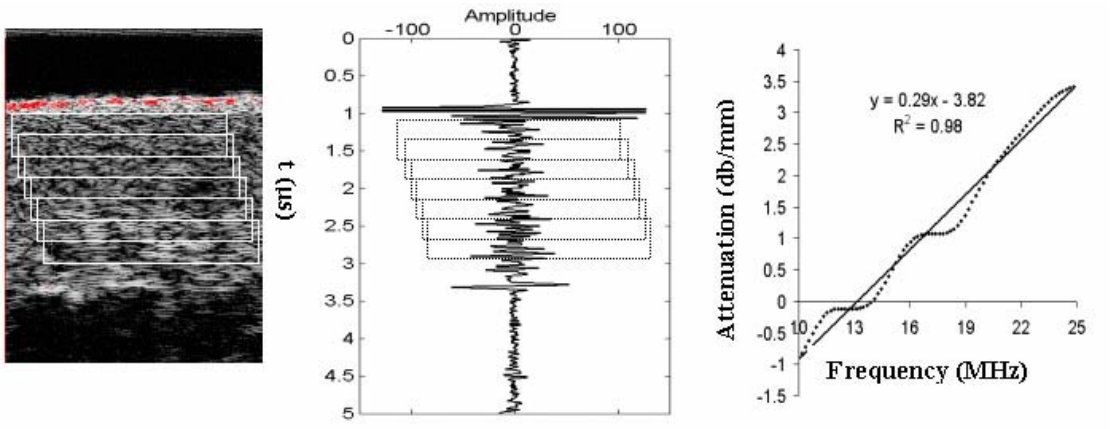

(a) **(b)** **(c)**

Figure 3-4. (a) A skin image showing the six regions of interest where the attenuation is calculated; (b) Six ROIs for a single RF-line; (c) Typical frequency-dependent attenuation coefficients obtained from a skin tissue *in vivo*.

Attenuation slope (β) and integrated attenuation (IA).

Attenuation coefficient was calculated by a regression of the power spectra with respect to the corresponding penetration depth in the skin. The Hamming window was set to be in a length of 50 points (0.395 mm). An ROI ranging approximately from 40 points (0.316 mm) to 165 points (1.304 mm) in a step of 25 points (i.e. 50% overlapping) after the skin entry echo was defined to extract the ultrasonic parameters (Figure 3-4a). The skin entry echo was automatically detected in the program of calculation based on the sudden change of the signal intensity. Totally six gated short signals were obtained from each line of the image (Figure 3-4b). Each gated signal was zero-padded to 512 points and FFT was then performed to obtain the power spectrum. The power spectra from the 28 independent lines in each image were then averaged before they were divided by the power spectra of reference signals, which were calculated by applying the same window to the signals reflected from a plane steel plate in the water at the same distance as that of ROIs. During the calculation, the signals which were saturated in the ROIs were excluded for averaging in order to avoid adding noise frequency components to the mean power spectra. If we hypothesized that the skin was ultrasonically homogeneous, the compensated power spectrum could be written as:

$$\langle S_{cal}(f,z)\rangle = B(f)\cdot 10^{-2\alpha(f)2z/20} \tag{2-9}$$

where $B(f)$ is the backscatter transfer function, $\alpha(f)$ is the frequency-dependent attenuation in unit of dB/mm and $2z$ is the whole propagation distance from the probe surface. The relationship of the compensated spectrum and the propagation distance could be observed more clearly after logarithmically transforming the two sides of the Eq. (2-9):

$$10\,lg\langle S_{cal}(f,z)\rangle = 10\,log\,B(f) - \alpha(f)\cdot 2z \tag{2-10}$$

Then at each frequency point f_i in the range of 10 to 25 MHz, $\alpha(f_i)$ could be obtained by regressing the logarithmic compensated spectra over the axial distance z. If a linear frequency dependence of attenuation coefficients was assumed in the skin tissues (Raju and Srinivasan, 2001), it could be expressed as:

$$\alpha(f) = \beta \cdot f + \alpha_0 \tag{2-11}$$

where β is the attenuation slope in the unit of dB/mm/MHz (Figure 3-4c). Figure 3-5 shows the whole processing. For the integrated attenuation (IA, unit: dB/mm), it was defined here as:

$$\mathrm{IA} = \frac{1}{f_2 - f_1}\int_{f_1}^{f_2} \alpha(f)df \tag{2-12}$$

where $f_1 = 10\mathrm{MHz}$ and $f_2 = 25\,\mathrm{MHz}$ are the upper and lower limits of the frequency range used, respectively. The integration was performed by an approximation of the trapezoid area. In this study, β and IA were used as quantitative ultrasonic parameters to test the feasibility of ultrasonic characterization of tissue fibrosis.

Backscatter parameters (IBS).

In this case, the window length was chosen to be 125 points (approximately 0.988 mm), from 40 points to 165 points where the attenuation was calculated. The power spectra of the data of the independent lines of each image in this region were averaged by applying the 125-point Hamming window before they were divided by the spectra of the reflection signals from the plane steel plate using gate window of the same length. The systemically corrected spectra were then logarithmically transformed to obtain the backscatter spectra $B(f)$ in this region. The integrated backscatter (IBS, unit: dB) was defined similarly to that of IA in the frequency range of 10 to 25 MHz as follows:

$$\mathrm{IBS} = \frac{1}{f_2 - f_1}\int_{f_1}^{f_2} B(f)df \tag{2-13}$$

where $f_1 = 10\mathrm{MHz}$ and $f_2 = 25\,\mathrm{MHz}$ are the upper and lower limits of the frequency range used, respectively. It should be noted that the backscatter in this region was not corrected by the attenuation of the epidermis and potentially partial dermis outside the ROI and the difference of reflection of skin-water interface was neglected. This parameter was used to describe the characteristics of average level of backscatter for the skin studied.

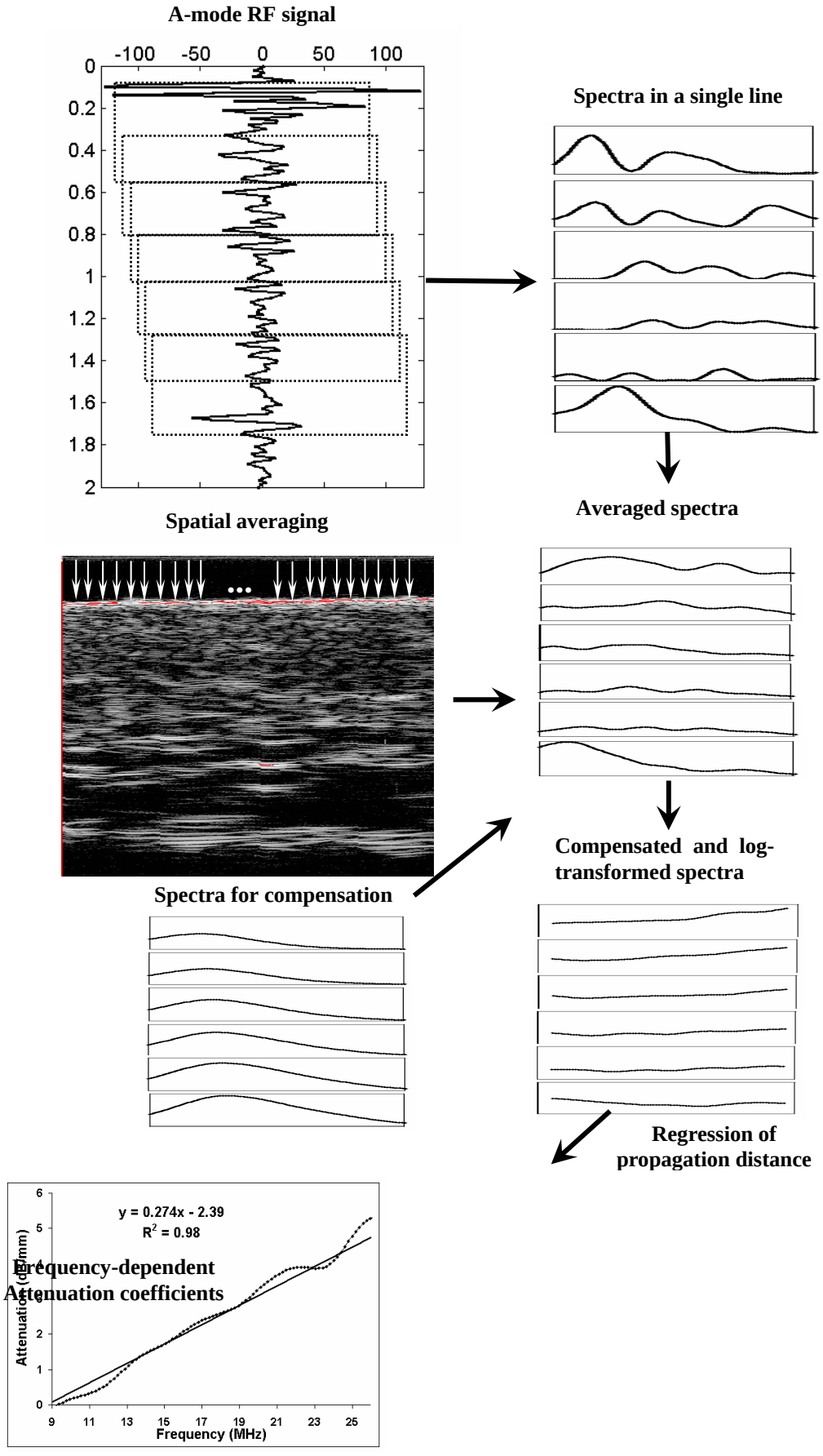

Figure 3-5. Processing of the ultrasonic signals to calculate the attenuation coefficients.

3.1.2.2 Statistical Parameters of Signal Envelope

The envelope of the signal was obtained by taking the Hilbert transform of the original RF signal (Komiyama et al., 2000). If the original temporal signal was assumed to be $s(t)$ and the Hilbert transform of this signal was $\hat{s}(t)$, the envelope $s_e(t)$ was computed as the magnitude of the analytical signal $s_a(t) = s(t) + j\hat{s}(t)$:

$$s_e(t) = \sqrt{s^2(t) + \hat{s}^2(t)} \tag{2-14}$$

Concerning the discrete form of data stored in the computer, the corresponding form of Eq. (2-14) was written as:

$$s_e(n) = \sqrt{s^2(n) + \hat{s}^2(n)} \tag{2-15}$$

where $s(n)$ and $\hat{s}(n)$ are the sequences of original and its Hilbert transformed signal, and $s_e(n)$ is the envelope of the original RF signal (Figure 3-6).

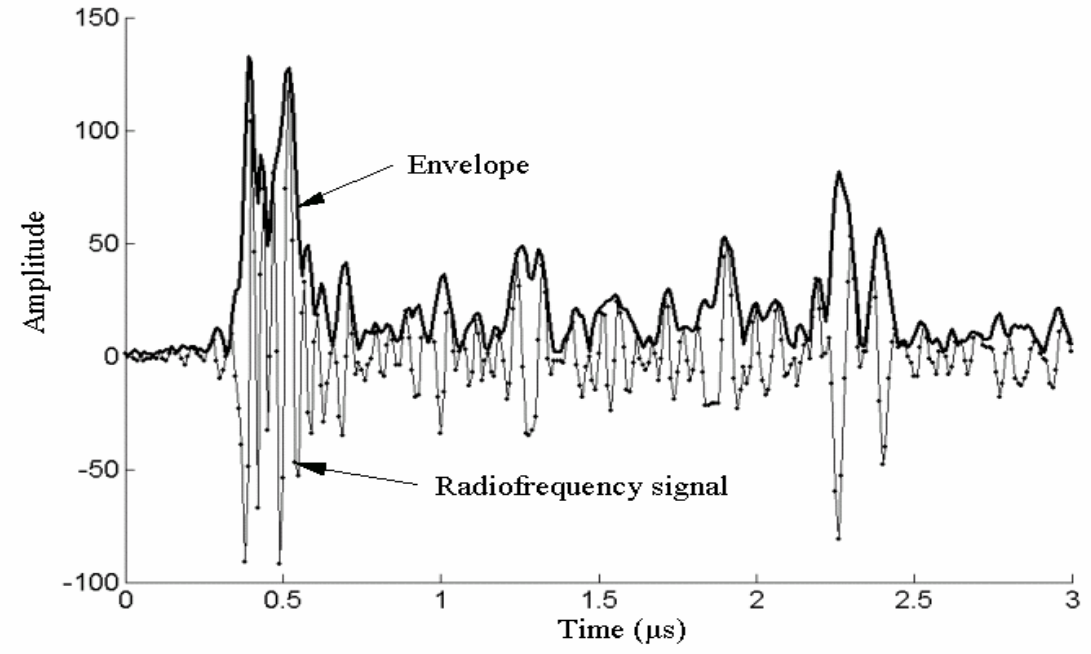

Figure 3-6. Envelope-detected radiofrequency signal backscattered from *in vivo* skin.

The envelope of the backscattered signal was related to the ultrasonic scatterers inside the tested skin. In order to characterize the ultrasonic scatterers, the statistical

information of the envelope was helpful. An important requirement for analyzing the points of the envelope was that they should be independent. Ultrasonic pulse had a finite duration and any scattering from one scatterer might influence the scattering by other scatterers in this limited duration. Therefore it was not necessary to count all the points in one pulse duration (Komiyama et al., 2000). A simple way to tackle this problem is to sample the envelope with an interval of this duration. With respect to our system, the pulse duration was measured to be approximately 18 points (0.18 μs). Thus for each line in the analyzed ROI for the extraction of the ultrasonic properties, 7 points were chosen and totally 196 points were included for computation from the 28 independent lines of each image for every testing site.

After sampling, statistical parameters could be computed from the envelope signal. In this study, three parameters including mean-to-standard deviation ratio (MSR), skewness and kurtosis (not corrected by 3) were calculated for each envelope (Komiyama et al., 2000). The MSR was very useful to characterize the dimension and distribution of the scatterer especially in view of differentiating from the famous Rayleigh scattering. In Rayleigh scattering where a large number of smaller scatterers are randomly distributed in a resolution cell, MSR is theoretically verified to be 1.91 as a constant. The skewness and kurtosis were called as “shape factors”, with the skewness referring to the asymmetry of the shape relative to the mean and the kurtosis referring to the distribution of the peak and tails of the data in relation to the Gaussian distribution with the same variance. These parameters of each testing site were averaged for all the tests on this site. All the analyses including the extraction of ultrasonic properties and statistical parameters were performed by custom-designed programs using the scientific computing tool: Matlab (MathWorks, Natick MA, USA).

3.1.2.3 Measurement of Skin thickness

Skin thickness was measured using the B-mode RF images. From the image, a cutis-subcutis interface was often evidently observed and the skin thickness was computed as the distance from the start of the entry echo to this interface. Each RF image had a number of 1024 pixels in the direction of depth of the cross-section, corresponding to 1024 data points sampled by the A/D card in each line. Therefore, numbers of pixels from the entry echo to the cutis-subcutis interface were multiplied by the sampling period (0.01 μs) and the result was regarded as the propagation time.

Again if a constant velocity of 1580 m/s was assumed, the transmission distance in the propagation time through the epidermis and dermis was regarded as the whole thickness of the skin. The measurement was performed at three randomly chosen places in the image and their average was used for the mean thickness of the skin. In addition to the real thickness (in mm), the thickness ratio of the two regions was also calculated. It was found that the thickness of the neck was generally larger than the forearm, so the employed neck/forearm thickness ratio was generally larger than one.

3.1.3 Subjects and *In-Vivo* Test

3.1.3.1 Normal Subjects and Reliability Test

The *in vivo* study was first conducted on a group of 20 normal subjects (age: 27 ± 3, range: 23-32; sex: 14 males, 6 females) under room temperature (approximately 25 °C). Two pairs of standardized positions, one pair on the palmar and dorsal sides of the distal forearm and the other pair, on both sides of the neck were chosen for testing. For the palmar forearm, the site was selected to be 3 cm away from the radiocarpal joint and laterally along the media nerve. While for the dorsal side, the site was on the center of the forearm and at 2 cm proximal to the ulnar styloid. In the neck region, the testing site was defined as 5 cm under the mastoid bone, which was also selected in tests on the patients, because this was the region where the patients received radiotherapy. The forearm sites were selected to be the reference sites of the same subject as compared to the neck sites because we tried to compensate some of the effects induced by factors such as ageing and nutrition differences which may be different among individuals. Two sites at the palmar and dorsal sides of the forearm were selected to test whether the current measurement of ultrasonic properties could differentiate the skins at the two sides of the forearm which have sunlight exposure to different extents. Subjects were asked to be seated when the forearm sites were tested and lying on their sides when the neck sites were tested. Before test, testing site was located and marked. The probe was applied onto the skin surface of those sites using a very small pressure in order to avoid significant change of ultrasonic properties induced by a large pressure (Fournier et al., 2001, 2003). The whole test was completed within 20 minutes. During the data collection, the subjects were asked to keep silent and fully relaxed. Three tests were conducted and the results were averaged for the repeated tests at each test site.

In order to test the intra- and inter-rater reliability of this measurement, two investigators were involved in this study. The first was the author of the thesis and the second was the author's colleague who knew well the principles and details of measurement. Tests on 10 normal subjects were conducted by the first investigator on two different occasions in two weeks. For the first time of testing, the test using the same protocol as defined earlier was also carried out by the second investigator in order to estimate the inter-rater reliability of the measurement. The study on the normal and patient subjects was approved by the Research Ethics Committee of the author's affiliated institution and formal consent was obtained from each subject before testing.

To assess the reliability, two types of analysis, i.e., the intraclass correlation coefficient (ICC) (Rankin and Stokes, 1998) and the Bland and Altman tests (Bland and Altman, 1986) were used. Four sites were tested for each subject, and all the values from these four sites were used for computing. Thus the measurement of 10 subjects totally generated totally 40 pairs of data from the intra- and inter-rater test. Therefore, we used $n = 40$ as reference of freedom. The ICC generally represented a proportional contribution of the between-subject variance to the total variance. In our study, ICC(1,3) as explained more clearly by Rankin and Stokes (1998) was used to assess the intra-rater reliability and ICC(3,3) was used for the inter-rater reliability. For the Bland and Altman test, difference versus mean would be plotted, and the mean of difference $\bar{d}$, the standard deviation of the differences and the coefficient of reliability were calculated. The reliability coefficient was the range for 95% of the difference. It was computed to be $2s_w$, where $s_w = \sqrt{\sum_{i=1}^{n} d_i^2 \Big/ n}$, assuming that the mean difference was zero (Bland and Altman, 1986). From the statistical meaning of the reliability coefficient, it is known that a small value indicates a more reliable test. These two types of analysis were broadly used to quantify the reliability of measurement of continuous data.

3.1.3.2 Clinical Trials on Patients after Radiotherapy

Clinical trials were performed in a local hospital (Department of Clinical Oncology, Princess of Wales Hospital). The test was arranged by an experienced doctor in this department. Totally 38 patients (age: 54 ± 11, range: 36-76; sex: 33

males, 5 females) were involved in the study. All the patients were recruited in their clinical follow-up by the oncologists and each had radiotherapy in the neck region due to a history existence of NPC and showed some symptoms of fibrosis in the time of recruitment. The median follow-up time was 3 years, with the range of 1 to 19 years.

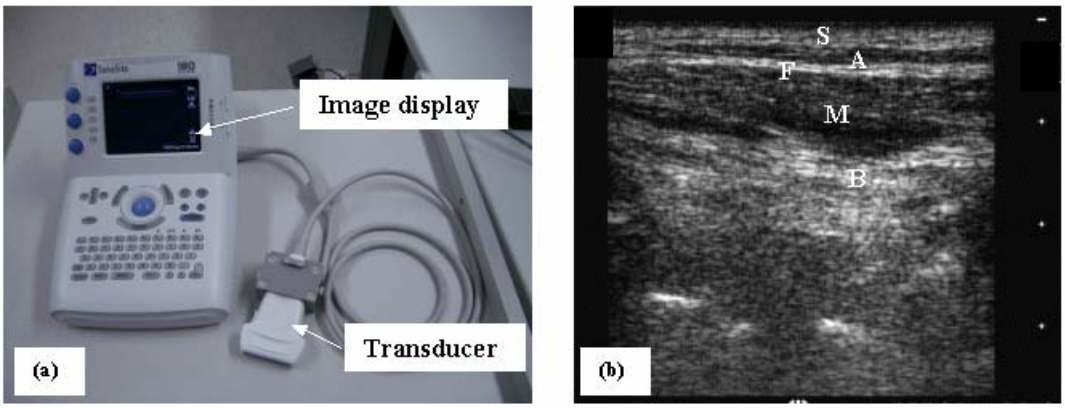

Figure 3-7. (a) The portable B-mode imaging system for soft tissues; (b) A typical image of tissues beneath the skin along the neck in the coronal plane. Typical tissue components include: S: epidermis and dermis (skin); A: subcutaneous fat; F: fascia; M: Muscle, and B: bone. Two points at the right side indicate a distance of 1 cm in the depth direction.

Four types of measurement were employed for the study in the patients. Firstly, the neck rotation range was recorded prior to the measurement of the high frequency ultrasound. The subject was asked to wear a hat with a line as the marker through the center of its visor. A protractor was held over the hat and the rotation was measured in reference to the movement of the linear marker of the hat. During measurement, the shoulder movement and the flexion and extension of the head were tried to be avoided. Secondly, RF signals were collected from the corresponding four sites of the patient using the high frequency ultrasonic imaging system with the same protocol as that used for the normal subjects. Thirdly, in the same neck region as tested for the collection of RF signals, a portable B-scan imaging system (SonoSite Inc., MA, USA) with a 7.5 MHz linear scanning probe was used to collect a cross-section image from tissues beneath the skin along the neck in the coronal plane (Figure 3-7). Typical three images were collected on each side of the neck for each patient using a maximum depth of 3.7 cm. The B-mode images were used to observe whether any evident symptoms existed in these images as indications of the tissue changes associated with different degrees of fibrosis. Finally, each patient also received an indentation test in the neck region and tissue stiffness was obtained from the corresponding sites. An

improved mini-TUPS system comprising of a main box with the ultrasonic unit and a notebook was used for collection of force and ultrasound signals (Figure 3-8). The main box was connected to the notebook using a USB interface. The transient responses of the force and deformation were further processed offline and the parameter of YM was computed using a Matlab program based on the model of Hayes et al. (1972) and with a compensation of effect of large deformation (Zhang et al., 1997). QLV parameters were not calculated from these data because in the current stage YM was almost thought to be as effective as QLV parameters to indicate the degree of fibrosis. For each patient, all the tests were completed in approximately 30 minutes.

Each patient in the follow-up was also given a palpation score from 0 to 3 by a clinical oncologist. More details of the definition of the palpation score were described in the first section of this chapter. According to the palpation score, the patients were further divided into four subgroups, named as from Group 0 to Group 3.

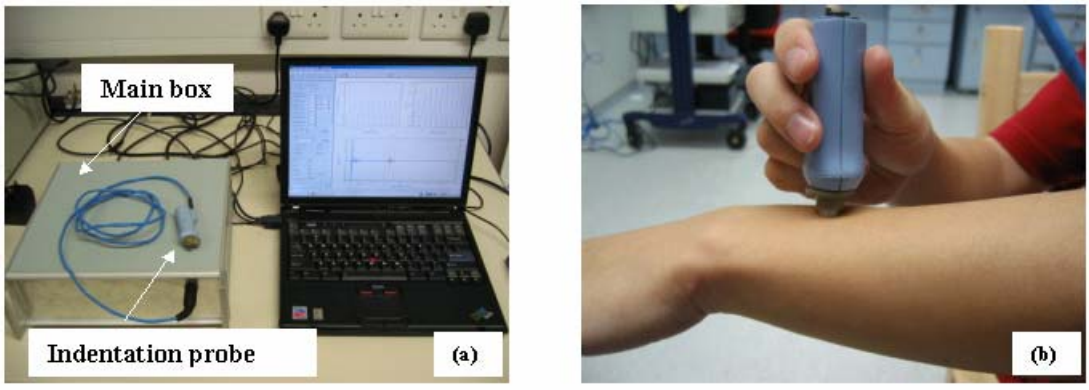

Figure 3-8. (a) The mini-TUPS system; (b) The operation of the probe on the soft tissues.

3.1.4 Data Analysis Methods

Data were expressed as mean ± standard deviation (SD). For normal subjects, comparison of various parameters was made using the paired *t*-test between two sites in the forearm and neck regions of the same subject. If no significant difference was found in the two regions, the parameters from the two testing sites were pooled and averaged values were given to the skins of the forearm and neck. The results of the two forearm sites of the patients were also compared with each other using the paired *t*-test. If no significant difference was found between them, averaged values from the two sites would be used as reference values. Otherwise, the palmar site was regarded as the reference site, because it was hypothesized that the skin on this side was less

varied among individuals by processes such as photoaging, which was a chronic process induced by sunlight and especially evident for the elderly. The results of the patients were compared with those of normal subjects in two ways: 1) direct comparison and 2) comparison based on the individual difference of the neck region to the reference point. The difference of various parameters between skins in the neck region and at the reference point of the same subject was denoted by a subscript "*d*" such as β_d, IA_d and IBS_d for the ultrasonic properties. Normal subjects and patients were compared using the unpaired *t*-test to show whether there was any significant change induced by the skin fibrosis. The correlations among three ultrasonic parameters were also calculated for both the normal skins and the skins after radiotherapy. Patients among different subgroups were further compared using one-way *ANOVA* in order to find whether various parameters were different across patients with different degrees of fibrosis. Post-hoc *t*-test was used if *ANOVA* showed significant difference. The parameters were also correlated to the age, the clinical symptoms, i.e., neck rotation range and the quantitative parameters of fibrosis, i.e. the effective YM. The comparison between genders was not considered because the severely biased population of the male and female subjects. All the statistical analyses were conducted by using either the commercial software SPSS (SPSS Inc., Chicago, IL, USA) or the Matlab (MathWorks, Natick MA, USA). $P < 0.05$ was used to indicate a significant difference.

3.2 Results

3.2.1 Ultrasonic Properties

3.2.1.1 Measurement Reliability

Table 3-1 shows the results of ICC for the analysis of the intra- and inter-rater reliability. The 95% confidence interval (CI) of the ICC is also presented. It was found that the inter-rater measurement carried out by the two investigators at the same occasion was generally higher than the intra-rater measurement. All the ICCs, except the intra-rater reliability for the IBS, were larger than 0.80, which is generally regarded to indicate a highly reliable measurement (Lobnig et al., 2003).

Table 3-1 The intra-rater and inter-rater reliability of the measurement of ultrasonic properties

US parameters	*Intra-rater measurement*		*Inter-rater measurement*	
	ICC(1,3)	*95% CI*	*ICC(3,3)*	*95% CI*
β (dB/mm/MHz)	*0.87*	*0.75 - 0.93*	*0.83*	*0.67 - 0.91*
IA (dB/mm)	*0.86*	*0.73 - 0.92*	*0.91*	*0.83 - 0.95*
IBS (dB)	*0.56*	*0.17 - 0.76*	*0.97*	*0.94 - 0.98*

Table 3-2 The results of the Bland and Altman test for intra-rater reliability

US parameters	$\bar{d}$	$SD_{\bar{d}}$	*95% limits of agreement*	$SE_{\bar{d}}$	*95% CI of* $\bar{d}$	*Reliability coefficient*
β (dB/mm/MHz)	*-0.001*	*0.031*	*-0.063 -> 0.060*	*0.005*	*-0.011 -> 0.009*	*0.063*
IA (dB/mm)	*0.52*	*1.10*	*-1.63 -> 2.67*	*0.17*	*0.17 -> 0.87*	*2.43*
IBS (dB)	*-2.40*	*1.82*	*-5.97 -> 1.17*	*0.29*	*-2.98 -> -1.82*	*6.07*

$\bar{d}$ is the mean difference; $SD_{\bar{d}}$ of $\bar{d}$ is the standard deviation of the mean difference calculated from the real data; $SE_{\bar{d}}$ of $\bar{d}$ is the standard error of the difference; 95% CI for $\bar{d}$ is the 95% confidence interval for the mean difference, which is defined as $\bar{d} \pm t_{n-1} \cdot SE_{\bar{d}}$. The reliability coefficient is calculated to be $2\sqrt{\sum_i d_i^2 / n}$, where n = 40 is the number of overall measurements (Rankin and Stokes, 1998).

Table 3-3 The results of the Bland and Altman test for inter-rater reliability

US parameters	$\bar{d}$	$SD_{\bar{d}}$	*95% limits of agreement*	$SE_{\bar{d}}$	*95% CI of* $\bar{d}$	*Reliability Coefficient*
β (dB/mm/MHz)	*0.004*	*0.035*	*-0.065 -> 0.073*	*0.006*	*-0.007 -> 0.015*	*0.071*
IA (dB/mm)	*-0.11*	*0.91*	*-1.89 -> 1.68*	*0.14*	*-0.40 -> 0.18*	*1.84*
IBS (dB)	*0.15*	*1.02*	*-1.84 -> 2.15*	*0.16*	*-0.17 -> 0.48*	*2.06*

Note the definitions of the notations are similar to that in Table 3-2 except that all the calculation here were with respect to the inter-rater measurement.

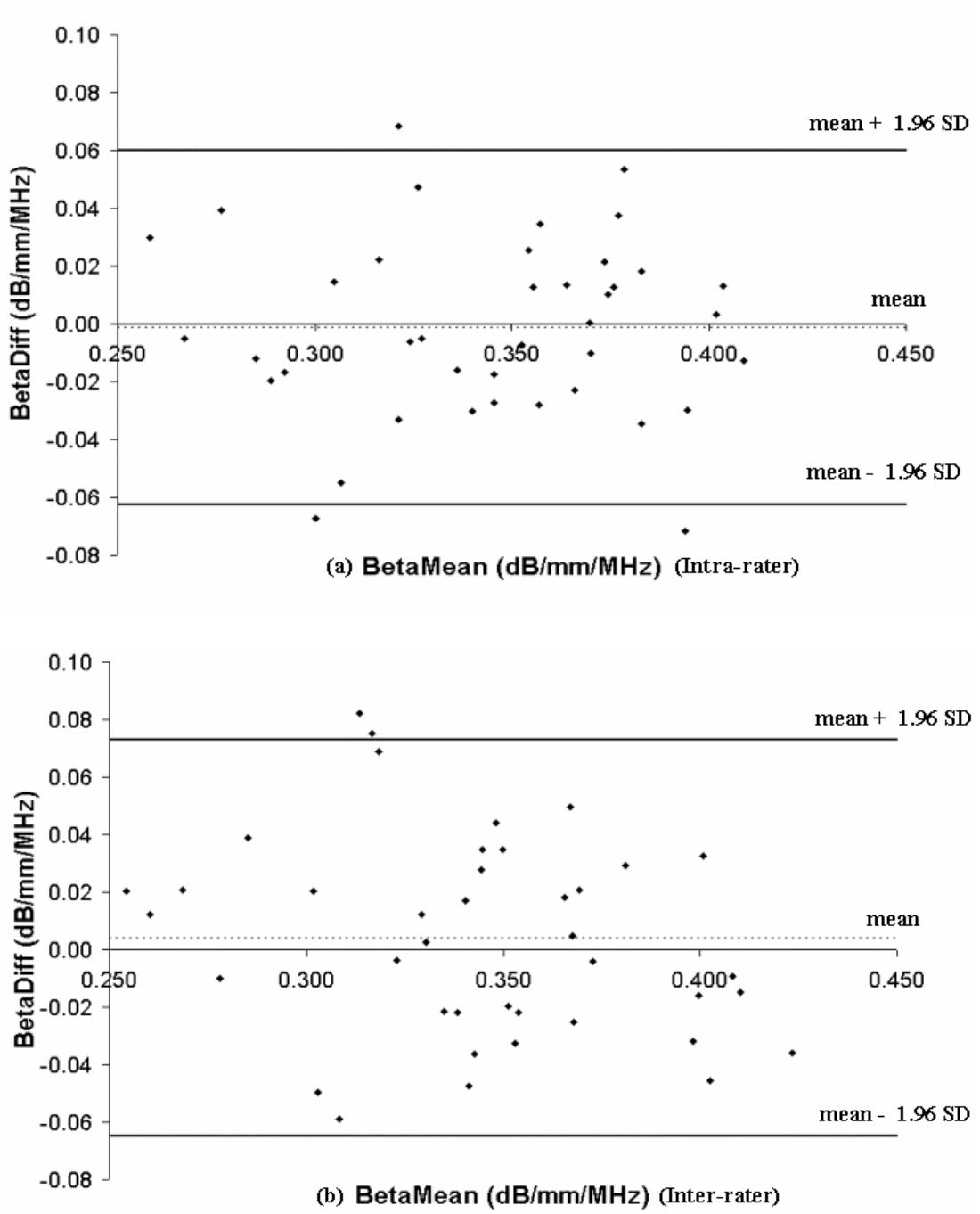

Figure 3-9. Distribution plot from the Bland and Altman test showing the mean values of the attenuation slope (Beta) against the differences of the (a) intra-rater and (b) inter-rater measurements. BetaMean is the intra-rater mean of the two measurements by the first investigator or the inter-rater mean of the measurements by the two investigators. BetaDiff is the intra-rater difference of the first and second measurements by the same investigator or the difference of the measurements taken by the first and second investigators. The dashed line indicates the mean of the difference, and the two real lines indicate the range of $mean \pm 1.96\, SD_{diff}$ **, showing where 95% of the difference is observed.**

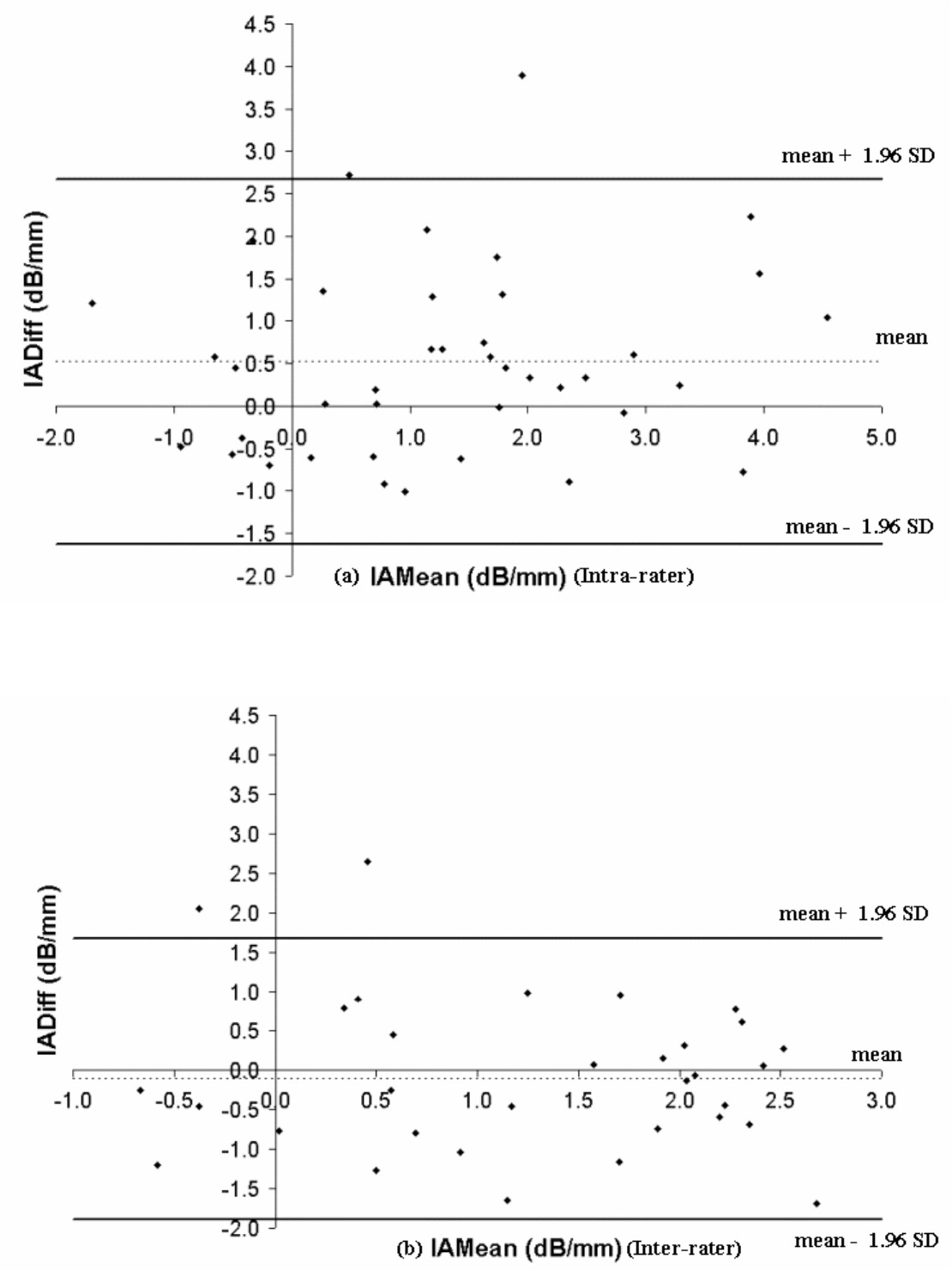

Figure 3-10. Distribution plot from the Bland and Altman test showing the mean values of the integrated attenuation (IA) against the differences of the (a) intra-rater and (b) inter-rater measurements. IAMean, IADiff, and the real and dotted lines are similarly defined as in Figure 3-5.

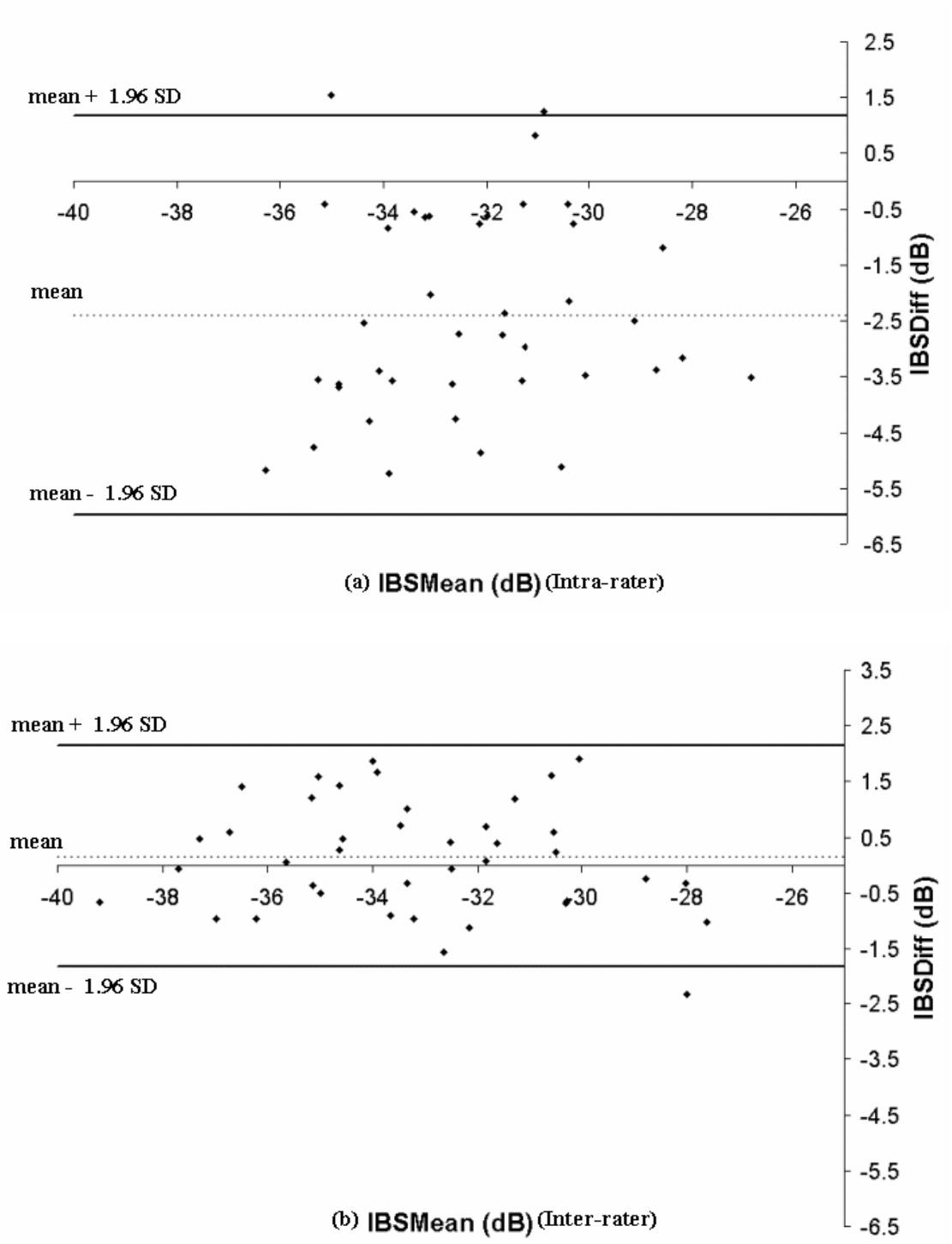

Figure 3-11. Distribution plot from the Bland and Altman test showing the mean values of the integrated backscatter (IBS) against the differences of the (a) intra-rater and (b) inter-rater measurements. IBSMean, IBSDiff, and the real and dotted lines are similarly defined as in Figure 3-5.

Figure 3-9, Figure 3-10 and Figure 3-11 show the distribution plot of the difference of the three parameters for intra- and inter-rater measurement (Bland and Altman, 1986). From these figures, no evident correlation of the difference with the mean of the parameters was observed for the three parameters. Table 3-2 and Table 3-3 show the quantitative results of the Bland and Altman test (Rankin and Stokes, 1998) for the intra- and inter-rater reliability of the measurement. A difference of 0.52 dB/mm for IA and –2.40 dB for IBS were found for the intra-rater measurement. Zero did not lie in the 95% CI of $\bar{d}$, indicating a bias between two measurements for these two parameters. Again, the coefficients of reliability were generally smaller for the inter-rater measurement than for the intra-rater measurement except the small difference between that of β. In average, the inter-rater reliability appeared to be higher than the intra-rater reliability, which could be reasonably explained concerning the design of the current study. This is explained in detail in the Discussion section.

3.2.1.2 Results of Normal and Irradiated skins

Figure 3-12 shows the typical images obtained from both sites of the forearm and the neck region of a normal subject. It was observed that the neck skin in the dermal region appeared generally less echogenic compared with the forearm skin. Therefore, in some cases the gain was adjusted when the testing site was changed from the forearm to the neck in order to achieve a higher SNR. Figure 3-13 shows the ultrasonic properties measured on the normal subjects. Table 3-4 shows the results of the comparison among the sites tested in the normal subjects. For all the parameters, no significant difference between two sites of the forearm and between two sites of the neck was found ($P > 0.05$). Because the difference of the palmar and dorsal sides of the forearm was found in patients (Table 3-4), the palmar side was chosen as reference of the forearm in the subsequent analyses. There was generally a linear relationship between the attenuation coefficient and the frequency, with a correlation coefficient larger than 0.90, showing that the linear relationship was sufficient to describe the frequency-dependent characteristics of the attenuation coefficients (Figure 3-4c). The attenuation slope (β) among the normal subjects was 0.378 ± 0.039 dB/mm/MHz and 0.328 ± 0.029 dB/mm/MHz in the palmar forearm skin and in the neck region, respectively. It was found that β was significantly smaller for the

skin in the neck region than in the forearm region ($P < 0.001$). IA for the normal subjects was 0.64 ± 1.40 dB/mm and 1.93 ± 1.81 dB/mm in the palmar forearm and in the neck, respectively. Negative IA was occasionally obtained especially for the forearm skin. It was found that IA was significantly larger in the neck region than in the palmar forearm region ($P = 0.001$). IBS for the normal subjects was –31.57 ± 2.94 dB and –33.55 ± 2.98 dB in the palmar forearm and in the neck, respectively. It was found that IBS was significantly smaller in the neck region than in the forearm region ($P < 0.001$), which was also indicated by a weak dermal echogenicity observed in the RF mode images.

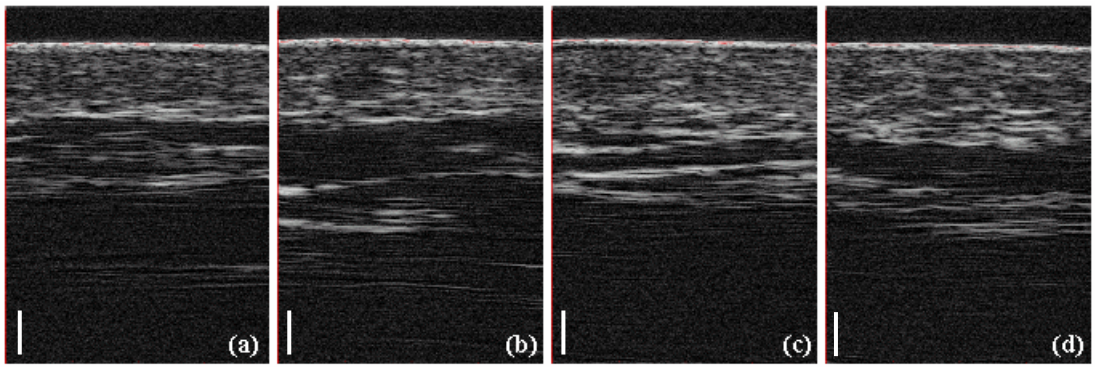

Figure 3-12. Ultrasonic images of the skin collected from a normal in sites: (a) palmar forearm; (b) dorsal forearm; (c) left neck; and (d) right neck. Note the different patterns of echogenicity observed in the skin and subcutaneous fat. The thickness of the skin measured in these four sites was: (a) 1.76 mm (b) 1.96 mm (c) 2.35 mm (d) 2.20 mm. The white bar indicates a scale of 1 mm.

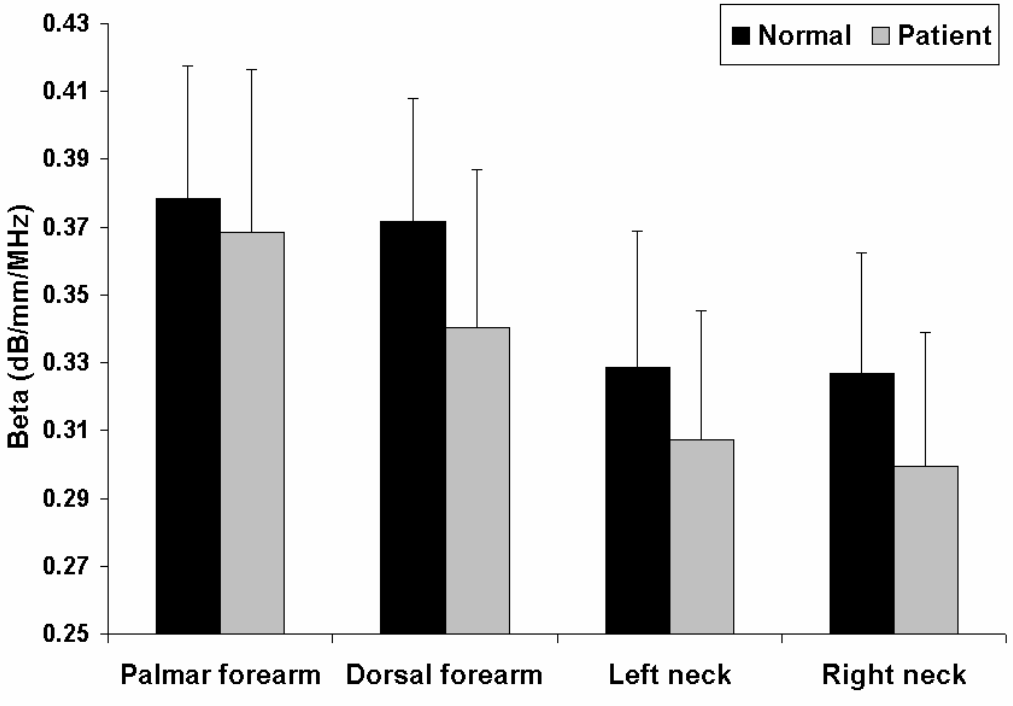

(a)

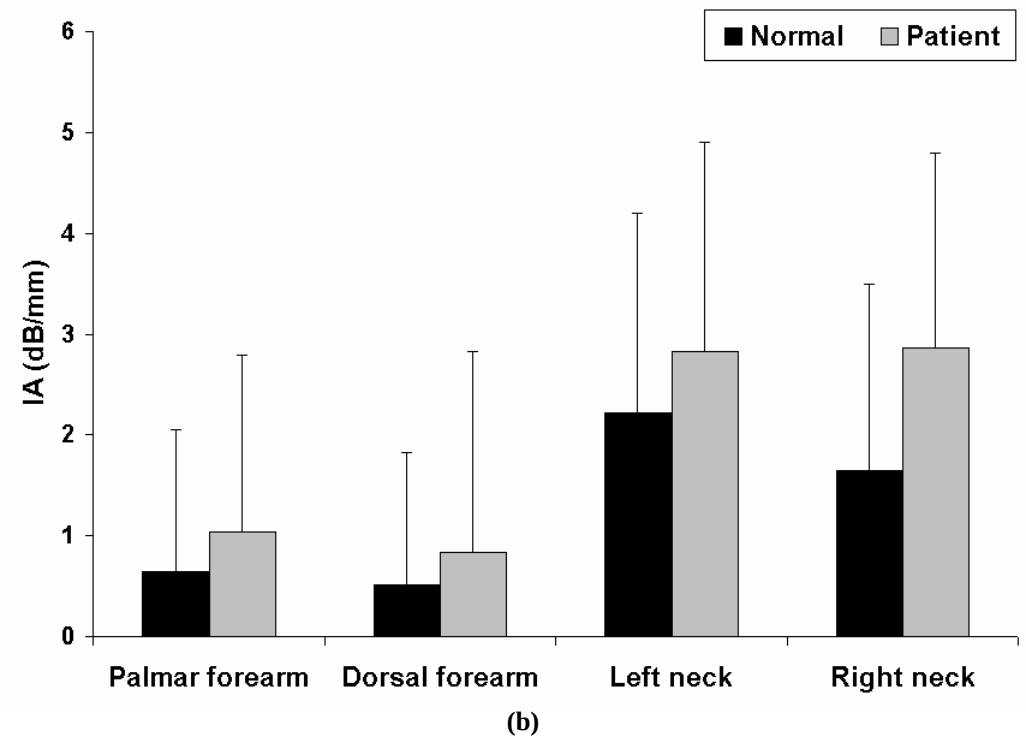

(b)

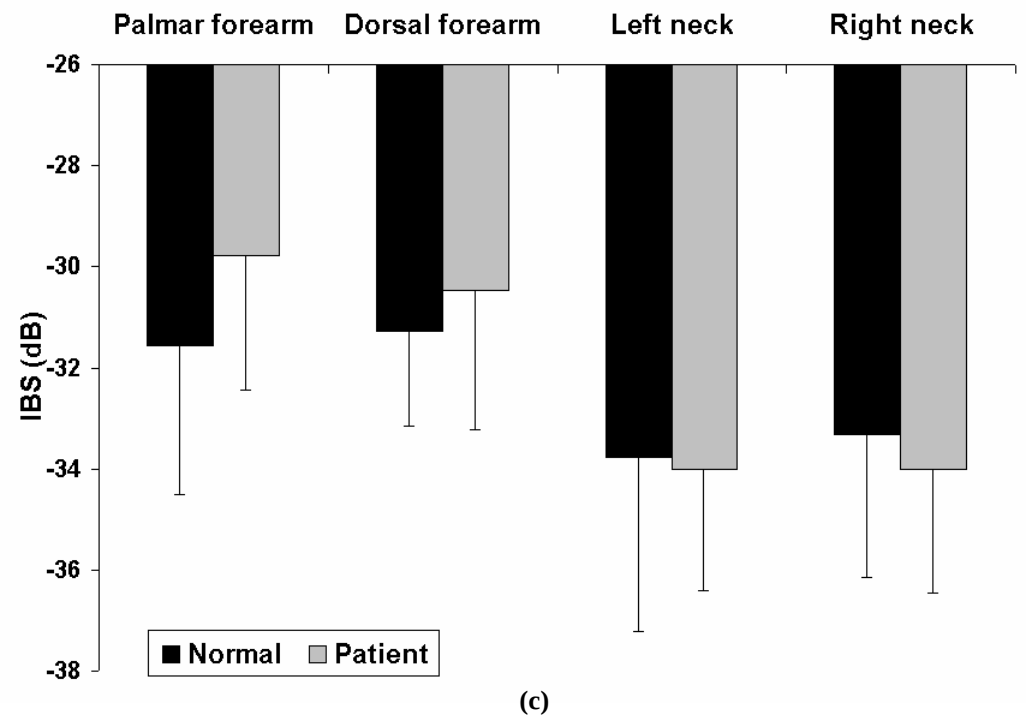

(c)

Figure 3-13. Ultrasonic properties measured in the skins of the normal subjects and patients. (a) Attenuation slope (Beta); (b) Integrated attenuation (IA); (c) Integrated backscatter (IBS).

Table 3-4 The *P* values of the comparison of ultrasonic parameters for the various testing sites

Paired t-test	β			*IA*			*IBS*		
	P arm & D arm	***L neck & R neck***	***P arm & neck***	***P arm & D arm***	***L neck & R neck***	***P arm & neck***	***P arm & D arm***	***L neck & R neck***	***P arm & neck***
Normal	*0.28*	*0.44*	*<0.001**	*0.37*	*0.07*	*0.001**	*0.26*	*0.17*	*<0.001**
Patient	*0.001**	*0.09*	*<0.001**	*0.20*	*0.41*	*<0.001**	*0.006**	*0.49*	*<0.001**
Unpaired t-test	***P arm***		***neck***	***P arm***		***neck***	***P arm***		***neck***
Normal & patient	*0.21*		*0.005**	*0.20*		*0.04**	*0.01**		*0.26*
Unpaired t-test for difference	***neck – P arm***			***neck – P arm***			***neck – P arm***		
Normal & patient	*0.17*			*0.18*			*0.001**		

Note the abbreviations presented in the table are defined as follows: P arm – palmar forearm, D arm – dorsal forearm, L – left, R – right. "*" stands for a significant difference at the significant level of P < 0.05.

Figure 3-14 shows the typical images obtained from both sites of the forearm and the neck region of a patient. Figure 3-13 also shows the results of measurement in 38 patients after radiotherapy. Table 3-4 also shows the comparison among the sites tested in patients. For the two sites in the forearm region, significant difference was found for β (P = 0.001) and IBS (P = 0.006). While for the two sites on the left and right side of the neck, no significant difference was found (P > 0.05). Therefore, the ultrasonic parameters were averaged in the neck region and compared to the palmar side due to the reason as explained in the Methodology section. The comparison between the normal subjects and patients was also restricted to the palmar site of the forearm and the two neck sites. It was found that β and IBS were significantly smaller, and IA was significantly larger in the neck than in the palmar forearm (P < 0.001). Overall speaking, the anatomic patterns of the ultrasonic parameters in terms of the forearm and neck skins ($\beta_{neck} < \beta_{forearm}$, $\mathrm{IA}_{neck} > \mathrm{IA}_{forearm}$ and $\mathrm{IBS}_{neck} < \mathrm{IBS}_{forearm}$) were similar in the normal subjects and patients, even though the neck skin of the patients was potentially affected by the radiotherapy.

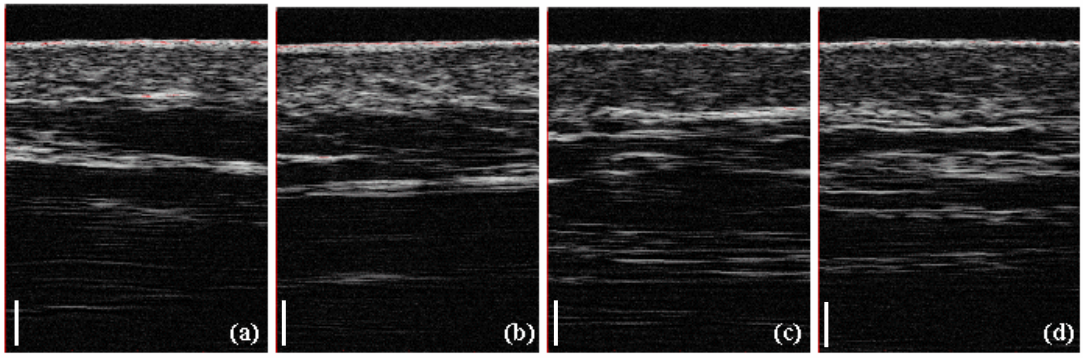

Figure 3-14. Ultrasonic images of the skin of a patient in sites: (a) palmar forearm; (b) dorsal forearm; (c) left neck; and (d) right neck. The thickness of the skin measured in these four sites was: (a) 1.39 mm (b) 1.58 mm (c) 1.88 mm (d) 2.05 mm. The white bar indicates a scale of 1 mm.

However, there was a change of ultrasonic parameters both in the neck region affected by irradiation and in the forearm region unaffected in patients compared with the normal subjects. Table 3-4 also shows the comparison of the ultrasonic parameters between the normal subjects and the patients in terms of the direct and relative comparison. For the direct comparison between the normal subjects and the patients, the results were as follow. In the normal and the fibrotic neck skins, β ranged from 0.270 to 0.388 dB/mm/MHz with a mean of 0.328 ± 0.029 dB/mm/MHz, and from 0.217 to 0.365 dB/mm/MHz with a mean of 0.303 ± 0.034 dB/mm/MHz, respectively. A significant decrease of β was found in the neck (P = 0.005), but not in the forearm (P > 0.05). IA ranged from –1.01 to 5.03 dB/mm with a mean of 1.93 ± 1.81 dB/mm and from -1.53 to 7.66 dB/mm with a mean of 2.85 ± 1.93 dB/mm in the normal and fibrotic neck skins, respectively. A significant increase of IA was found in the neck region of the patients (P = 0.04), but not in the forearm (P > 0.05) compared with that of the normal subjects. IBS ranged from –37.60 to –28.53 dB with a mean of –33.55 ± 2.98 dB, and from –38.13 to –27.75 with a mean of –34.00 ± 2.29 dB in the normal and fibrotic neck skins, respectively. A significant difference was found not in the neck with radiotherapy (P > 0.05), but in the unaffected forearm (P = 0.01). Among the three parameters of the patients, the changes had the same trend for β (increase) and IA (decrease) in the two regions (forearm and neck), but the change of IBS was opposite (increase in the forearm and decrease in the neck). For the comparison of the difference between the neck and the palmar side, the trends were a little different. The mean of β_d was –0.051 ± 0.050 dB/mm/MHz in the normal subjects and –0.065 ± 0.056 dB/mm/MHz in the patients, but no significant

difference was found ($P > 0.05$). The mean of IA_d was 1.29 ± 2.15 dB/mm in the normal subjects and 1.81 ± 2.10 dB/mm in the patients, and still no significant difference was found ($P > 0.05$). The mean of IBS_d was –1.98 ± 2.13 dB and –4.23 ± 2.59 dB in the normal subjects and in the patients, respectively, with the latter one significantly less than the former one ($P = 0.001$).

Significant Pearson correlations among the three ultrasonic parameters were found ($P < 0.01$, Figure 3-15) in both the non-fibrotic forearm skins of normal subjects and patients and the fibrotic neck skin of patients. The strongest correlation was found between IA and IBS in the neck skin of the patients ($r^2 = 0.45$).

3.2.1.3 Correlations with Other Measurements

The demographic information of the four patient subgroups was shown in Table 3-5. Therefore the four subgroups appeared to be age-matched and their results could be compared directly (Figure 3-16). β increased from the score 1 to 3 except for score 0. No evident trend was observed for IA. IBS was similar for score 0 and score 1 but increased from score 1 to score 3. However, no significant difference was demonstrated across different subgroups for all the 3 parameters ($P > 0.05$, one-way *ANOVA*).

Table 3-5 The demographic information of the 4 patient subgroups

Group	***Population (n)***	***Age (mean ± SD)***
0	*13*	*54 ± 10*
1	*11*	*54 ± 13*
2	*8*	*57 ± 12*
3	*6*	*53 ± 10*

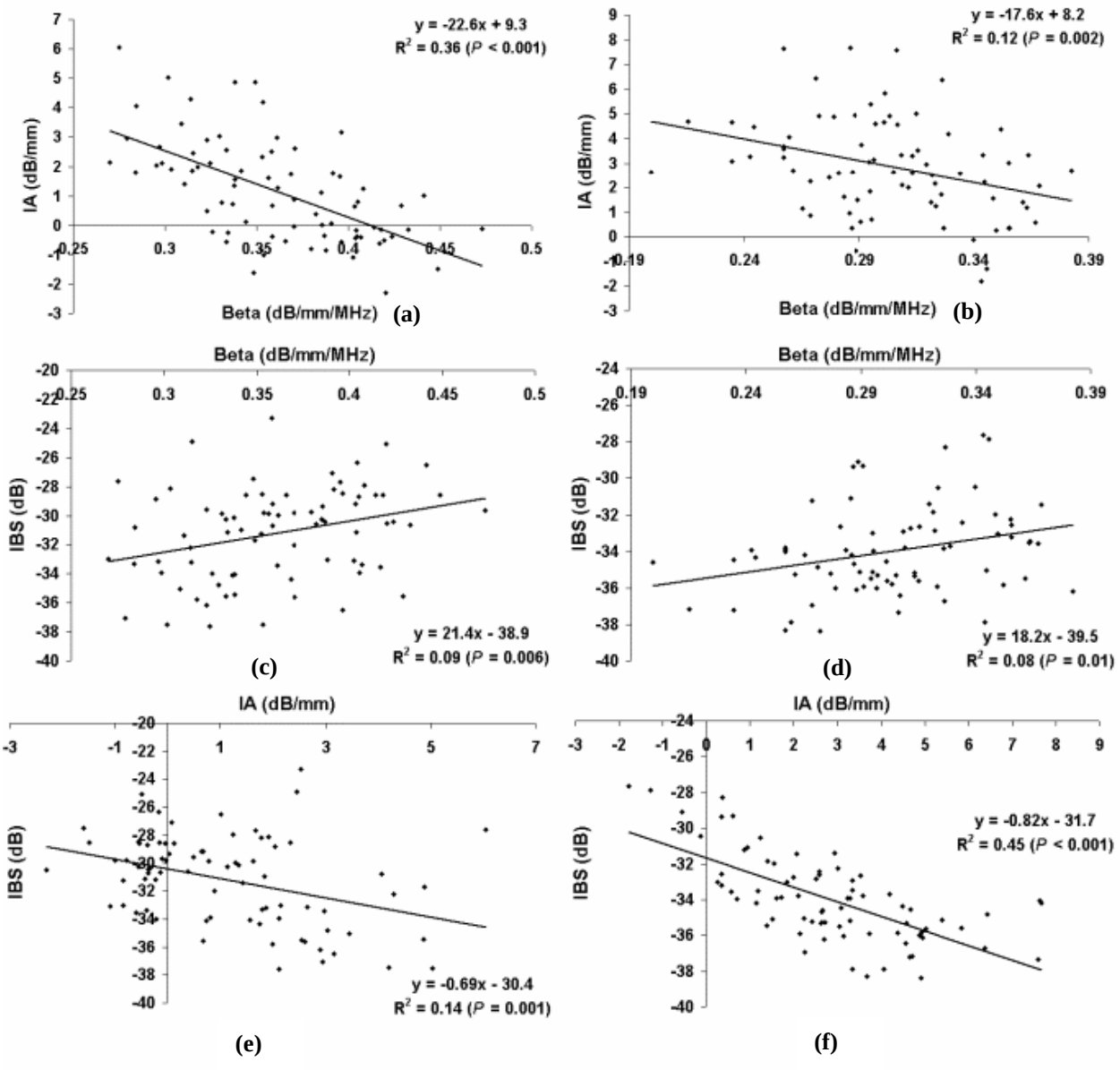

Figure 3-15. The Correlations among the three ultrasonic parameters in (a) (c) (e) the unaffected skins and (b) (d) (f) the affected skins. The unaffected skins include those in the forearm and neck of the normal subjects and the palmar forearm of the patients. The affected skins include those in the neck region of the patients.

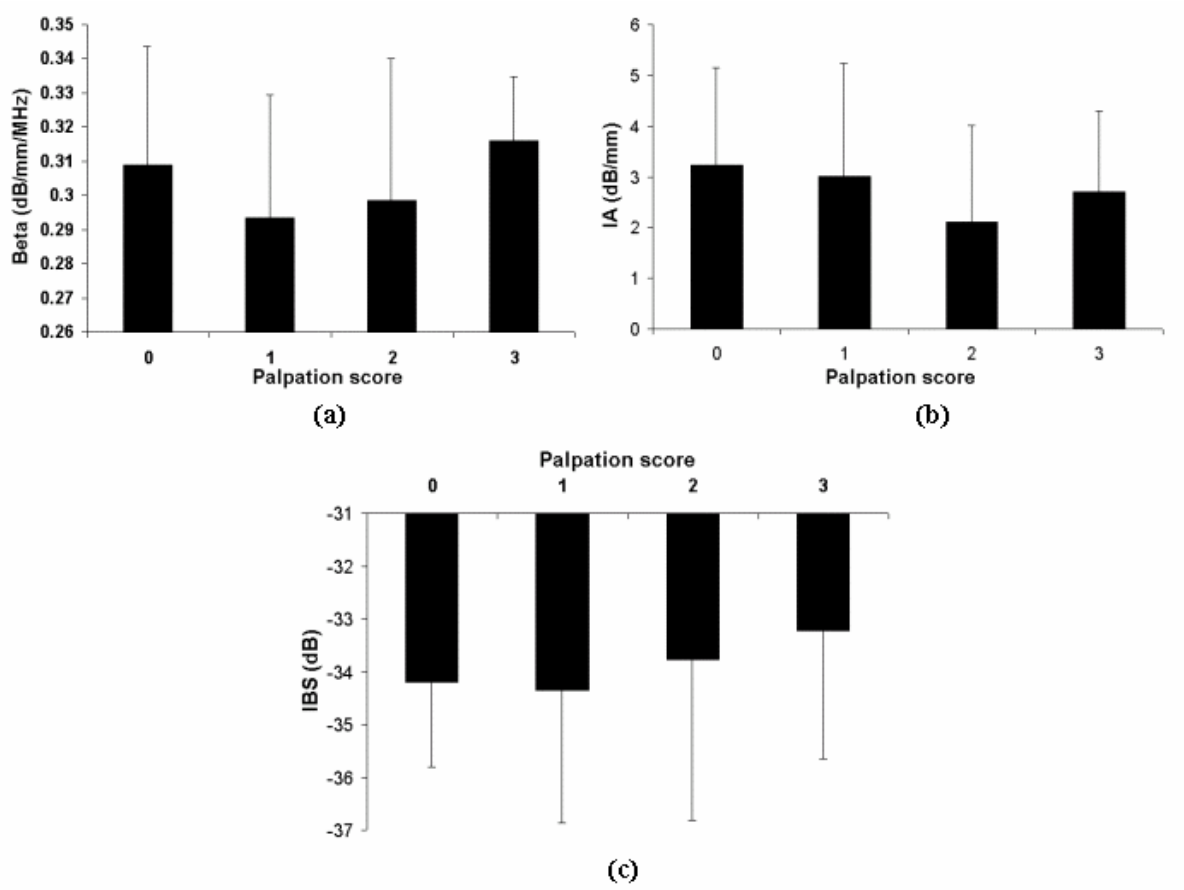

Figure 3-16. Comparison of the ultrasonic parameters across the patient subgroups. (a) The attenuation slope β; (b) The integrated attenuation IA; and (c) The integrated backscatter IBS.

For the measurement of stiffness of the neck soft tissues, 5 out of 38 patients were not completed due to the malfunction of the system during experiment. Therefore totally 33 patients were successfully measured for the stiffness. Figure 3-17 shows the effective YM measured in the four subgroups. Significant difference was found between different subgroups. The results were similar to those reported earlier (Leung et al., 2002). When the measured effective YM was correlated to the three ultrasonic parameters, positive, negative and positive correlations were found for β, IA and IBS, respectively. However, all the correlations did not reach a significance level ($P > 0.05$), indicating that the stiffness was not strongly related to the ultrasonic parameters (Figure 3-18).

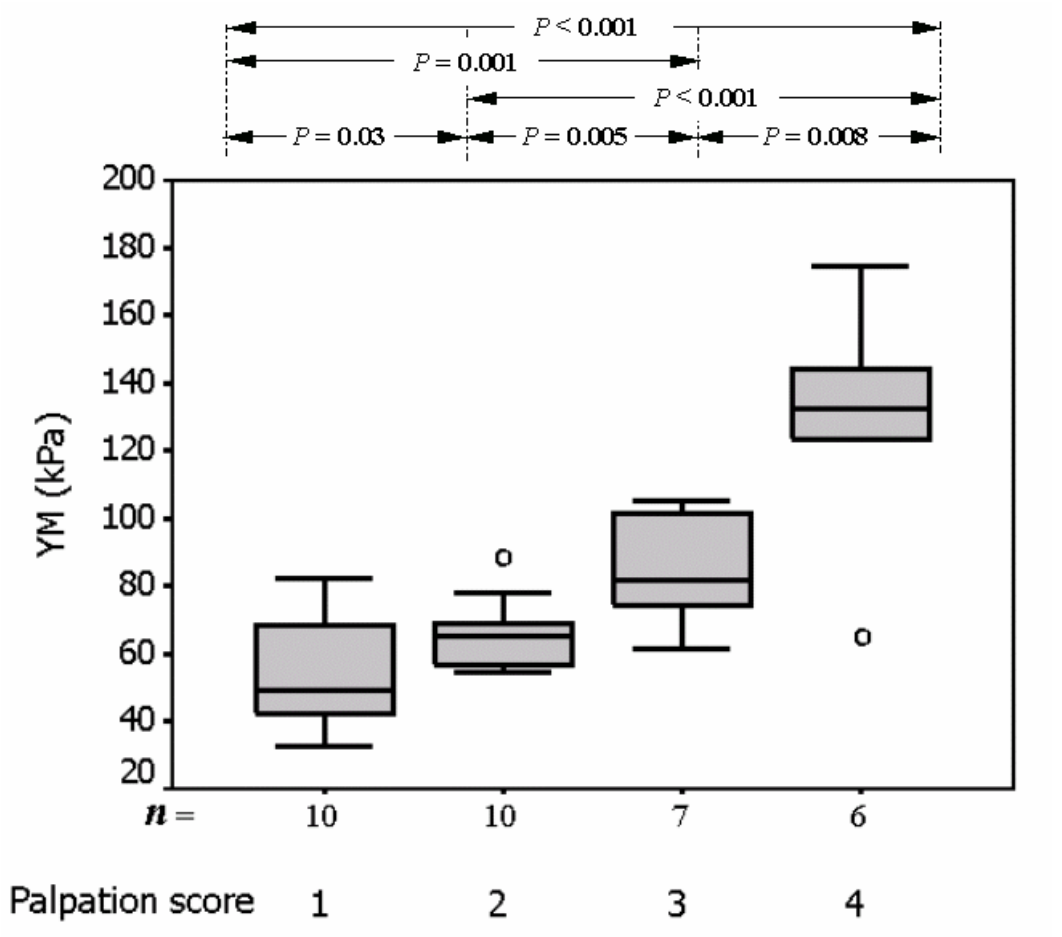

Figure 3-17. The Boxplot of the YM measured in the four patient subgroups. The *P* value of the *t*-test between two subgroups is also indicated. "*n*" indicates the number of patients in each subgroup. For a detailed description of the Boxplot, please refer to Figure 2-5.

The ultrasonic parameters were also correlated to the neck rotation ranges. Each ultrasonic parameter of the left neck side was correlated to the range of the rotation to the right because it was regarded that the right rotation range was related to the fibrotic degree of the left neck, and vice versa. Table 3-6 shows the results of the correlations. No significant correlation was found for all the three cases ($P > 0.05$).

Table 3-6 The correlations of neck rotation range and ultrasonic properties. No significant correlation was found for all the three cases ($P > 0.05$)

Relations	*Rotation and* β	*Rotation and IA*	*Rotation and IBS*
Correlation (r)	*0.03*	*0.10*	*0.01*
P value	*0.78*	*0.41*	*0.92*

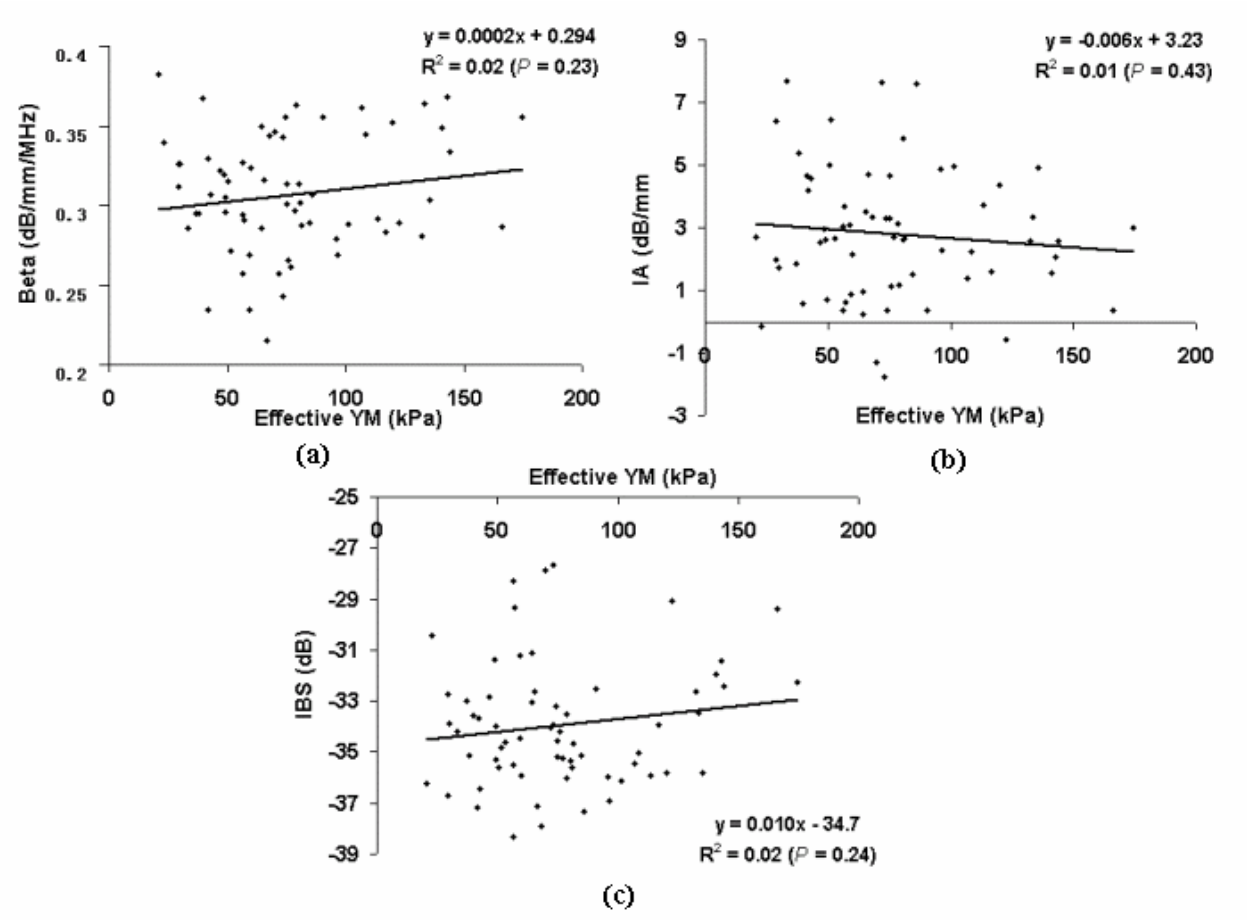

Figure 3-18. Correlations of the effective YM and (a) the attenuation slope β, (b) the integrated attenuation IA and (c) the integrated backscatter IBS. All the P values for the correlations are larger than 0.05.

In order to estimate the effect of aging, the correlation of ultrasonic properties and aging was calculated (Figure 3-19). For the unaffected skins in both normal subjects and patients, only a significantly positive correlation with the age was found for IBS (P = 0.01), but not for β and IA (P > 0.05). For the skins having received radiotherapy, no significant correlation was found for the ultrasonic properties and age (P > 0.05). Multivariable regression of ultrasonic properties in terms of the age and effective YM also did not demonstrate any significant correlation (P = 0.49 for β, P = 0.70 for IA, and P = 0.16 for IBS).

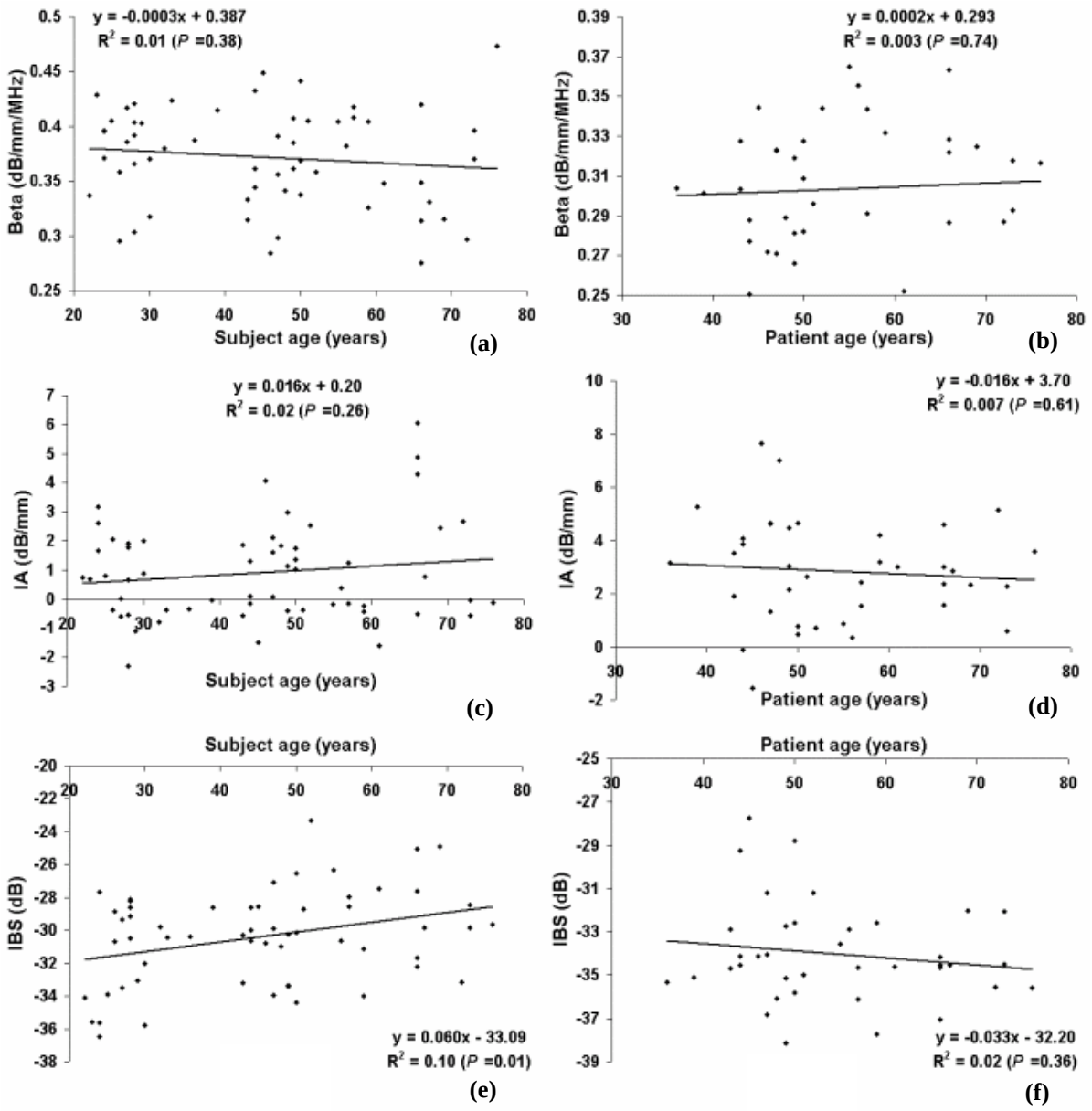

Figure 3-19. Correlation of age and the ultrasonic properties in (a) (c) (e) the unaffected skins of both the normal subjects and the patients and (b) (d) (f) the affected skins of patients. The significant level of the correlation is also shown in the figure.

3.2.1.4 Sonographic Observations

No quantitative analysis was performed for the image collected from the neck soft tissues by the SonoSite imaging system. A general observation was that for patients with a lower degree of fibrosis, the tissue morphology was kept better in the image, while for the patients with a severe degree of fibrosis, the tissue structure appeared to be more inhomogeneous, and the margins between different tissues were blurred (Figure 3-20). Although attempts have been made to grade the liver fibrosis based on

B-mode ultrasound images (Yeh et al., 2003), it appeared not possible for the fibrotic neck tissue till now due to too much heterogeneous structures presented in this region.

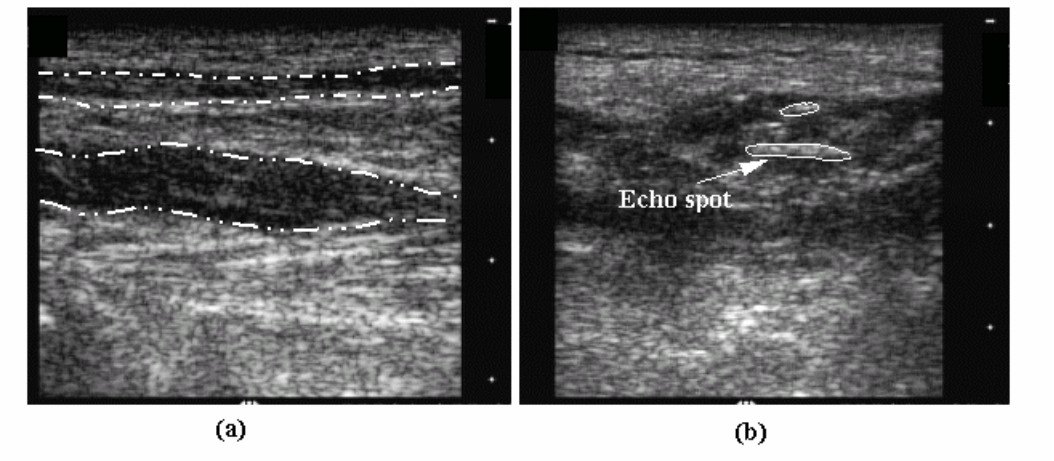

Figure 3-20. Ultrasonic imaging of the tissues under the skin of the neck. (a) Taken from a patient with fibrosis score of 0. The morphology of the tissue was well kept as indicated by the dotted lines; (b) Taken from a patient with fibrosis score of 3. Note that more echo spots were observed, which may be caused by the existence of additional fibrotic plaques. The distance between the two adjacent points at the right side of the image is 1 cm.

3.2.2 Statistical Parameters

Figure 3-21 shows the comparison of the statistical parameters including the MSR, skewness and kurtosis between the normal subjects and patients. Table 3-7 shows the P values for various comparisons. For the normal subjects, a significant difference was found at the two sites of the forearm for all the three parameters ($P < 0.02$), but not on the left and right sides of the neck ($P > 0.05$). Thus the palmar side was used for the comparison between the forearm and the neck. Within the normal subjects, no significant difference was found for the palmar forearm and for the neck region ($P > 0.05$). While in the patients, MSR was significantly smaller ($P = 0.02$), skewness was significantly larger ($P = 0.04$) and kurtosis was significantly larger ($P = 0.05$) in the neck than in the palmar forearm, although the significance level was not high. Comparison between the normal subjects and patients showed significant differences for all statistical parameters ($P < 0.001$).

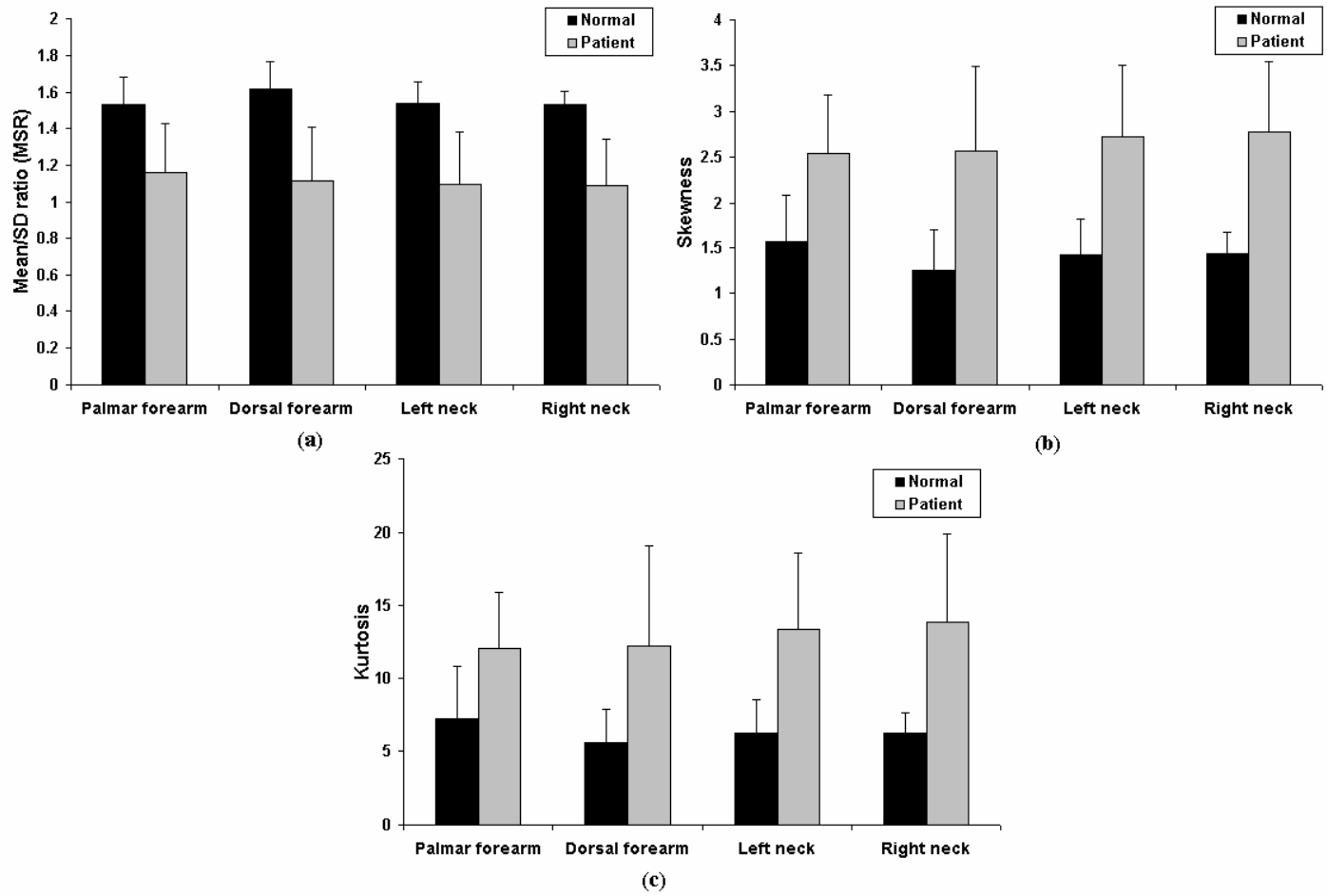

Figure 3-21. Comparison between the normal subjects and patients at the four sites for the statistical parameters: (a) MSR, (b) skewness and (c) kurtosis.

Table 3-7 The *P* value of the comparison of statistical parameters for the various tested sites

Paired t-test	***MSR***			***Skewness***			***Kurtosis***		
	P arm & D arm	***L neck & R neck***	***P arm & neck***	***P arm & D arm***	***L neck & R neck***	***P arm & neck***	***P arm & D arm***	***L neck & R neck***	***P arm & neck***
Normal	*0.02**	*0.36*	*0.46*	*0.006**	*0.40*	*0.16*	*0.01**	*0.47*	*0.14*
Patient	*0.06*	*0.41*	*0.02**	*0.43*	*0.33*	*0.04**	*0.45*	*0.29*	*0.05**
Unpaired t-test	***P arm***		***neck***	***P arm***		***neck***	***P arm***		***neck***
Normal & patient	*< 0.001**		*< 0.001**	*< 0.001**		*< 0.001**	*< 0.001**		*< 0.001**

Note the abbreviations are defined as in Table 3-4. "*" stands for a significant difference at the level of 0.05.

Statistical parameters were also computed among the 4 subgroups (Table 3-8). One-way *ANOVA* showed that there was significant difference among the four

subgroups for the three parameters ($P < 0.05$). Subsequent *t*-test showed that the difference between two neighbor subgroups only existed between Group 1 and Group 2 ($P = 0.007$ for MSR, $P = 0.004$ for skewness and $P = 0.02$ for kurtosis). But if Groups 0 & 1, and Groups 2 & 3 were further grouped into two patient sections with equivocal and evident fibrosis, respectively, significant differences were demonstrated ($P < 0.001$ for MSR and skewness, and $P = 0.004$ for kurtosis). The correlations of statistical parameters with the effective YM were shown in Table 3-9. It partially supported the significant correlations of statistical parameters and the fibrotic degree.

Table 3-8 The statistical parameters across the 4 subgroups according to the palpation score

Statistical parameters	***Group 0***	***Group 1***	***Group 2***	***Group 3***
MSR	*0.96 (0.18)*	*1.04 (0.17)*	*1.26 (0.18)*	*1.28 (0.39)*
Skewness	*3.00 (0.54)*	*3.11 (0.51)*	*2.32 (0.66)*	*2.15 (0.76)*
Kurtosis	*14.3 (4.9)*	*16.1 (3.9)*	*11.6 (4.9)*	*10.1 (4.5)*

The value in the parentheses indicates the standard deviation.

Table 3-9 The correlation of the effective YM and the statistical parameters in radiation-affected skins

Relations	***Effective YM and MSR***	***Effective YM and skewness***	***Effective YM and kurtosis***
Correlations	*r = 0.24*	*r = -0.26*	*r = -0.19*
	*P = 0.05**	*P = 0.04**	*P = 0.13*

When the statistical parameters were plotted with the subject age in both the affected and unaffected skins, it showed that there was a significant correlation between the statistical parameters and the age in the unaffected normal skin, but not in the affected skin in the neck of the patient (Table 3-10).

3.2.3 Skin Thickness

Although there were bright reflective points in the hypodermis for the normal skin as shown in the ultrasound images, the margin between the dermis and hypodermis was often sharp enough to be differentiated (Figure 3-12). This margin was generally kept for the patients as well, thus making the measurement and comparison of skin thickness possible. Occasionally it was observed both in the normal and patient

subjects that the margin was not sufficiently parallel to the skin surface, and then a mean of values measured at different sites was taken in this case.

Table 3-10 The correlation of age and the statistical parameters in the radiation-unaffected and affected skins

Correlations	*Age and MSR*	*Age and skewness*	*Age and kurtosis*
*Unaffected skin**	*r = -0.56*	*r = 0.47*	*r = 0.35*
	*P < 0.001**	*P < 0.001**	*P = 0.007**
*Affected skin**	*r = -0.16*	*r = 0.15*	*r = 0.18*
	P = 0.35	*P = 0.36*	*P = 0.29*

***The unaffected skins include the palmar forearm skin of both normal and patient subjects and the affected skin indicates the neck skin of the patient subjects. "*" stands for a significant correlation at the significance level of 0.05.**

The thickness of the skin measured at different sites between the normal subjects and the patients was plotted and compared (Figure 3-22). The *P* values of the comparison within and between the normal and patient groups were also tabulated (Table 3-11). For the normal subjects, the skin thickness of the two sides of the forearm was not significantly different ($P > 0.05$). The mean value for the forearm was 1.52 ± 0.21 mm. The skin thickness of the two sides of the neck was also not significantly different ($P > 0.05$). The mean skin thickness for the neck was 1.85 ± 0.30 mm. The skin thickness was significantly larger in the neck than in the forearm ($P < 0.001$). For the patient subjects, the thickness of the forearm skins was also not significantly different ($P > 0.05$). The mean value for the forearm was 1.53 ± 0.20 mm. It was unexpectedly found that the skin thickness of the two sides of the neck showed a significantly difference using the paired *t*-test ($P < 0.001$). The mean thickness for the left and right neck was 2.06 ± 0.34 mm and 2.18 ± 0.35 mm, respectively. Thus both sides of the neck were separately compared with the mean forearm skin thickness. The thickness of the two neck sides was both significantly larger than that of the forearm ($P < 0.001$). There was no significant difference in the forearm skin between the normal subjects and the patients ($P > 0.05$). The skin thickness of the both sides of the neck showed significant increases in the patients than in the normal subjects ($P < 0.01$). When the ratio of the neck thickness to the forearm thickness was used, it showed the same trend, i.e., the ratio increased in the patients in comparison with that of the normal subjects ($P < 0.01$). The skin thickness

ratio was 122 ± 16% in the normal subjects, 136 ± 24% and 145 ± 29% for the left and right sides of the neck in the patients.

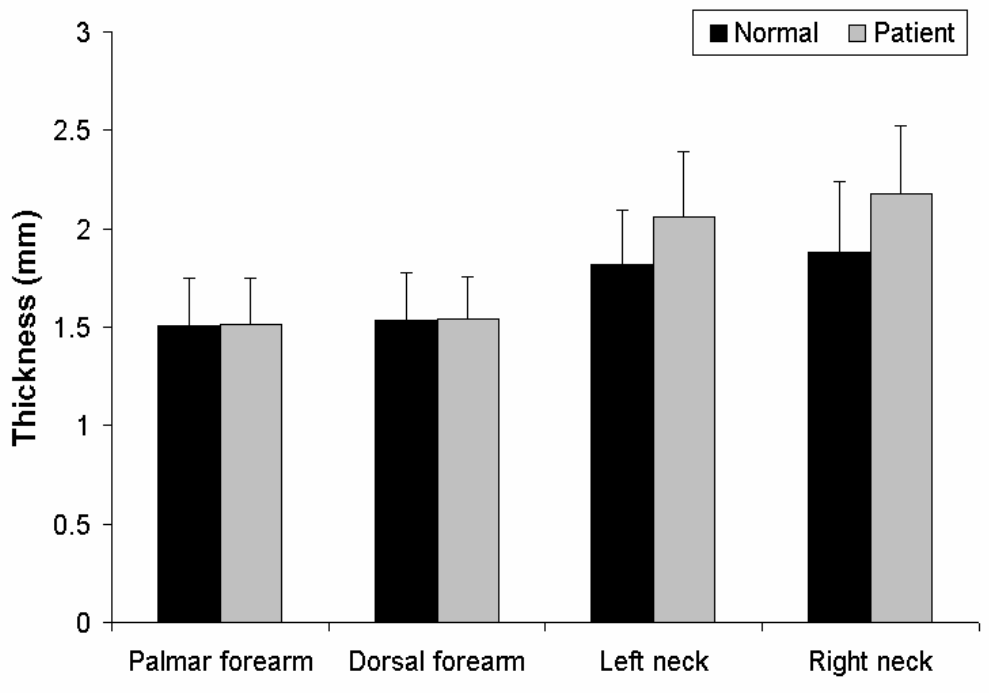

Figure 3-22. Skin thickness at different sites for the normal and patient subjects.

Table 3-11 The *P* values of various comparisons within and between the normal and patient groups

Paired t-test	***P arm & D arm***	***L neck & R neck***	***L neck & arm***	***R neck & arm***	***neck & arm***
Normal	*0.31*	*0.11*	-	-	*< 0.001**
Patient	*0.21*	*< 0.001**	*< 0.001**	*< 0.001**	-
Unpaired t-test	***arm***		***Patient L neck & Normal neck***	***Patient R neck & Normal neck***	
Normal & patient (direct comp)	*0.45*		*0.01**	*< 0.001**	
Unpaired t-test	***Thickness ration of Patient L neck/arm & normal subject neck/arm***			***Thickness ratio of Patient R neck/arm & normal subject neck/arm***	
Normal & patient (comp of thickness ratio)	*0.01**			*0.001**	

Note the abbreviations are defined as in Table 3-4. "*" stands for a significant difference at the significant level of 0.05.

Skin thickness was also calculated among the 4 subgroups (Table 3-12). One-way ANOVA showed that there was no significant difference among the four subgroups

($P > 0.05$). The skin thickness was also correlated to the effective YM measured for the neck soft tissues of the patient. No significant correlation was found between the two parameters ($r = 0.007$, $P = 0.95$). When the skin thickness was plotted with the subject age in both the radiation-affected and unaffected skins, it showed that there was no significant correlation between the two parameters in the neck ($r = -0.11$, $P = 0.43$ for the unaffected skin, $r = 0.20$, $P = 0.23$ for affected skin).

Table 3-12 Skin thickness and neck/forearm thickness ratio across the 4 subgroups according to the palpation score

Patient subgroups	*Group 0*	*Group 1*	*Group 2*	*Group 3*	*P value of one-way ANOVA*
Thickness (mm)	*2.07 (0.34)*	*2.18 (0.32)*	*2.16 (0.42)*	*2.05 (0.20)*	*0.80*
Thickness ratio	*134% (26%)*	*148% (25%)*	*147% (30%)*	*131% (16%)*	*0.35*

The value in the parentheses indicates a standard deviation.

While the age dependence of the skin thickness was not significantly demonstrated, there was a significant variation of the presence of a subepidermal low-echogenic band (SLEB) (Figure 3-23). The presence of the SLEB was counted in the various regions of both the normal subjects and patients. Although the presence of SLEB at the palmar side of the forearm was generally associated with its presence in the volar forearm, it did not necessarily happen for all the cases. This kind of observation was similar for both sides of the neck. For the normal subjects, the presence of the SLEB in 40 sites of the forearm was 10% and it was 28% in 40 sites of the neck region. However, the difference was not significantly established ($P = 0.12$, Wilcoxon signed rank test). In the patients, the proportion of the presence of the SLEB was 62% in the forearm and 30% in the neck, for which the difference was significant ($P < 0.001$, Wilcoxon signed rank test). The presence possibility of the SLEB was significantly higher in the forearm in the patients than in the normal subjects ($P < 0.001$, Wilcoxon rank test), but no significant difference was found in the neck between the two groups ($P = 0.76$, Wilcoxon rank test). The high prevalence of the SLEB in the older subjects observed in this study was similar to that reported in other literature (Gniadecka, 2001).

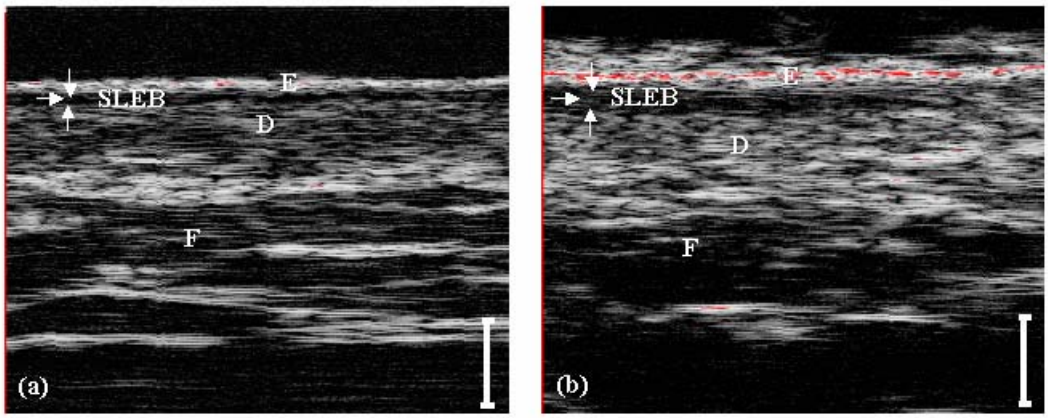

Figure 3-23. The subepidermal low-echogenic band (SLEB) observed in (a) a normal subject with age of 33 years and (b) a patient with age of 69 years. Note a broader band was observed in the older subject. E: epidermal entry echo, D: dermis and F: subcutaneous fat. The white bar in the image indicates a scale of 1 mm.

3.3 Discussion

There is a need to quantitatively and objectively assess the radiation-induced fibrosis, and high frequency ultrasound is a helpful and potential tool to characterize the tissue pathologies. Therefore, attempts were made in the design of our study to use high frequency ultrasound to assess the skin fibrosis in patients after radiotherapy. In this thesis, we reported and compared the results of ultrasonic properties in terms of the attenuation slope, integrated attenuation and integrated backscatter, the statistical parameters, and the skin thickness measured from the ultrasonic skin image in the forearm and neck region in both the normal subjects and patients. The potential of these parameters to assess the different degrees of fibrosis was also evaluated. For the measurement of the ultrasonic properties, the reliability with respect to intra- and inter-rater operation was quantified. To the best of our knowledge, this is the first time in the literature that results of the *in-vivo* ultrasonic properties in view of comparing dermal tissues with and without cutaneous fibrosis were reported.

3.3.1 Ultrasonic Properties

High frequency sonography has been widely used in dermatology to detect the skin modifications induced by sex, chrono-ageing, chronic sun-exposure and various skin diseases. There were also clinical trials that introduced this noninvasive facility to assess the postirradiation cutaneous and subcutaneous reactions (Gottlober et al., 1997; Warszawski et al., 1997). Those analyses were based on the thickness and the texture of the dermis using B-mode ultrasonic imaging while quantitative information

on the ultrasonic properties extracted from the echographic RF signals was lacking. It was reported that the ultrasonic properties were sensitive to the variations of tissue compositions such as collagen and water in skin (Olerud et al., 1990; Moran et al., 1995), and thus the measurement of ultrasonic parameters *in vivo* using RF signals collected by a 20 MHz ultrasonic probe was included in the current study to assess the skin tissues.

3.3.1.1 Reliability of the Measurement

To make a test method clinically meaningful, the measurement should be reliable. In fact, the reliability of the *in-vivo* measurement of ultrasonic properties was reported in a few studies for skin (Guittet et al., 1999b; Fournier et al., 2001). The reliability was reported in terms of CV or standardized CV in their studies, but in the current study neither the test methods nor the parameters used to represent the reliability were the same as those reported previously. Although the scanning of the transducer inside the probe was mechanical, the test itself generally involved artificial effects caused by the raters' operation. It was therefore necessary to study the reliability of our current measurement. Concerning the parameters used to represent the reliability of the continuous data, CV was not used here because it is only proper for describing the data with a standard deviation proportional to the mean, which was not necessarily the case especially for the integrated attenuation in our study (Rankin and Stokes, 1998). The correlation coefficient is generally used to describe two groups of relevant data but it is sometimes not appropriate due to its some shortcomings. One is that it tests the linear association, instead of agreement of two pairs of data. It is also not proper to use the correlation coefficient when the sequence of two measurements, which needs to be separated for the computation of the correlation coefficient, makes no sense. In such a case, the correlation coefficient will give different values if the sequences of the paired data are changed, but in fact this kind of change does not affect the reliability of the test. Paired *t*-test was also not proper because it compares the mean of the difference but neglects the distribution of the difference. Significant scattering of the individual differences but a zero-mean may induce the difference of measurement being non-significant. The intraclass correlation coefficient (ICC) describes the true variance as a fraction of the total variance and is thus a better choice for characterizing the test reliability. It was used in this study to investigate the intra- and inter-rater reliability of our measurement.

In general, an ICC larger than 0.80 was regarded as a high reliability (Altman, 1991). From the current results, our measurement was demonstrated to be highly reliable with ICCs larger than 0.80 except the case of intra-rater measurement for the IBS (0.56). The distribution plot of the Bland and Altman test did not show a correlation of the individual differences with the mean value. Generally speaking, the ICCs of the inter-rater measurement were larger than those of the intra-rater measurement, and the reliability coefficients of the inter-rater test were smaller than those of the intra-rater test. According to the design of our measurement protocol, the superior reliability of the inter-rater measurement was most probably due to the reason that the second rater operated the probe and conducted the test in a short time after the test of the first rater was finished. Therefore, the effects of factors such as the mislocation of the probe that might cause the measurement discrepancies were minimized and became neglectable. This effect of probe mislocation was relatively small as the same mark was used for locating the testing site by the two raters. While for the intra-rater test, experiment was conducted on two different occasions with an interval of one week so that the effects of mislocation, room and skin surface temperature, probe pressure applied and personal activity status of the skin were exaggerated compared with those for the inter-rater operation conducted on the same occasion. The intra-rater reliability of IBS was lower than that of other measurements. It was a little biased because the 95% CI of the difference was negative (Table 3-2). Possible reasons might be that this parameter was affected not only by those aforementioned factors but also by the coupling between the thin film of the probe and the skin. Any inconsistency of coupling would be expressed as significant variations of the signal intensity, which was directly related to the integrated backscatter as defined in this study. Coupling might not be so problematic for attenuation coefficients as these coefficients were extracted from relative change of ultrasound signal with different depths of skin, but rather with the absolute value of the signals, given the SNR of the ultrasound signal was large enough in the skin. The issue of coupling for backscatter parameters seemed to be a problem faced by all investigators when *in vivo* experiments were conducted for tissue characterization by use of absolute backscatter coefficients. Thus it was paid special attention to when the clinical trials were carried out. In the clinical trials, a good coupling was assured while keeping a gentle pressure on the skin. This was secured from the B-mode image that no shadowing and large variations of the intensity which were most probably

induced by the poor coupling of the contact were observed. The coefficient of reliability shows the range in which the difference of two measurements locate for 95% of the pairs of observations, and if the variation induced by processes to be detected was significantly larger than that range, it was very useful to use the current measurement to assess those processes.

3.3.1.2 Ultrasonic Properties of Normal and Irradiated Skins

In this study, the measurement of ultrasonic properties was performed in both the normal subjects and patients with fibrosis. In the normal subjects, the skins at different anatomic regions were differentiable by the ultrasonic properties. It is generally known to us that the skin varies substantially in thickness, components, structure and tension at different anatomic sites and it also changes chronologically with age. It has been demonstrated that ultrasonic properties of skin *in vivo* or *in vitro* were sensitive to some of these variations (Olerud et al., 1990; Moran et al., 1995; Pan et al., 1998; Fournier et al., 2001). The difference of the ultrasonic properties found in this study was regarded as the reflection of anatomic difference of skin in these two regions. For example, Raju et al. (2001) reported that a larger attenuation slope in the dermis of the fingertip region than that of two locations in the forearm. They attributed this difference to the possible variations in skin tension and collagen structure of the two regions. In this study, a higher β, with a lower IA was found in the forearm region than in the neck region. For IBS, a significantly smaller value in the neck region was found than in the forearm region. Comparatively related study about skin echogenicity by Pellacani and Seidenari (1999) reported that the facial skin was much less reflective compared to the forearm skin. If the neck skin is anatomically assumed be more similar to the facial skin, our current findings were not contradictive to their results. Pan et al. (1998) studied the effect of transverse stress on the ultrasonic properties. Their study demonstrated a large decrease of the IA, a minor decrease of β and a minor non-significant increase of the backscatter associated with the increase of the stress. One possible reason that might cause the dissimilarity of ultrasonic properties in the two regions could be the difference of the internal tension. However, if the findings of Pan et al. (1998) were the fact, the current results might not to be simply explained by a difference of tension of the skin in the two regions because the attenuation slope and integrated attenuation changed inversely rather than consistently in our case. Others factors such as the network of the collagen and elastic

fibers with the ground substances including the water content might also contribute to the difference of ultrasonic properties in the two regions. The current observation warrants the further investigation of data collection from more body sites in order to establish the regional variations in the ultrasonic properties of skin.

In patients who had received radiotherapy, the distribution of the ultrasonic parameters in the neck and forearm regions was similar to that of the normal subjects, except that the palmar and dorsal side of the forearm showed significant difference in β and IBS. The most possible reason for the difference between the two sides of the forearm was the actinic elastosis, which was a skin damage induced by the exposure to sunlight (Altmeyer et al., 1992b). All the subsequent comparison on the forearm was made on the palmar side, which was less affected by this phenomenon individually. The anatomic characterizations of the ultrasonic properties were maintained in the patients regardless of the pathological status of the neck which had received therapeutic radiation.

The ultrasonic properties of the irradiated skins in patients were compared with those of the normal subjects in two ways: direct and relative comparisons. The direct comparison showed that β was significantly decreased and IA was significantly increased in the irradiated than in the normal neck skins, but this was not demonstrated in the non-irradiated forearm skins of both the patient and normal subjects. It appeared that the irradiated skin had changes of its attenuation coefficients in terms of β and IA. The direct comparison of IBS was a little contrary. The significant change was not found on the neck skin, but on the palmar forearm skin. This phenomenon might be explained by the age dependence of IBS as shown in Figure 3-19. In normal skins IBS was age-dependent but this age-dependence had been interfered by the fibrotic process and thus became unclear in the fibrotic skins. Therefore, no significant difference was found in the neck skins between the young normal subjects and the older patients. When the relative difference of ultrasonic parameters between the neck skin and the palmar skin was used for comparison, all the results showed an increase in the patients than in the normal subjects. The increase of IBS_d was significant while it had not reached significant levels for β_d and IA_d. The two kinds of comparison both demonstrated that β and IBS were decreased, and IA was increased by the skin fibrotic process. To explain the results, however, was not

so straightforward. The observation could not be explained by a variation of internal transverse stress based on the results of Pan et al. (1998) because the change of β and IA was reverse rather than consistent in this study. The increase of IA was most probably induced by the increase of collagen content in the skin with fibrosis as indicated by previous investigations (Olerud et al., 1990; Moran et al., 1995). Goss and Dunn (1980) studied the ultrasonic propagation properties of the collagen suspension and found that collagen exhibited greater absorption than the globular proteins. Therefore, the increase of collagen content in fibrotic tissues was a most conceivable candidate who contributed to the increase of IA. The relationship between β and the collagen in skin has not been well established in the literature yet, but it was proposed that β was related to water content such as in the case of dermal edema induced by contact dermatitis (Raju et al., 2003). It was not quantified to what extent the fibrotic skin had the edema after radiotherapy, which could be studied in future investigations. Our findings of β and IA were similar to a study in the different regions of the human aortae (Bridal et al., 1997). In their study, a slight decrease of β and a slight increase of IA were demonstrated in the regions with dense collagen in comparison with normal regions. Meanwhile, the change of the IBS found in our study was consistent with that reported in terms of the echogenicity in the dermis (Warszawski et al., 1997). In their investigation, the breast skin showed an even much larger decrease of the signal intensity in the early skin reactions. Although the intensity increased slightly in the late reactions, it was still lower than that of the original status as indicated by the non-irradiated contralateral breast skin. They attributed the reduction of signal intensity most probably to the oedematous changes or papillary dermal inflammatory lymphocyte infiltration. The current observation of IBS was a little contradictive to the fact that collagen generally had a positive correlation with the ultrasonic backscatter. However, it should be noted that the ultrasonic backscatter was greatly dependent on the orientation of the collagen fiber to the insonification direction (Roberjot et al., 1994). Typically, the backscatter of ultrasound propagating across the fiber would be stronger than that when propagating along the fiber. Although the collagen increased in the fibrotic skin, it was possible that its structure might change to be more randomly aligned instead of parallel to the skin surface so that the backscatter was not significantly improved. In addition, the water content increased significantly in the fibrotic dermal tissues, as probably

indicated by the concurrent decrease of β, and it caused the decrease of the ultrasonic backscatter. It was therefore very important at the next stage to find out how the collagen and water varied in the skin with radiation-induced fibrosis. The exact reasons for our findings should be confirmed by associated biochemical examinations or other relevant tests to extract the information of collagen and water of the tissue samples in further investigations.

The advantage of the direct comparison was that the anatomic region was the same and the structure of the skin compared was similar. But this kind of comparison did not exclude the potential effects induced by the chronic ageing process. The change of ultrasonic properties with the ageing process had been reported by some researchers although the results seemed not to be so consistent to date. Guittet et al. (1999a, 1999b) reported a decrease of β with age while Fournier et al. (2001, 2003) obtained a correlation between IBS and the age but not between β and age on the skin of palmar forearm. In the current clinical trials, the patients generally were older than the normal subjects. An analysis of the correlation of the ultrasonic parameters and age in both the forearm skin of the normal and patient subjects and the neck skin of the patients showed that only the IBS in the unaffected palmar forearm skin was significantly correlated with age (Figure 3-19). Thus, it was assumed that direct comparison was effective for β and IA. In consideration of the individual difference caused by age, the measurement of the forearm skin as an individual reference was also conducted in the current study to assess the relative change of ultrasonic properties in skin with fibrosis. For the unaffected two sides in the forearm of patients, statistical analyses showed a significant difference for β and IBS. This was expected in our initial design of this study because the exposure of sunlight of the two sides of the forearm was quite different for each individual. This effect caused by so-called photoaging was much obvious for the elderly than the young (Gniadecka, 2001). In the normal subjects, this effect was not detectable as indicated by a non-significant difference between the two sides. In the elderly patients, the palmar side was much less exposed to sunlight in comparison with the dorsal side. Our results showed an increase of IBS with the age in the unaffected normal skins in the palmar side, which was consistent with those reported in the literature (Seidenari et al., 1994; Fourier et al., 2001). While correlation between either β or IA and age was not confirmed in this study, which was inconsistent with those reported previously

(Guittet et al., 1999a, 1999b; Fourier et al., 2003). The exact reason on this point was unclear. Possible reasons included the different sites chosen for data collection and the difference of data acquisition systems and processing techniques. The site we tested was in the distal palmar forearm instead of the middle palmar forearm in their study.

The mutual correlations of the three ultrasonic parameters in both irradiated and non-irradiated skins were demonstrated (Figure 3-15), which was unexpected in the original design of our study. The correlation of IA and IBS was explainable because the "IBS" as defined in this study represented the averaged capability of the backscattering in the whole region of interest (from the depth 0.3 mm to 1.3 mm). This capability was inherently related to two factors, i.e. scattering in the interested tissue volume and the attenuation caused by the tissue before the ultrasound reaching this volume. If the scattering of the selected tissue volume was assumed to be constant for the skin, the backscatter was then determined by the internal attenuation. Therefore, the IBS was directly related to IA, which was an indicator of the level of the internal attenuation. However, the reason for the correlations of β with IA and IBS was unclear because they were independently derived from the signals collected from the tissue. The correlations might represent some intrinsic relationships among these parameters in skin tissues. A reasonable explanation would be that all three parameters were dependent on certain skin compositions so that they were correlated to each other due to the common compositions as deterministic factors, even though these parameters were independently extracted. The collagen might serve as such a candidate component. However, the validity of such a hypothesis needs to be further confirmed. To the best of our knowledge, no such relationship was reported previously in the literature. Although significant mutual correlation of ultrasonic parameters was demonstrated, to measure them separately was still of interest because they represented different characteristics of ultrasound propagation in biological tissues.

3.3.1.3 Ultrasonic Properties of Irradiated Skins and Degrees of Fibrosis

If the palpation score served as an indicator to divide the patients into small subgroups with different fibrotic degrees, the ultrasonic properties of different patient subgroups could be compared directly due to their matched-age. From Figure 3-16, the most possible correlation might exist between the IBS and the palpation score. Although not significantly, it appeared that IBS increased as the fibrotic degree

increased. One possible reason would be that the collagen content increased more in the skin with more severe fibrosis. For β and the IA, no consistent trend in relation to the palpation score was observed from the current results. Quantitative measurement of the stiffness of the neck soft tissue was achieved and the stiffness well correlated with the palpation score (Figure 3-17), which was consistent with the results obtained in a previous study (Leung et al., 2002). Olerud et al. (1987) reported that the ultrasonic attenuation measured by a scanning acoustic microscopy was significantly positively correlated with the tensile strength of the skin tissue. However, in our study when the stiffness was correlated to the ultrasonic parameters, no significant correlation was demonstrated (Figure 3-18). Analysis of the relationship of the ultrasonic properties with the neck rotation range as one clinical symptoms of fibrosis also showed no significant correlation (Table 3-6). Therefore, no consistent conclusion on the relation between the degree of neck tissue fibrosis and the ultrasonic parameters could be drawn. However, it should be noted that a trigger effect of the ultrasonic parameters induced by fibrosis might exist as significant difference between normal subjects and patients was found. The ultrasonic parameters in the patients might have changes triggered as a result of fibrosis while in the patient subgroups differences could not be uniformly established after triggering. Therefore, fibrosis could be seen as a trigger factor for the change of ultrasonic parameters.

It should be noted that the degree of the skin fibrosis was judged by the hand palpation of the neck soft tissue given by a clinical oncologist in the current study. The measured stiffness indicated the mechanical properties of the entire neck soft tissues, i.e., the skin as well as the subcutaneous tissues. The change of the neck rotation range was functional reflection of the neck tissue fibrosis. The palpation score, the tissue stiffness, and the neck rotation range obtained in such ways might be a more accurate characterization of the fibrosis of the entire soft tissues especially the underneath muscular tissue instead of the nature of the skin tissues. Thus further study should include specific measure of the mechanical properties of the skin tissue in order to correlate the exact mechanical properties of the skin to the ultrasonic properties. The development of our microscopic system for the skin elastography is potential regarding this aspect.

3.3.1.4 Results of Literature and Limitations of Current Measurement

Some of the values of β reported in the literature for the forearm skin tissues *in vivo* were in the range of 0.07 to 0.36 dB/mm/MHz measured at 40 MHz (Guittet et al., 1999a), 0.08 to 0.39 dB/mm/MH measured between 14 and 50 MHz (Raju et al., 2001), and 0.02 to 0.50 dB/mm/MHz measured between 11 and 27 MHz (Fourier et al., 2003). Our results of the β of the skin in the palmar forearm was in the range of 0.28 to 0.47 dB/mm/MHz with a mean value of 0.37 ± 0.04 dB/mm/MHz measured between 10 and 25 MHz. The β measured in this study was generally in the range that reported previously. The IA range of –12.9 to 2.12 dB/mm with a mean value of –4.6 ± 3.8 dB/mm was reported by Fourier et al. (2003) between 11 to 27 MHz in the middle palmar forearm skin. In their study, diffraction correction was lacking and it was found that a large portion of the IA was negative. A mean IA of 13.5 ± 3.7 dB/mm was reported by Lebertre et al. (2002) between 22 to 45 MHz for the female abdominal skins *in vitro*. The IA measured in the current study was from –2.3 to 6.0 dB/mm with a mean value of 0.8 ± 1.6 dB/mm between 10 to 25 MHz in the palmar forearm skin, which was quite different from that of the aforementioned studies. The difference of the attenuation parameters in this study compared with values reported previously might be caused by the data acquisition system, signal processing methods, the experimental conditions and the population of subjects studied. Thus standard measurement methods should be proposed in the future to facilitate the inter-lab comparisons. Because the IBS was defined specifically in this study, to the best of our knowledge, no comparative results existed in the literature.

There were several limitations that were worth paying attention to in the current study. Firstly, the studied region in this study was generally anterior to the focal region of the transducer and thus in this region the ultrasound energy was increasing along with the penetration depth. It was necessary to correct this effect called as “diffraction”. A reference method was used in the current study to correct the system-dependent and diffraction effects for the received signals backscattered from the skin tissue (Fournier et al., 2001). However, this kind of correction method would lead to some bias. For the attenuation parameters, the diffraction could be better compensated by an axial translation of the transducer to keep the focal zone in the studied region (Ophir and Mehta, 1988). This approach has not been used in our study due to the positional uncertainty that might be induced by the movement of the tissue during the

measurement and the too long time for applying such a method to a large population of subjects. Secondly, a homogeneous backscatter was assumed in the whole region of interest for the calculation of attenuation parameters. Such a hypothesis was not necessarily upheld in practice as indicated by previous investigators due to the intrinsic non-homogeneity of the dermal tissue and the existence of some echo-rich spots in the cutaneous and subcutaneous fibrosis (Gottlober et al., 1997; Fourier et al., 2001). The heterogeneity of the ultrasonic scattering in the dermal tissue made the calculation of attenuation parameters unstable and the calculated attenuation coefficients not true values inherent to the skins but rather relative. This might be the reason why occasionally negative integrated attenuation occurred, but not as frequently as observed in the study of Fourier et al. (2003). However, a special case was that if the heterogeneous backscatter in the region of interest was only depth-dependent rather than frequency-dependent, the attenuation slope would not be affected because the backscatter inhomogeneity only caused the attenuation slope to shift in parallel along the ordinate. A general issue that theoretical algorithms may face when they are applied to clinical experiments is that not all the theoretical assumptions are necessarily practically matched, such as the case in the current study. Thirdly, the IBS as defined in this study was not compensated by the attenuation of the tissue located before the region of interest and the reflection by the film-skin interface. Therefore, all the IBS was underestimated considering the incident signal attenuated by the skin interface, the epidermis and some of the dermis located before the studied region. Finally, some conclusions were made based on the comparison of the difference of the ultrasonic parameters of the fibrotic neck skin and the forearm skin, with the hypothesis that the ageing caused the ultrasonic properties for the skin in different region to change in the same direction. Whether such a hypothesis was acceptable has not been further verified in this study. A better way to do the comparison is to recruit age-matched normal subjects for data collection and then the comparison of the parameters between normal and fibrotic skins became more feasible.

3.3.2 Statistical Parameters

Our results showed that the statistical parameters were not significantly different in the neck and palmar forearm skin in the normal subjects, for which the characteristics were not the same as those of the ultrasonic parameters. In the patients,

the statistical parameters all showed a significantly change in both the neck and forearm region as compared with the normal subjects (Figure 3-21). The age-dependence was the most probable reason that caused such a difference, and this was verified by an analysis of the correlation between the statistical parameters and age (Table 3-10). However, in the irradiated skin of the patients, all the statistical parameters showed significant difference between the neck and forearm region. All the statistical parameters were larger in the neck than those in the palmar forearm, although the significance level was a little weak. Thus, if the difference of the ageing effect in the neck and forearm was neglectable, the fibrotic process tended to provoke the variation of the distribution of the envelope of the signal backscattered from the skin.

The scattering in the skin of the normal subjects was pre-Rayleigh but closer to Rayleigh conditions because the MSR was closer to 1.91 in the normal subjects than in the patients. The lower MSR in the patients indicated that a larger variation was associated with the mean of the envelope signal. The skewness was significantly larger in the patients than that in the normal subjects. A larger and positive skewness indicated that the data was more spread out to the large value. For the kurtosis, it was larger than 3 for the normal subjects and the patients, which indicated that the scattering was longer-tailed than the Gaussian distribution. A significantly larger kurtosis was observed in the patients, indicating that in the skins of the patients the distribution of the envelope was even longer-tailed. All the changes between the normal subjects and the patients were most probably ascribable to the chronic change of the dermal microstructures that contributed to the ultrasonic scattering. In the ageing process, especially after 40 years of age, the tissue constitutes such as the collagen and elastin fibers changed in a drastic manner (Vitellaro-Zuccarello et al., 1994; Quaglino et al., 1996). In order to estimate the effect of the fibrotic degree on the statistical parameters, they were correlated to the palpation score and the quantitative stiffness of the neck soft tissue. No consistent trend was observed among the four subgroups. However, if the four subgroups were further grouped into 2, one representing the patients with equivocal fibrosis and the other with severe fibrosis, significant difference was then demonstrated. The results were a little interesting because the direction of change was just contrary to that induced by the ageing. The correlation of the ultrasonic parameters with the stiffness of the neck soft tissue did

not contradict this observation. The difference of the statistical parameters in age-matched patients with different degrees of skin fibrosis was most probably caused by the modifications of the skin components that were associated with the fibrotic process, such as the collagen content and structure.

The use of statistical parameters of the amplitude of backscattered signals has already been applied to ultrasonic tissue characterization (Wagner et al., 1987). For example, the probability distribution of the backscattered envelope signal in terms of the parameters as defined similarly in this study was studied by Komiyama et al. (2000) to test its capability in differentiating among the subtypes of coronary atherosclerosis and detecting the vulnerable coronary plaque, for which the discrimination was sometimes not possible based on conventional IVUS video images. In their study the MSR of the plaque without a lipid core was very close to Raleigh-scattering (2.01 ± 0.27). The MSR of the plaque with a lipid core (1.52 ± 0.27) was similar to that of our study in the skin of the normal subjects. Their results of the skewness and kurtosis seemed to be significantly different from the current ones. However, one thing we should bear in mind was that the frequency of the data collection system was different between the two studies (10 to 25 MHz in our study and 30 MHz in their study). In their study, it was demonstrated that the lipid core could be detected with a higher sensitivity and specificity by the statistical parameters than the visual video image analysis. Furthermore, the statistical parameters were also demonstrated to be significantly correlated to the size of the core area. Thus it was found that the statistical parameters were very helpful for predicting the pathological conditions of coronary plaque together with the use of IVUS image. Another study (Ciulla et al., 1997) correlated the skewness and kurtosis of the pixels of the echocardiogram to the collagen volume fraction of the myocardial tissues and found that these two parameters were significantly correlated with collagen content. The collagen content was closely relevant to the myocardial fibrosis in the patients with hypertension. Therefore, the noninvasive measurement of the statistical parameters might enhance the prediction of the fibrotic extent and help to choose proper therapeutic regimens for the regression of the hypertrophy. In our test, the quantification of the collagen content in the dermal tissue was not achieved and a direct analysis of their correlation was not possible. Further study may include the quantitative analysis of the statistical parameters and the skin compositions.

3.3.3 Skin Thickness

The high frequency ultrasonic B-mode image was introduced in this study for the measurement of skin thickness because of its successful applications in dermatology (Serup et al., 1984; Ihn et al., 1995; Gottlober et al., 1997). Although there might be some difference between the thickness measured by ultrasound and other established techniques (Tan et al., 1981), the comparison still could be conducted because the same device was used. The skin thickness measured in the present study showed a strong regional variation. The mean skin thickness of the neck was 122 ± 16% longer than that of the forearm in the normal subjects. Our results were not in contrast to that reported by Lee and Hwang (2002). In their biopsic study, the mean skin thickness of the Korean adults as a standard of Asian race was 1.13 to 1.18 mm in the middle forearm and 1.41 mm in the anterior neck region, respectively. The thickness of our study (1.52 ± 0.21 mm and 1.85 ± 0.30 mm in the forearm and neck skin, respectively) seemed to be generally larger than their values, probably due to the differences caused by the different measurement methods and the different experimental conditions (*in vitro* vs. *in vivo*) and the bias of positions chosen for testing. Although the age of the patients was larger than that of the normal subjects, the skin thickness in the forearm region did not show any difference between these two groups of subjects. A negative but not significant correlation with the age was obtained for the thickness of the forearm skin, which was consistent with that reported by Gniadecka and Jemec (1998). For the neck skin in the patients, both direct and relative (to his/her own forearm skin) comparisons showed it was significantly thicker than that in the normal subjects. This increase was most probably attributable to the skin fibrosis, because no age-dependence was found for the neck skin. The thickness of the two sides of the neck skin was unexpectedly slightly but significantly different, with the right larger than the left. The reason for such an observation was unclear till now. It was likely that the dosage of radiation absorbed by the two sides of the neck was biased to the right and thus this side developed more serious fibrosis and had a larger thickness in comparison with the other side.

Although significant increase of the thickness was demonstrated in fibrotic skin, the comparison among different patient subgroups and the correlation between skin thickness and the stiffness of the neck tissue did not disclose a strong relationship between the thickness and the fibrotic degree. Although not biochemically verified,

the skin thickness could be used as a prognostic parameter for the assessment of the cutaneous fibrosis according to some of the previous reports (Gottlober et al., 2001). The reduction of the skin thickness was regarded to be the therapeutic improvement for the treatment of the cutaneous fibrosis. It should be noted in those studies that the cutaneous fibrosis was very obvious with other severe syndromes caused by radiation therapy and it was not typical and comparable to this study because in our case the fibrosis was relatively less severe and with less other late sequelae. The collagen content was directly related to the dermal thickness in the normal skin, but the large variations of the collagen content in pathological skins might limit the function of collagen as a predictive factor for the skin thickness (Shuster et al., 1975).

3.3.4 Study Limitations and Further Improvement

Some limitations of the current study using the high frequency ultrasound and relevant measurement of skin fibrosis should be discussed. The limitation of the measurement of the ultrasonic properties has been discussed in Section 3.3.1.4. Further studies are to exclude other factors that potentially affected the uncertainty of the measurement such as the operation of the probe and the match of the age for the normal and patient subjects. A more direct way to study the effect of late sequela of radiation is to conduct the comparison before and after the therapeutic radiation. In this way, chronological monitoring of the change of the various parameters is also possible. In the analysis of the statistical parameters, the non-uniformity of the ultrasonic beam size along the skin depth direction, which could cause the variations of the number of scatterers in the beam were not emphasized. This non-uniformity would naturally make the echo statistics fluctuant even though the tissue was homogeneous along the depth direction. Raju et al. (2003) used reference values collected in normal skin tissues at different regions of interest along the axial direction to correct this effect. However, in our study, all the computation was conducted in the fixed depth so that this effect would only cause a systematic difference rather than random difference.

The largest limitation in the current study came from the grading of the skin fibrosis based on the hand palpation and the measurement of the soft tissue stiffness. The palpation score and the quantified effective YM were most conceivably the reflection of the fibrosis of the entire neck soft tissues especially the underlying muscular tissues, rather than the skin. Therefore, this raised the question that whether

these measurements were truly related to the fibrotic degree of the cutaneous tissue. Two directions may be needed to answer such a question in future investigations. One is to conduct the biochemical or histological examinations such as the needle biopsy of the skin tissues or to quantitatively evaluate the fibrotic extent using some reference tissue components such as the collagen content. The other is to specifically measure the physical properties such as the elasticity of the skin layer as indicators of cutaneous fibrosis. The advantage of the first research direction is that the assessment is straightforward, accurate and intrinsic to the fibrosis state so that our comparison can be much more meaningful. But the disadvantage is its invasive nature and may cause severe complications to the fibrotic tissues (Yeh et al., 2003). In contrast, the second direction may often be noninvasive and it is more preferable. However, its shortcoming is that the measurements are generally also indirect reflections of the fibrosis, and thus may not be recognized as a golden standard. One potential candidate for this kind of measurement is the system still being developed in our group to measure the elastic properties of the skin layer, as discussed in the section to follow.

4. Development of System for Measuring Skin Elasticity

4.1 Methodology

4.1.1 Preliminary System Setup

Inspired by the tissue ultrasound palpation system, a load cell can be added to the skin imaging system, thus making it possible to simultaneously measure the force and the deformation in the B-mode image. In order to compress the specimen, the soft thin film on the tip of the probe was substituted by a harder and thicker (approximately 0.24 mm) plastic plate. The reflection of the modified film was thus increased but it did not affect the measurement of the deformation, which was based on the echoes of the interfaces. A plastic sheath was designed for holding the probe and fixed it onto the load cell of the Hounsfield material testing machine. The cover at the tip of the probe was ensured to be tightly attached to the probe and to avoid any movement between the cover and its main body during the compression so that all the force was applied to the tested specimen.

4.1.2 Tests on Phantoms and *in-Vitro* Skin Tissues

4.1.2.1 Phantom Fabrication and Test Procedures

In order to construct thin phantoms that mimic the thickness and scattering of the skin, a type of polyvinyl alcohol (PVA) cryogel was used (Fromageau et al., 2003). Possible selections of materials also include the gelatin and agar that have been broadly used in fabricating tissue-mimicking phantoms for ultrasound detection (De Korte et al., 1997; Ryan and Foster, 1997). After several trials, they were not adopted in this study due to the fragility of the fabricated samples and the difficulty in storage. While for the PVA cryogel, it was not so complex to fabricate and could be kept easily in the water with no or little alteration of its properties, at least for the shape of the phantom, if the water was regularly changed and maintained to be fresh. The fabrication procedure of the phantoms was described as follow. PVA powders were first mixed with water in a weight concentration of 10% and then heated to and kept in a temperature of approximately 70 °C. During the heat, the solution was stirred in order to avoid the coagulation of the PVA powder. After the power was totally dissolved and no large PVA pellet was observed, heating was stopped and the solution naturally cooled. After the PVA solution almost completely cooled down to the room

temperature, graphite powder at a weight concentration of 5% was added to the mixture to increase the ultrasonic scattering of the material. Again the mixture was agitated to make the graphite powder uniformly distributed. Then the mixture was cyclically processed to be frozen at –20 °C for 14 hours and thawed at the room temperature for 10 hours. Each cycle of freezing and thawing took approximately 24 hours. After the first freeze-thaw cycle, the mixture became solid and as the cycles increased, the stiffness increased continuously. However, the increase of stiffness of the phantoms per cycle appeared not to be a constant and the stiffness increase per cycle was observed to decrease as the cycle number increased, provided other conditions were the same (Fromageau et al., 2003). In this study, phantoms with two layers were fabricated with the first frozen and thawed for 6 cycles and the second for 2. The mixture was poured into a container (dimension: 130×70 mm with a thickness of approximately 2.4 mm), the depth of which could be increased to be integral times of the original value. For the first layer, it was cyclically processed for 4 times and then the depth of the container was doubled. After mixture was poured to the increased space of the container, it was further processed for another 2 cycles. Then the phantoms were fetched out and kept in the water before testing. Totally six phantoms were constructed with the same protocols. According to the similar fabrication process as described in Fromageau et al. (2003), the two layers had different stiffness.

The phantoms were then tested using the setup shown in Figure 4-1. After the phantom was placed on a rigid base, it was compressed on the central part by the probe with a slight contact (Figure 4-2a). The phantom was compressed with a speed of 5 mm/min in approximately 20 steps, with each step approaching approximately 0.5% of the total thickness and the total compression ratio controlled in the range of 10%. The time interval between each step was approximately 20 s. The force data were recorded at approximately 10 s after the end of the ramp compression. For the PVA phantom, the relaxation for a typical test was recorded to be larger than 120 s so that the force was regarded to be an instantaneous one. At the same time, the movement of the Hounsfield cantilever defined as the displacement of the probe was recorded in order to extract the sound of speed in the phantoms. An ultrasonic image was also saved for each step in order to compute the respective deformation of the two layers. The surface of the phantom was moistened during the test due to two reasons:

1) to serve as ultrasound coupling between probe and phantom and 2) to avoid the dehydration of the phantom which was exposed to the air.

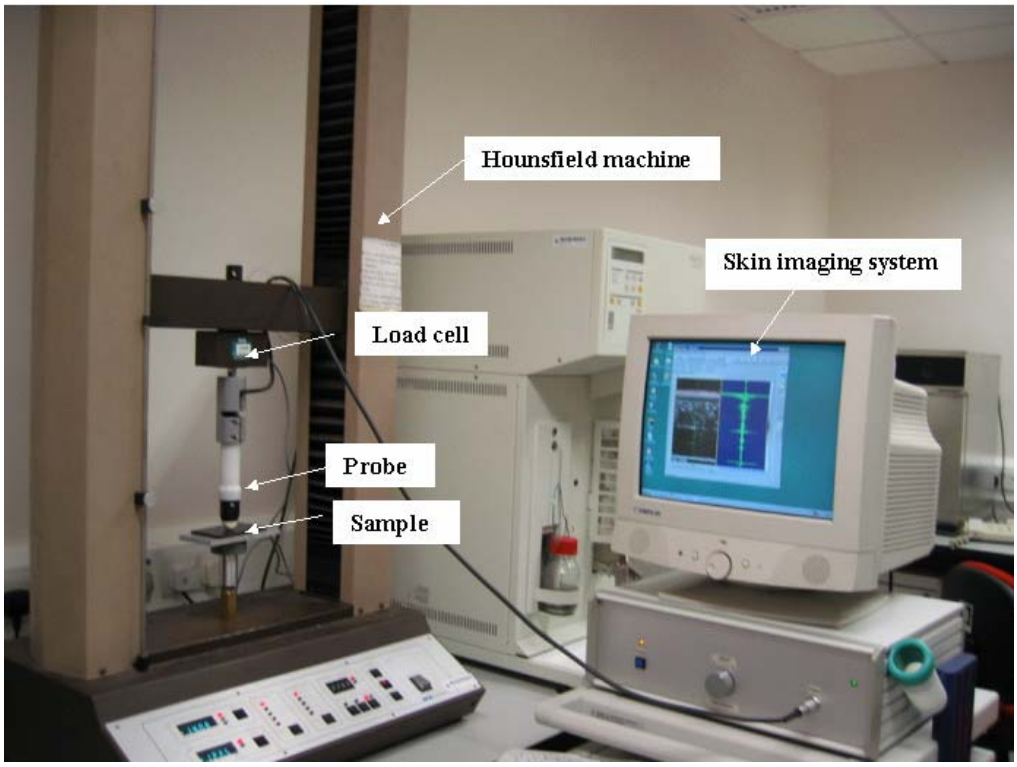

Figure 4-1. System configuration to test the two-layer PVA phantoms using the Hounsfield machine and the skin imaging system.

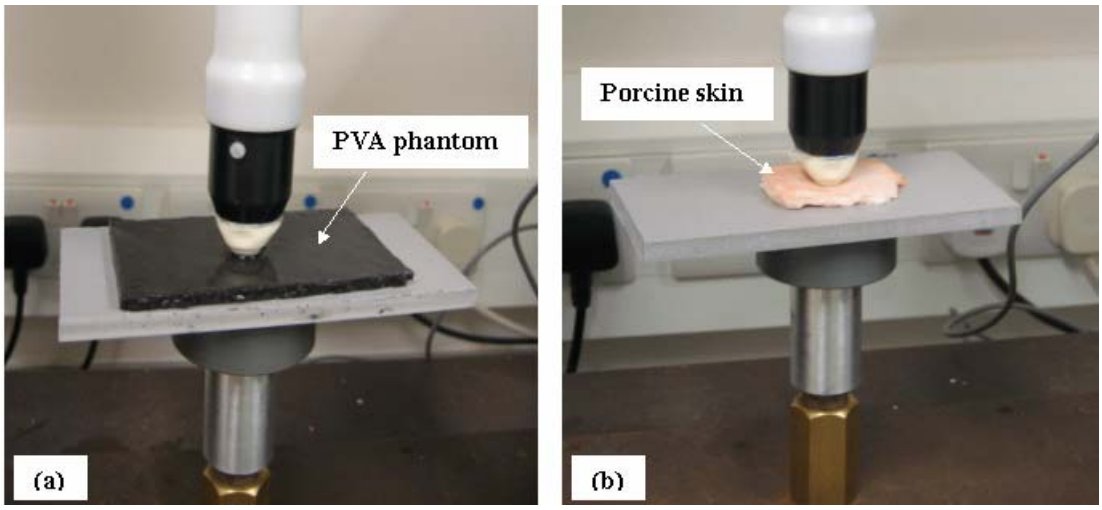

Figure 4-2. Zoomed pictures showing the experiment on (a) PVA phantom and (b) procine skin.

To test the repeatability of the measurement, three separate phantoms were fabricated and repeatedly tested for three times at the same site for each phantom. The six phantoms were first tested with the softer side down and then with the harder side down in order to confirm the hypothesis that in both cases the distinct stiffness of the

two layers could be differentiated. As the total surface area of the phantom was larger than that of the probe, the "compression" was not a purely uniaxial compression as used in conventional material testing and nonlinear effects could be caused by the non-standard boundary conditions. To simplify the problem, it was assumed that the two layers were "compressed" with the same pressure and the pressure/relative compression ratio was used to represent the stiffness of the tested phantoms.

4.1.2.2 Experiment on *in-Vitro* Porcine Skin

Three pieces of fresh porcine meat were bought from the supermarket. All the tissues under the subcutaneous fat were totally excised by a lancet, while part of the fat was preserved to serve as the second layer, like that of the phantom. The specimen was tested under the Hounsfield machine using the same procedure as described for the phantoms. The speed of sound was assumed to be 1540 m/s in the porcine skins. The stiffness of the dermis and hypodermis was obviously different (Gennisson et al., 2004) and therefore it was hypothesized that this system was effective to discriminate this difference.

4.1.2.3 Data Analysis Methods

The speed of sound in the sample was calculated by:

$$v = \frac{d}{\Delta t} \tag{2-16}$$

where d is the movement of the cantilever read from the Hounsfield machine, and Δt is converted from the detected displacement of the echo reflected from the bottom surface of the sample. The speed of sound was computed in the repeatability test and its averaged value was used for all the remained tests to extract the deformations of the two layers by ultrasound. For the test in phantoms and porcine skin tissues, the stiffness was defined as:

$$E = \frac{F / S}{\Delta L / L} \tag{2-17}$$

where F is the force from the load cell, S is the contact surface area of the probe, ΔL is the deformation of the layer, and L is the original thickness of the layer. ΔL and L were both computed from the peak of the echo of the two-layer interface and the echo of the bottom base. The ratio F / S is called as the probe pressure and $\Delta L / L$ is called as the deformation ratio. Any shift of the contact surface was also counted in

the analysis by calculating the movement of the skin surface echo. The deformation information was calculated as the average of the results of the three typical lines in a RF image. The stiffness of the two layers was compared with each other both in the phantoms and *in-vitro* porcine skins.

4.1.3 Preliminary Tests on *in-Vivo* Human Skin

Tests were also conducted on human skin for three times in the forearm skin of one subject. Pressure was not recorded due to the absence of a portable force sensor in the current stage. A gentle pressure was gradually applied to the skin and a series of images were recorded continuously. The interval between two images recorded was approximately 0.1 ms. Recorded image series were used to calculate the deformation of the skin layer during the compression by employing a cross-correlation algorithm for two ROIs selected as the skin surface and the dermis-subcutaneous fat interface. Experiment was carried out to see whether the deformation of the skin layer could be successfully extracted under the compression. If this was successful, then measurement of the skin stiffness would be easier to be accomplished given that the applied force is simultaneously recorded in the future experimental setup.

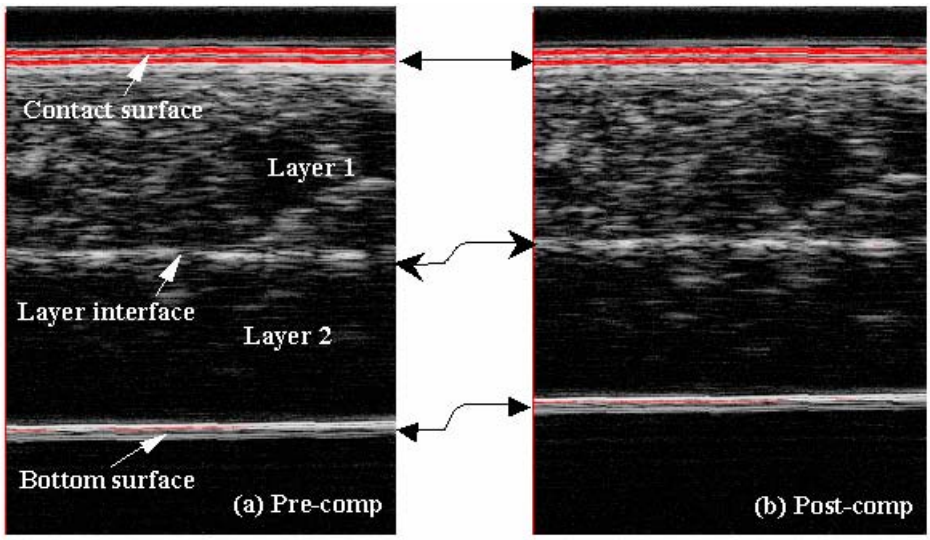

Figure 4-3. Two images show the PVA phantom (a) before and (b) after the compression.

4.2 Preliminary Results

4.2.1 Phantom Test

Figure 4-3 shows the phantom images before and after the compression. In the upper layer, there was quite a lot of ultrasonic scattering due to the existence of

graphite powder while in the lower layer the scattering was very weak, probably due to the attenuation and the reflection of ultrasound at the layer interface. The interface between the two layers could be obviously seen in the images. The shifting of the layer interface and the bottom reflection was evidently observed in the figure. The tracking of the interface shifting was quite successful and the deformation of the two layers could be computed separately.

The speed of the sound in the test phantom was calculated (Table 4-1). The mean speed of sound was 1541 ± 25 m/s, which was in the range reported in previous literature (Fromageau et al., 2003). In the subsequent analysis, the mean speed of sound was used.

Table 4-1 The speed of sound measured in the three phantoms

Phantoms	***1***	***2***	***3***	***Overall mean***
Speed (m/s)	*1570 (72)*	*1525 (22)*	*1528 (15)*	*1541 (25)*

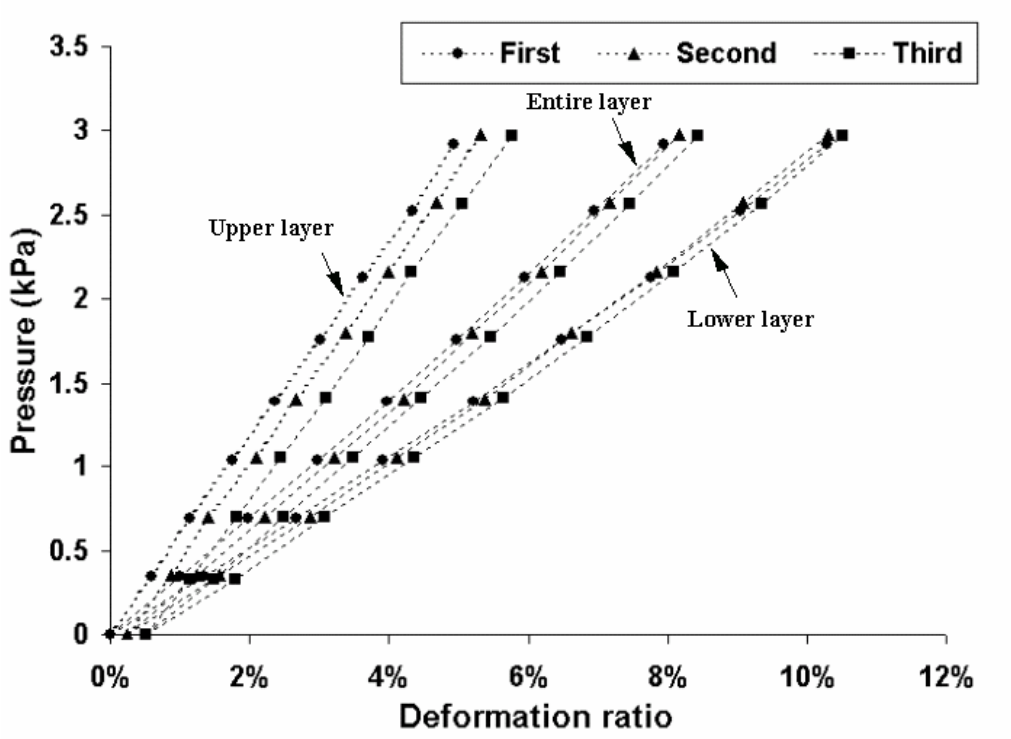

Figure 4-4. Typical relationship of the applied pressure and the deformation ratio for three repeated tests of one phantom. Note that the deformation ratios of the second and third test are shifted to the right by 0.25% and 0.50%, respectively, to make the curves more clearly displayed in the figure.

Figure 4-4 shows the typical relationship between the probe pressure and the deformation ratio of the separate and the entire layers. The deformation was generally

less than 15% of the original thickness and the test was highly repeatable. Quantitative results showed that the coefficient of variance for the stiffness was small, usually less than 4% with one exception (Table 4-2). Therefore, it suggested that this method was reliable for measuring the elasticity of thin materials.

Table 4-2 Reliability test for the three phantoms

Phantom		*First (kPa)*	*Second (kPa)*	*Third (kPa)*	*Mean (kPa)*	*CV (%)**
1	*Upper*	*59.9*	*52.8*	*47.3*	*53.3*	*11.8*
	Lower	*27.3*	*28.5*	*29.2*	*283*	*3.4*
2	*Upper*	*48.0*	*48.4*	*49.0*	*48.5*	*1.0*
	Lower	*26.8*	*27.3*	*27.7*	*27.3*	*1.7*
3	*Upper*	*58.8*	*58.3*	*56.9*	*58.0*	*1.7*
	Lower	*28.4*	*29.6*	*29.5*	*29.2*	*2.3*

***CV: coefficient of variance.**

Figure 4-5 shows the typical relationship between the applied pressure and the deformation ratio of the two separate layers for two tests of one phantom. The results all showed a larger slope for the stiffer layer no matter whether this layer was on top or not during the test. However, due to the geometrical nonlinearity of the compression configuration, i.e. not a pure uniaxial compression, the stiffness obtained for each layer in these two cases changed a lot, especially for the soft layer. Figure 4-6 and Table 4-3 show the results from the paired tests on the six phantoms. The mean thickness of the stiff and soft layer of the phantom was 2.47 ± 0.23 mm and 2.98 ± 0.21 mm, respectively. For all the six phantoms, the results showed that the stiffness was larger in the phantoms with more cycles of frozen-thawing processes, which was consistent with the physical observation. Another observation was that the difference of the two layers could be discriminated more obviously when the stiff layer was on the top. The difference was 15.2 ± 4.7 kPa when the stiff layer was in contact with the probe, while it became 5.2 ± 1.5 kPa when the soft layer was on the top. This indicated that a severe nonlinear nature of the compression configuration given that the mechanical properties of the two layers in the phantom was not varied during the test.

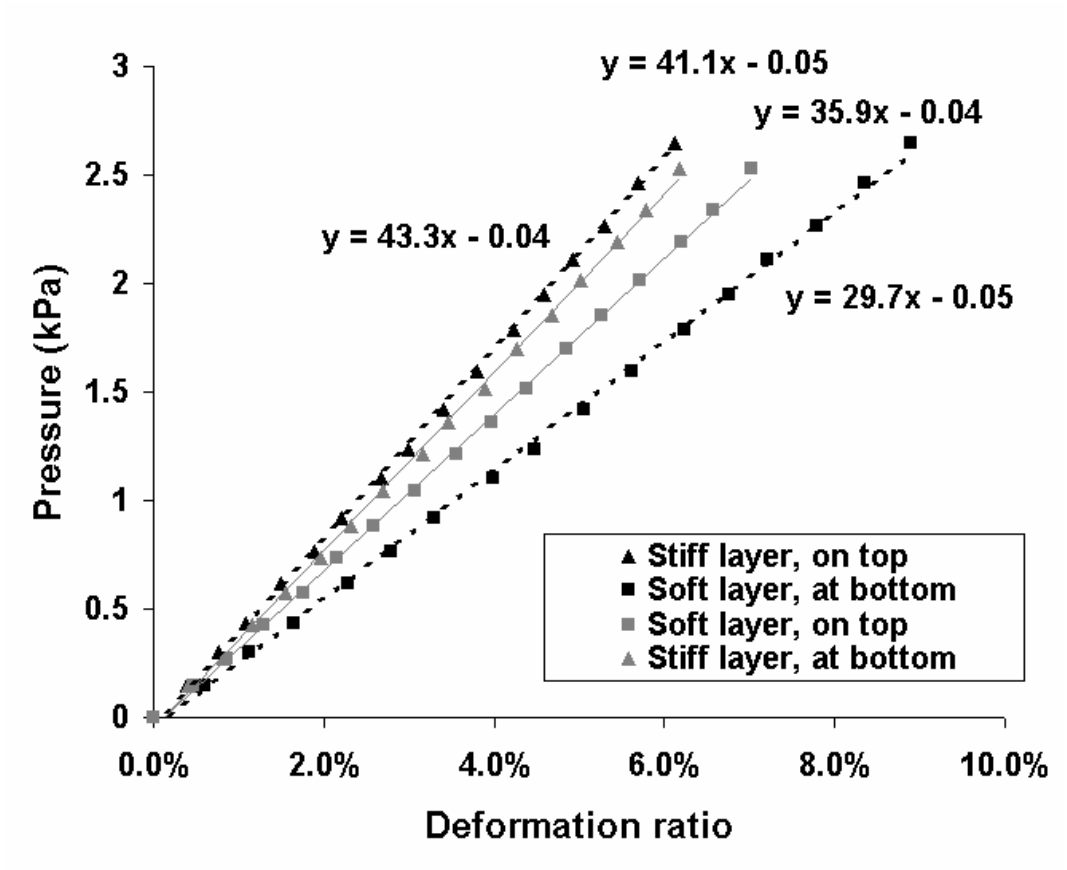

Figure 4-5. Typical relationship of the applied pressure and the deformation ratio for the two tests on one phantom. The phantom was tested twice with a change of the layer which contacted the probe.

Table 4-3 Test results of the stiffness of the six phantoms

Phantoms	***Stiff layer***			***Soft layer***		
	On top (kPa)	*At bottom (kPa)*	*Variation* (%)*	*On top (kPa)*	*At bottom (kPa)*	*Variation (%)*
1	*41.8*	*42.7*	*2.1*	*34.6*	*17.9*	*63.6*
2	*37.8*	*35.0*	*7.7*	*31.1*	*27.2*	*13.4*
3	*41.0*	*39.8*	*3.0*	*35.6*	*28.6*	*21.8*
4	*45.6*	*37.7*	*19.0*	*32.9*	*28.7*	*13.6*
5	*44.7*	*41.5*	*7.4*	*36.7*	*30.7*	*17.8*
6	*43.3*	*41.1*	*5.2*	*35.9*	*29.7*	*18.9*
Mean (SD)	*42.4 (2.8)*	*39.6 (2.8)*	*7.4 (6.1)*	*34.5 (2.1)*	*27.2 (4.7)*	*24.8 (19.3)*

Variation: ratio of the absolute difference to the mean. The data with the same shadowing indicate that they were obtained in pairs within one test.

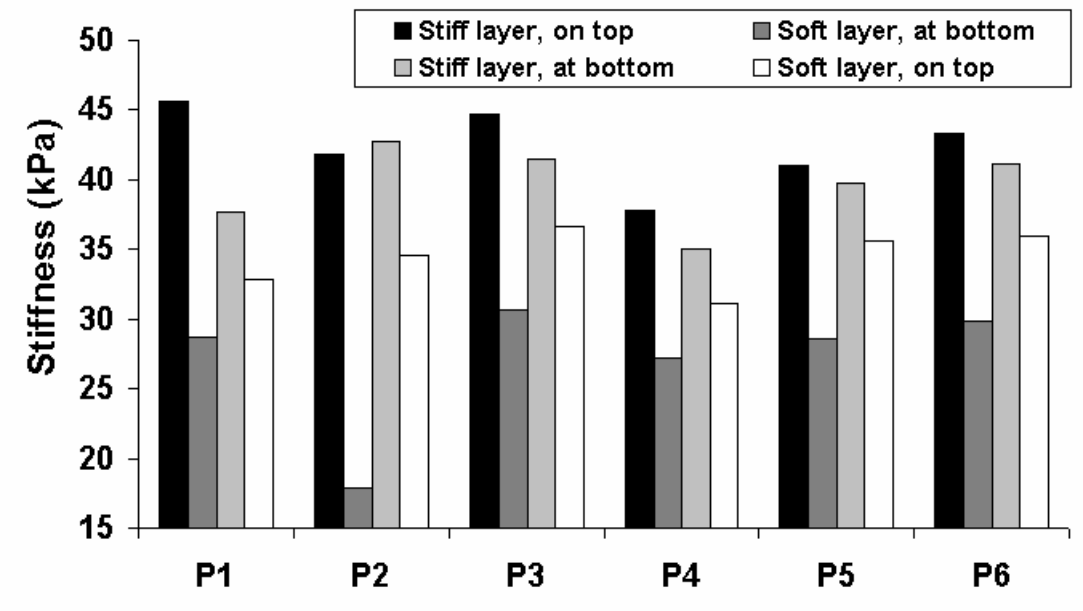

Figure 4-6. The stiffness of two layers for the 6 phantoms.

4.2.2 Experiment on Porcine Skin

The dermis appeared to be anechoic for the porcine skin *in vitro*, instead of a strong scattering observed *in vivo*, which might be induced by the change of physiological conditions in excised tissues, such as the removal of the internal tension. However, the interface between the dermis and hypodermis was still clear enough to be distinguished (Figure 4-7). Therefore, using this information, the measure of the deformation of the two layers was still possible.

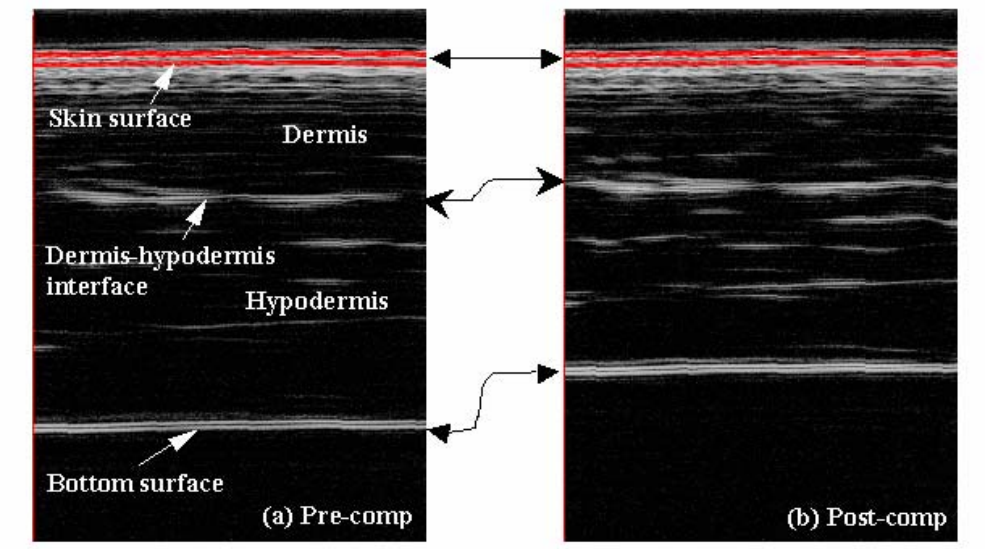

Figure 4-7. Two images show the *in-vitro* porcine skin (a) before and (b) after the compression.

The results showed that the slope of the pressure-deformation ratio curves was larger in the dermis than in the hypodermis for the three porcine tissues tested (Figure 4-8). The slope for the Specimen S1 was 24.8 kPa for the dermis and 11.5 kPa for the fat, respectively. It was 13.5 kPa and 5.7 kPa for the Specimen S2, 31.2 kPa and 9.0 kPa for the Specimen S3, respectively. The test not only showed layer difference, but also the inter-specimen variations. It should also be noted that the difference of the stiffness of different layer was partially caused by the nonlinearity of the compression configuration used in this study.

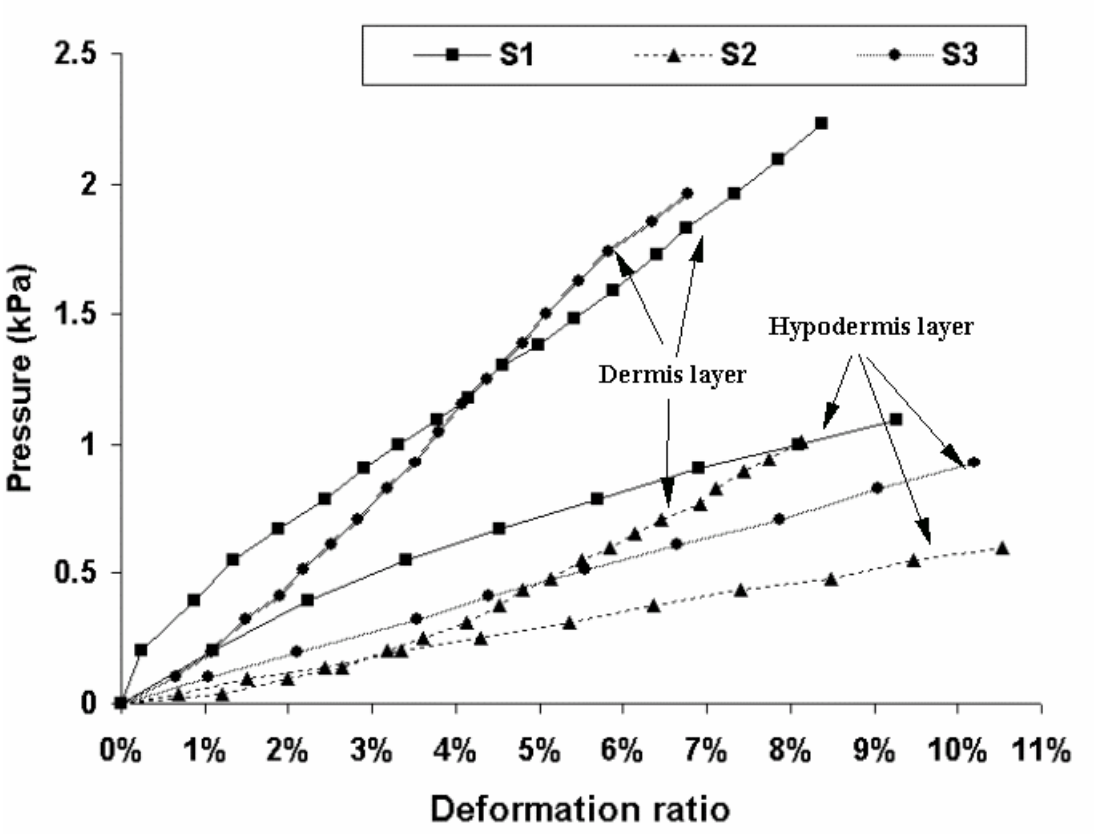

Figure 4-8. The relationship of the applied pressure and the deformation ratio of the dermis and hypodermis of the three porcine skin specimens tested *in vitro*.

4.2.3 Preliminary Results on Human Skin *in Vivo*

Preliminary *in vivo* tests showed that the deformation of the skin could be successfully derived from the images obtained by the high frequency ultrasonic skin imaging system (Figure 4-9). Due to the unavailability of the force information during loading, to calculate the skin stiffness was not possible. The preliminary measurements served as a feasibility test for this modified skin scanner to measure the skin elasticity. Further investigations are suggested in the Discussion section.

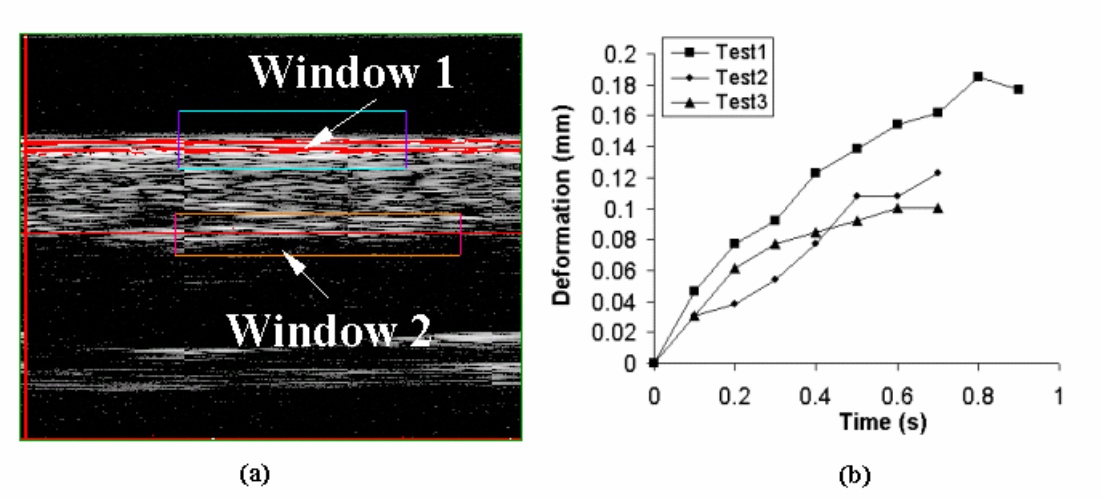

Figure 4-9. (a) An image of a human skin *in vivo* with two tracking windows for the extraction of its deformation; (b) The deformation of the *in-vivo* skin of three tests without the record of the load. The deformation is defined as the displacement difference of the two tracking windows.

4.3 Discussion

With the minor revisions and some improvements, the 20-MHz ultrasonic imaging system for skin had been utilized as a tool to measure the elasticity of thin materials. In this study, it was used associated with the standard testing machine in lack of attaching a proper load sensor to the probe. Our results of phantoms (n = 6) showed that the test was reliable with a CV less than 4% with only one exception. In this preliminary study, the ultrasound probe of the skin scanner was used to compress the phantoms and tissues. The test configuration was actually an indentation because the surface of the phantom was much larger than that of the probe. During the compression, the phantom was not confined and thus inhomogeneous bound conditions would cause some uncertainties to the repeatability of the test.

Results of the 6 phantoms comprising of two layers with different stiffness showed that the stiffness depended on whether the layer was placed on the top or at the bottom. The results of the 6 phantoms consistently showed that the stiffness of the stiff layer became smaller and that of the soft layer became larger when the top layer was changed from the stiffer layer to the softer layer. The stiffness of the two layers could be differentiated more distinctively when the stiff layer was on the top. This observation appeared difficult to be explained by the theoretical axial stress distribution in a semi-infinite elastic medium (Ophir et al., 1991, Appendix A). This might due to the reason that in this study the thickness of the phantom was small rather than infinite to the dimension of the probe tip. The axial stress distribution

might be different when the thickness of the phantom was less than the indenter. Theoretical analysis or computational simulation using tools such as the finite element analysis is necessary in further investigations in order to extract the stiffness of the two layers more precisely (Han et al., 2003). All the tests on six phantoms showed that the stiffer layer fabricated with more cycles of freezing and thawing could be discriminated by the test. The results of the porcine skin were similar to those of the phantoms. These preliminary tests demonstrated that the modified ultrasound skin scanner was able to measure and distinguish the stiffness of several layers of a thin tissue.

The preliminary test on human skins *in vivo* showed that the deformation of the skin layer was trackable on the B-mode images. The deformation of the skin layer could be up to 0.2 mm as tested using a normal pressure. Therefore, if a load sensor could be attached to the probe, the measurement of the load during the compression was also feasible and the quantification of the skin layer stiffness could come into reality. The potential applications of the measurement of the skin stiffness include the assessment of the degree of skin fibrosis and the efficacies of cosmetic medicines. Future studies toward the improvement of the system and its applications are definitely required before meaningful results can be achieved based on the preliminary study presented in this part.

5. Summary on Objectives and Achievements of This Study

For the first objective, the nonlinear and viscoelastic parameters indicating the mechanical properties of the irradiated neck soft tissues were obtained. Correlations of the mechanical properties and the severity of fibrosis were found for the two elastic parameters but not for the two viscous parameters. Thus the nonlinear elastic parameters appeared to be more powerful than the viscous parameters to characterize the degree of fibrosis.

For the second objective, basic information about the ultrasonic parameters, the statistical parameters and the skin thickness were reported and compared between the normal subjects and the patients and among patient subgroups. Some of these parameters had been demonstrated to be significantly different between the patients and the normal subjects. These differences were attributable to the typical changes of collagen and water content in the fibrotic tissues. However, to use them as a standard to assess the severity of radiation-induced fibrosis was not possible at the current stage. Further studies are necessary to clarify the relationship between these parameters and the severity of fibrosis.

For the third objective, the preliminary ultrasonic elasticity measurement was demonstrated to be capable of differentiating the stiffness of two layers in the phantoms and porcine skins *in vitro* and measuring the deformation of the skin layer *in vivo* in a compression test. Thus with further improvement of the system (combined with a load cell), it could be used to measure the stiffness of skin *in vivo*.

6. Conclusions and Future Research Directions

In this thesis, the nonlinear viscoelastic properties of the fibrotic neck soft tissues were studied using the quasi-linear viscoelastic model extended from a nonlinear solution of the indentation test. The feasibility of the use of high frequency ultrasound in terms of both RF signal and B-mode image to measure the acoustic properties, the statistical parameters and the skin thickness in order to quantitatively and objectively assess the skin fibrosis was investigated by comparing the results obtained from the normal subjects and the patients after radiotherapy who had different degrees of this late sequela. In addition, an ultrasonic microscopic system was preliminarily developed to measure and differentiate the stiffness of thin materials with different layers. Conclusions were drawn as follows:

1. The initial modulus and nonlinear factor of the patients with neck tissue fibrosis were significantly larger than those of the normal subjects. In fibrotic tissues, the stiffness was initially larger and increased more rapidly with higher degree of fibrosis;

2. The irradiated neck soft tissue in patients required a significantly longer time to relax after step indentation and relaxed to a significantly less extent at the equilibrium in the indentation process. In fibrotic tissues, no trend of the viscous properties was demonstrated to be associated with the severity of fibrosis;

3. The measurement of the acoustic properties of the skin using the 20-MHz ultrasonic imaging system was reliable and it was thus applied to test the feasibility of such measurement for the quantitative and objective assessment of skin fibrosis;

4. The attenuation slope and integrated attenuation was demonstrated to be age-independent. A significant decrease of attenuation slope and a significant increase of integrated attenuation were found in the fibrotic neck skin, but not in the palmar forearm skin. While the integrated backscatter was found to be age-dependent in the normal forearm skin, its relative representation in terms of the individual difference between the neck skin and the forearm skin showed a significant decrease in the fibrotic neck skin. In the neck skins of the patient subgroups with different degrees of neck tissue fibrosis, comparison of age-matched patients showed neither a consistent trend for the acoustic properties and the degree of fibrosis, nor a significant correlation between the acoustic properties and the effective Young's modulus of the

neck soft tissue. This might be due to the factor that the palpation score and the Young's modulus were a direct reflection of fibrosis of the entire neck soft tissue, but not specifically that of the skin;

5. The three ultrasonic parameters (β , IA , IBS) were correlated with each other, which might imply common elements existing in the skin that interact with the ultrasound and strongly affect the acoustic properties of the skin;

6. The statistical parameters of the envelope signal were demonstrated to be age-dependent. However, a weakly significant difference was found between the irradiation-affected neck skin and the non-affected forearm skin in the patients. In the skins of the patients who were divided into two subgroups with equivocal and severe fibrosis respectively, the effects of fibrosis were demonstrated to be significant and inverse to those of the ageing process;

7. The skin thickness increased significantly as a result of fibrosis. But a significant correlation of the skin thickness with the palpation score and the stiffness was not demonstrated;

8. Preliminary experiments showed that the test of the ultrasonic system for measuring skin elasticity was reliable and this system was capable of measuring and differentiating the stiffness of two layers in thin phantoms and porcine skins. The potential of this system to measure the stiffness of skin layer *in vivo* was demonstrated.

However, it should be noted that some of the conclusions were preliminary and some were drawn based on a series of hypotheses as explained in the context. Some uncertain factors were associated when the conclusions were claimed. Further investigations are still necessary to clarify those uncertainties and confirm the accuracy of the current conclusions. Research directions that are worth being investigated in the future studies include:

1. To investigate the factors such as the tissue compositions that are intrinsically related to the various aspects studied in the current project, including the nonlinear mechanical properties, the acoustic properties and the statistical parameters. Based on the current findings and those reported in the literature, it is especially important to measure the change of collagen and water content in the fibrotic tissue because the mechanical and acoustic properties are closely related to these two elements;

2. To incorporate some other methods such as the creep and stress relaxation test or develop other models in simulations of the indentation data to study the mechanics of soft tissues so that more quantitative information can boost the evaluation of soft tissue fibrosis;

3. To quantify the accuracy and sensitivity of fibrosis assessment using elastic parameters of QLV model by incorporating gold standard for assessing fibrosis;

4. To improve the algorithms for extracting acoustic properties from the collected radio frequency signal. The extraction of the acoustic properties inherent to tissue involves a lot of processing to exclude the data acquisition system dependent effects and a lot of compensation algorithms have been proposed to achieve such a goal. It is necessary to pursue more robust algorithms that will improve the stability, accuracy and precision of our measurement so that our method can be more sensitive to detect the skin modification induced by fibrosis. However, it is of importance that the improved test should not be time-consuming and must be cost effective because a clinical environment will not permit too complex a test;

5. To introduce the advancing techniques of digital image processing to process the skin images using the high frequency ultrasonic imaging system so that more features can be extracted from the fibrotic skin which may be helpful for the diagnosis of fibrosis;

6. To perform experimental tests by recruiting patients before and after the radiotherapy in order to observe the genuine effect of fibrosis on the ultrasonic properties by excluding other confounding factors that might exist in this study;

7. To measure the mechanical properties of skin as the representation of its fibrosis. One limitation of the current study was that the degree of the skin fibrosis was assessed by indirect evaluation of the fibrosis of the bulk soft tissue. Although it is reasonable to assume that the elastic properties of the skin are related to the degree of fibrosis due to the increased collagen content, no evidence shows in practice that the fibrosis of the entire soft tissue is also a reflection of that of the skin. Measurement of skin elasticity using other approaches is desired;

8. To further develop our elastomicroscopic system to make this system capable of measuring the stiffness of the skin layer in vivo.

Appendices

Appendix I Letter to Invite the Patients to Attend the Clinical Experiment

尊敬的先生/女士：

本人是香港理工大學賽馬會康復科技中心的研究生，現正在進行一個名為『超聲評估組織纖維化』的項目研究，目的是為了更好的對放射性治療後組織纖維化程度進行定量和客觀化的評估。我們已經得到閣下主診醫生的批准，在醫院進行研究工作。

此信之目的是邀請閣下參與此項研究，我們會利用超聲儀器在你的脖子和手臂部位採集一些數據，需時約 30 分鐘。

你並不必須參與此項研究，你的決定亦不會影響你的治療。如果參與研究，你的一切資料亦都會得到保密，我們不會把它泄漏給任何人。

如果你同意參加此項研究，請你填妥同意書。

如果你希望認識及了解更多關於此項的研究工作，請致電給我們：27667664

多謝閣下參與和合作。

研究人員
黃燕平
賽馬會康復科技中心
香港理工大學

指導研究人員
梁承暉博士
臨床腫瘤科
威爾斯親王醫院

研究負責人
鄭永平博士
賽馬會康復科技中心
香港理工大學

Appendix II Consent Form for Subjects Who Agreed to Attend the Experiment of Collection of Ultrasound Data in Skin

Consent Form

I, _____(name of subject), hereby consent to participate in, as a subject, the research program "Ultrasonic assessment of tissue fibrosis".

- I have understood the experimental procedures presented to me.
- I have been given an opportunity to ask questions about the experiment, and these have been answered to my satisfaction.
- I realize I can discontinue the experiment with no reasons given and no penalty received during the experiment.
- I realize that the results of this experiment may be published, but that my own results will be kept confidential. My personal information, including the experimental record, will be destroyed after the project is finished.
- I realize that the results of this experiment are the properties of The Hong Kong Polytechnic University and The Prince of Wales Hospital.
- I agree that the PI and the project research members, who obtained the authorization from the PI, can use my experimental data for this project study.

Subject name: _____ Signature: _____
Witness: _____ Signature: _____
Date: _____

同意書

我, _____ (受試者姓名), 在此同意作為受試者參加超聲評估組織纖維化"研究項目。

- 我已明白到該測試的步驟。
- 我已給予機會詢問有關該測試的問題, 並已獲得滿意的回答。
- 我已知道我可以終止測試而無需給予任何理由, 或由此而受到任何懲罰。
- 我已知道這個測試的結果可被發表, 但有關我個人的結果將獲得保密。我的個人信息包括我的實驗記錄在此項目結束後會被消除。
- 我已知道這個測試的結果屬香港理工大 學和香港威爾斯親王醫院。
- 我同意本項目負責人及其受權的項目研究人員使用我的實驗記錄以作此項目的研究。

受試者姓名_____ 簽署_____
作證人姓名_____ 簽署_____
日期_____

Bibliography

Alexander H, Cook TH, 1977. Accounting for natural tension in the mechanical testing of human skin. J Invest Dermatol 69:310-314

Alexander H, Miller DL, 1979. Determining skin thickness with pulsed ultra sound. J Invest Dermatol 72:17-19

Altman DG, 1991. *Practical Statistics for Medical Research*, 1st ed., Chapman & Hall, London

Altmeyer P, El-Gammal S, Hoffmann K, 1992a. *Ultrasound in Dermatology*, Spring-Verlag, Berlin Heidelberg

Altmeyer P, Hoffmann K, Stucker M, Goertz S, El-Gammal S, 1992b. General phenomena of ultrasound in dermatology. In "*Ultrasound in Dermatology*", (eds) Altmeyer P, El-Gammal S, Hoffmann K, Spring-Verlag, Berlin Heidelberg, pp.55-79

Balbir-Gurman A, Denton CP, Nichols B, Knight CJ, Nahir AM, Martin G, Black CM, 2002. Non-invasive measurement of biomechanical skin properties in systemic sclerosis. Ann Rheum Dis 61:237-241

Baldeweck T, Laugier P, Herment A, Berger G, 1995. Application of autoregressive spectral analysis for ultrasound attenuation estimation: interest in highly attenuating medium. IEEE Trans Ultrason Ferroelect Freq Contr 42:99-110

Bamber JC, Fry MJ, Hill CR, Dunn F, 1977. Ultrasonic attenuation and backscattering by mammalian organs as a function of time after excision. Ultrasound Med Biol 3:15-20

Best TM, McElhaney J, Garrett WE, Jr, Myers BS, 1994. Characterization of the passive responses of live skeletal muscle using the quasi-linear theory of viscoelasticity. J Biomech 27:413-419

Bhagat PK, Kerrick W, Ware RW, 1980. Ultrasonic characterization of aging in skin tissue. Ultrasound Med Biol 6:369-375

Bland JM, Altman DG, 1986. Statistical methods for assessing agreement between two methods of clinical measurement. Lancet 327:307-310

Bridal SL, Fornes P, Bruneval P, Berger G, 1997. Correlation of ultrasonic attenuation (30 to 50 MHz) and constituents of atherosclerotic plaque. Ultrasound Med Biol 23:691-703

Brink JA, Sheets PW, Dines KA, Etchison MR, Hanke CW, Sadove AM, 1986. Quantitative assessment of burn injury in porcine skin with high-frequency ultrasonic imaging. Invest Radiol 21:645-651

Chivers RC, 1981. Tissue characterization. Ultrasound Med Biol 7:1-20

Ciulla M, Paliotti R, Hess DB, Tjahja E, Campbell SE, Magrini F, Weber KT, 1997. Echocardiographic patterns of myocardial fibrosis in hypertensive patients: endomyocardial biopsy versus ultrasonic tissue characterization. J Am Soc Echocardiogr 10:657-664

Cole GW, Handler SJ, Burnett K, 1981. The ultrasonic evaluation of skin thickness in scleredema. J Clin Ultrasound 9:501-503

Cosnes A, Anglade MC, Revuz J, Radier C, 2003. Thirteen-megahertz ultrasound probe: its role in diagnosing localized scleroderma. Br J Dermatol 148:724-729

Culav EM, Clark CH, Merrilees MJ, 1999. Connective tissues: matrix composition and its relevance to physical therapy. Phys Ther 79:308-319

Dao TH, Rahmouni A, Campana F, Laurent M, Asselain B, Fourquet A, 1993. Tumor recurrence versus fibrosis in the irradiated breast: differentiation with dynamic gadolinium-enhanced MR imaging. Radiology 187:751-755

Davis AM, Dische S, Gerber L, Saunders M, Leung SF, O'Sullivan B, 2003. Measuring postirradiation subcutaneous soft-tissue fibrosis: state-of-the-art and future directions. Semin Radiat Oncol 13:203-213

De Korte CL, Ignacio Cespedes EI, Van der Steen AFW, Lancee CT, 1997. Intravascular elasticity imaging using ultrasound: feasibility studies in phantoms. Ultrasound Med Biol 23:735-746

De Korte CL, Doyley MM, Carlier SG, Mastik F, Van der Steen AFW, Serruys PW, Bom N, 2000. High resolution IVUS elastography in patients. IEEE Ultrason Symp Proc, pp.1767-1770

De Korte CL, Sierevogel MJ, Mastik F, Strijder C, Schaar JA, Velema E, Pasterkamp G, Serruys PW, Van der Steen AFW, 2002. Identification of atherosclerotic plaque components with intravascular ultrasound elastography *in vivo*: a Yucatan pig study. Circulation 105:1627-1630

De Korte CL, Van der Stein AFW, 2002. Intravascular ultrasound elastography: an overview. Ultrasonics 40:859-865

De Rigal J, Escoffier C, Querleux B, Faivre B, Agache P, Leveque JL, 1989. Assessment of aging of the human skin by *in vivo* ultrasonic imaging. J Invest Dermatol 93:621-625

Denham JW, Hauer-Jensen M, 2002. The radiotherapeutic injury – a complex 'wound'. Radiother Oncol 63:129-145

Dines KA, Sheets PW, Brink JA, Hanke CW, Condra KA, Clendenon JL, Goss SA, Smith DJ, Franklin TD, 1984. High frequency ultrasonic imaging of skin: experimental results. Ultrason Imag 6:408-434

Diridollou S, Patat F, Gens F, Vaillant L, Black D, Lagarde JM, Gall Y, Berson M, 2000. *In vivo* model of the mechanical properties of the human skin under suction. Skin Res Tech 6:214-221

Dische S, Saunders MI, 1999. The CHART regimen and morbidity. Acta Oncol 38:147-152

Eich HT, Eich PD, Stuschke M, Muller RD, Sack H, 1999. CT densitometry for the grading of subcutaneous fibrosis after the photon-neutron therapy of malignant salivary gland tumors. Strahlenther Onkol 175:128-132

Eisenbeiss C, Welzel J, Eichler W, Klotz K, 2001. Influence of body water distribution on skin thickness: measurements using high-frequency ultrasound. Br J Dermatol 144:947-951

Feleppa EJ, Yaremko MM, 1987. Ultrasonic tissue characterization for diagnosis and monitoring. IEEE Eng Med Biol Mag 6:18-26

Ferguson-Pell M, Hagisawa S, Masiello RD, 1994. A skin indentation system using a pneumatic bellows. J Rehabil Res Dev 31:15-19

Fink MA, Cardoso JF, 1984. Diffraction effects in pulsed-echo measurement. IEEE Trans Sonics Ultrason 31:313-329

Fink M, Hottier F, Cardoso JF, 1983. Ultrasonic signal processing for *in vivo* attenuation measurement: short time Fourier analysis. Ultrason Imag 5:117-135

Fornage BD, McGavran MH, Duvic M, Waldron CA, 1993. Imaging of the skin with 20-MHz US. Radiology 189:69-76

Forster FK, Olerud JE, Riederer-Henderson MA, Holmes AW, 1990. Ultrasonic assessment of skin and surgical wounds utilizing backscatter acoustic techniques to estimate attenuation. Ultrasound Med Biol 16:43-53

Fournier C, Bridal SL, Berger G, Laugier P, 2001. Reproducibility of skin characterization with backscattered spectra (12-25 MHz) in healthy subjects. Ultrasound Med Biol 27:603-610

Fournier C, Bridal SL, Coron A, Laugier P, 2003. Optimization of attenuation estimation in reflection for *in vivo* human dermis characterization at 20 MHz. IEEE Trans Ultrason Ferroelect Freq Contr 50:408-418

Franklin TJ, 1997. Therapeutic approaches to organ fibrosis. Int J Biochem Cell Biol 29:79-89

Fromageau J, Brusseau E, Vray D, Gimenez G, Delachartre P, 2003. Characterization of PVA cryogel for intravascular ultrasound elasticity imaging. IEEE Trans Ultrason Ferroelect Freq Contr 50:1318-1324

Fung YC, 1981. Bio-viscoelastic solids. In "*Biomechanics: Mechanical Properties of Living Tissues*", (eds) Fung YC, Springer-Verlag, New York, pp.196-260

Funk JR, Hall GW, Crandall JR, Pilkey WD, 2000. Linear and quasi-linear viscoelastic characterization of ankle ligaments. J Biomech Eng-Trans ASME 122:15-22

Garra BS, Cespedes EI, Ophir J, Spratt SR, Zuurbier RA, Magnant CM, Pennanen MF, 1997. Elastography of breast lesions: initial clinical results. Radiology 202:79-86

Gefen A, Megido-Ravid M, Azariah M, Itzchak Y, Arcan M, 2001. Integration of plantar soft tissue stiffness measurements in routine MRI of the diabetic foot. Clin Biomech 16:921-925

Gennisson JL, Baldeweck T, Tanter M, Catheline S, Fink M, Sandrin L, Cornillon C, Querleux B, 2004. Assessment of elastic parameters of human skin using dynamic elastography. IEEE Trans Ultrason Ferroelect Freq Contr 51:980-989

Glazer HS, Lee JK, Levitt RG, Heiken JP, Ling D, Totty WG, Balfe DM, Emani B, Wasserman TH, Murphy WA, 1985. Radiation fibrosis: differentiation from recurrent tumor by MR imaging. Radiology 156:721-726

Gniadecka M, 2001. Effects of ageing on dermal echogenicity. Skin Res Tech 7:204-207

Gniadecka M, Jemec GBE, 1998. Quantitative evaluation of chronological ageing and photoageing *in vivo*: studies on skin echogenicity and thickness. Br J Dermatol 139:815-821

Gniadecka M, Quistorff B, 1996. Assessment of dermal water by high-frequency ultrasound: comparative studies with nuclear magnetic resonance. Br J Dermatol 135:218-224

Gong QY, Zheng GL, Zhu HY, 1991. MRI differentiation of recurrent nasopharyngeal carcinoma from postirradiation fibrosis. Comput Med Imaging Graph 15:423-429

Goss SA, Dunn F, 1980. Ultrasonic propagation properties of collagen. Phys Med Biol 25:827-837

Goss SA, Johnston RL, Dunn F, 1978. Comprehensive compilation of empirical ultrasonic properties of mammalian tissues. J Acoust Soc Am 64:423-457

Goss SA, Johnston RL, Dunn F, 1980. Compilation of empirical ultrasonic properties of mammalian tissues. II. J Acoust Soc Am 68:93-108

Gottlober P, Kerscher MJ, Korting HC, Peter RU, 1997. Sonographic determination of cutaneous and subcutaneous fibrosis after accidental exposure to ionising radiation in the course of the Chernobyl nuclear power plant accident. Ultrasound Med Biol 23:9-13

Gottlober P, Steinert M, Bahren W, Weber L, Gerngross H, Peter RU, 2001. Interferon-gamma in 5 patients with cutaneous radiation syndrome after radiation therapy. Int J Radiat Oncol Biol Phys 50:159-166

Guittet C, Ossant F, Remenieras JP, Pourcelot L, Berson M, 1999a. High-frequency estimation of the ultrasonic attenuation coefficient slope obtained in human skin: simulation and *in vivo* results. Ultrasound Med Biol 25:421-429

Guittet C, Ossant F, Vaillant L, Berson M, 1999b. *In vivo* high-frequency ultrasonic characterization of human dermis. IEEE Trans Biomed Eng 46:740-746

Han L, Noble JA, Burcher M, 2003. A novel ultrasound indentation system for measuring biomechanical properties of *in vivo* soft tissues. Ultrasound Med Biol 29:813-823

Hayes WC, Keer LM, Herrmann G, Mockros LF, 1972. A mathematical analysis for indentation tests of articular cartilage. J Biomech 5:541-551

Hoffmann J, Gerbaulet U, El-Gammal S, Altmeyer P, 1991. 20-MHz B-mode ultrasound in monitoring the course of localized scleroderma (morphea). Acta Dermatol Venereol 164:S3-16

Hoffmeister BK, Wong AK, Verdonk ED, Wickline SA, Miller JG, 1995. Comparison of the anisotropy of apparent integrated ultrasonic backscatter from fixed human tendon and fixed human myocardium. J Acoust Soc Am 97:1307-1313

Hojris I, Andersen J, Overgaard M, Overgaard J, 2000. Late treatment-related morbidity in breast cancer patients randomized to postmastectomy radiotherapy and systemic treatment versus systemic treatment alone. Acta Oncol 39:355-372

Hopewell JW, 1990. The skin: its structure and response to ionizing radiation. Int J Radiat Biol 57:751-773

Hounsfield GN, 1973. Computerized transverse axial scanning (tomography). I. Description of system. Br J Radiol 46:1016-1022

Hsu TC, Wang CL, Shau YW, Tang FT, Li KL, Chen CY, 2000. Altered heel-pad mechanical properties in patients with type 2 diabetes mellitus. Diabet Med 17:854-859

Hsu TC, Wang CL, Tsai WC, Kuo JK, Tang FT, 1998. Comparison of the mechanical properties of the heel pad between young and elderly adults. Arch Phys Med Rehabil 79:1101-1104

Huisman HJ, Thijssen JM, 1996. Precision and accuracy of acoustospectrographic parameters. Ultrasound Med Biol 22:855-871

Huisman HJ, Thijssen JM, Wagener DJ, Rosenbusch GJ, 1998. Quantitative ultrasonic analysis of liver metastases. Ultrasound Med Biol 24:67-77

Ihn H, Shimozuma M, Fujimoto M, Sato S, Kikuchi K, Igarashi A, Soma Y, Tamaki K, Takehara K, 1995. Ultrasound measurement of skin thickness in systemic sclerosis. Br J Rheum 34:535-538

Jemec GBE, Gniadecka M, Ulrich J, 2000. Ultrasound in dermatology. Part I. High frequency ultrasound. Eur J Dermatol 10:492-497

Johansen J, Taagehoj F, Christensen T, Overgaard J, Overgaard M, 1994. Quantitative magnetic resonance for assessment of radiation fibrosis after post-mastectomy radiotherapy. Br J Radiol 67:1238-1242

Johnson GA, Tramaglini DM, Levine RE, Ohno K, Choi NY, Woo SLY, 1994. Tensile and viscoelastic properties of human patellar tendon. J Orthop Res 12:796-803

Kalis B, De Rigal J, Leveque JL, De Riche O, Corre YL, Lacharriere OD, 1990. *In vivo* study of scleroderma by non-invasive techniques. Br J Dermatol 122:785-791

Kawchuk GN, Elliott PD, 1998. Validation of displacement measurements obtained from ultrasonic images during indentation testing. Ultrasound Med Biol 24:105-111

Klaesner JW, Commean PK, Hastings MK, Zou D, Mueller JM, 2001. Accuracy and reliability testing of a portable soft tissue indentor. IEEE Trans Neur Sys Rehabil Eng 9:232-240

Klaesner JW, Hastings MK, Zou D, Lewis C, Mueller MJ, 2002. Plantar tissue stiffness in patients with diabetes mellitus and peripheral neuropathy. Arch Phys Med Rehabil 83:1796-1801

Komiyama N, Berry GJ, Kolz ML, Oshima A, Metz JA, Preuss P, Brisken AF, Pauliina Moore M, Yock PG, Fitzgerald PJ, 2000. Tissue characterization of atherosclerotic plaques by intravascular ultrasound radiofrequency signal analysis: an *in vitro* study of human coronary arteries. Am Heart J 140:565-574

Kuc R, Schwartz M, 1979. Estimating the acoustic attenuation coefficient slope for liver from reflected ultrasound signals. IEEE Trans Sonics Ultrason 26:353-362

Laugier P, Fournier B, Berger G, 1996. Ultrasound parametric imaging of the calcaneus: *in vivo* results with a new device. Calcif Tissue Int 58:326-331

Lauterbur PC, 1973. Image formation by induced local interactions: examples employing nuclear magnetic resonance. Nature 242:190-191

Lebertre M, Ossant F, Vaillant L, Diridollou S, Patat F, 2002. Spatial variation of acoustic parameters in human skin: an *in vitro* study between 22 and 45 MHz. Ultrasound Med Biol 28:599-615

Lee Y, Hwang K, 2002. Skin thickness of Korean adults. Surg Radiol Anat 24:183-189

Leontiou I, Matthopoulos DP, Tzaphlidou M, Glaros D, 1993. The effect of gamma irradiation on collagen fibril structure. Micron 24:13-16

Leung SF, Zheng YP, Choi CYK, Mak SSS, Chiu SKW, Zee B, Mak AFT, 2002. Quantitative measurement of post-irradiation neck fibrosis based on the Young modulus: description of a new method and clinical results. Cancer 95:656-662

Li C, Wilson PB, Levine E, Barber J, Stewart AL, Kumar S, 1999. TGF-β1 levels in pre-treatment plasma identify breast cancer patients at risk of developing post-radiotherapy fibrosis. Int J Cancer 84:155-159

Lin T, Ophir J, Potter G, 1988. Correlation of ultrasonic attenuation with pathologic fat and fibrosis in liver disease. Ultrasound Med Biol 14:729-734

Lizzi FL, Greenebaum M, Feleppa EJ, Elbaum M, Coleman DJ, 1983. Theoretical framework for spectrum analysis in ultrasonic tissue characterization. J Acoust Soc Am 73:1366-1373

Lizzi FL, Ostromogilsky M, Feleppa EJ, Rorke MC, Yaremko MM, 1986. Relationship of ultrasonic spectral parameters to features of tissue microstructure. IEEE Trans Ultrason Ferroelect Freq Cont 33:319-329

Lobnig BM, Bender R, Maslowska-Wessel E, 2003. Repeatability of heart rate variability measured via spectral analysis in healthy subjects. J Clin Basic Cardiol 6:29-33

Lu MH, Zheng YP, 2004. Indentation test of soft tissues with curved substrates: a finite element study. Med Biol Eng Comput 42:535-540

Madsen EL, Dong F, Frank GR, Garra BS, Wear KA, Wilson T, Zagzebski JA, Miller HL, Shung KK, Wang SH, Feleppa EJ, Liu T, O'Brien WD, Jr, Topp KA, Sanghvi NT, Zaitsev AV, Hall TJ, Fowlkes JB, Kripfgans OD, Miller JG, 1999. Interlaboratory comparison of ultrasonic backscatter, attenuation, and speed measurements. J Ultrasound Med 18:615-631

Mak AFT, Lai WM, Mow VC, 1987. Biphasic indentation of articular cartilage I: theoretical analysis. J Biomech 20:703-714

Mak AFT, Liu GHW, Lee SY, 1994. Biomechanical assessment of below-knee residual limb tissue. J Rehabil Res Dev 31:188-198

Malinauskas M, Krouskop TA, Barry PA, 1989. Noninvasive measurement of the stiffness of tissue in the above-knee amputation limb. J Rehabil Res Dev 26:45-52

Marinus J, Niel CG, De Bie RA, Wiggenraad RG, Schoppink EM, Beukema LH, 2000. Measuring radiation fibrosis: the interobserver reliability of two methods of determining the degree of radiation fibrosis. Int J Radiat Oncol Biol Phys 47:1209-1217

Martin M, Lefaix JL, Delanian S, 2000. TGF-β_1 and radiation fibrosis: a master switch and a specific therapeutic target? Int J Radiat Oncol Biol Phys 47:277-290

Martin M, Remy J, Daburon F, 1989. Abnormal proliferation and aging of cultured fibroblasts from pigs with subcutaneous fibrosis induced by gamma irradiation. J Invest Dermatol 93:497-500

Moran CM, Bush NL, Bamber JC, 1995. Ultrasonic propagation properties of excised human skin. Ultrasound Med Biol 21:1177-1190

Mutsaers SE, Bishop JE, McGrouther G, Laurent GJ, 1997. Mechanisms of tissue repair: from wound healing to fibrosis. Int J Biochem Cell Biol 29:5-17

Nuutinen J, Lahtinen T, Turunen M, Alanen E, Tenhunen M, Usenius T, Kolle R, 1998. A dielectric method for measuring early and late reactions in irradiated human skin. Radiother Oncol 47:249-254

Obuchowski NA, 2003. Receiver operating characteristic curves and their use in radiology. Radiology 229:3-8

Olerud JE, O'Brien WD, Riederer-Henderson MA, Steiger DL, Debel JR, Odland GF, 1990. Correlation of tissue constituents with the acoustic properties of skin and wound. Ultrasound Med Biol 16:55-64

Olerud JE, O'Brien WD, Riederer-Henderson MA, Steiger DL, Forster FK, Daly C, Ketterer DJ, Odland GF, 1987. Ultrasonic assessment of skin and wound with the scanning laser acoustic microscope. J Invest Dermatol 88:615-623

Ophir J, Alam SK, Garra B, Kallel F, Konofagou E, Krouskop T, Varghese T, 1999. Elastography: ultrasonic estimation and imaging of the elastic properties of tissues. Proc Instn Mech Engrs 213, Part H, 203-233

Ophir J, Cespedes I, Ponnekanti H, Yazdi Y, Li X, 1991. Elastography: a quantitative method for imaging the elasticity of biological tissues. Ultrason Imag 13:111-134

Ophir J, Mehta D, 1988. Elimination of diffraction error in acoustic attenuation estimation via axial beam translation. Ultrason Imag 10:139-152

Ossant F, Patat F, Lebertre M, Teriierooiterai ML, Pourcelot L, 1998. Effective density estimators based on the K distribution: interest of low and fractional order moments. Ultrason Imag 20:243-259

Ottani V, Raspanti M, Ruggeri A, 2001. Collagen structure and functional implications. Micron 32:251-260

O'Sullivan B, Levin W, 2003. Late radiation-related fibrosis: pathogenesis, manifestations, and current management. Semin Radiat Oncol 13:274-289

Padhani AR, Yarnold JR, Regan J, Husband JE, 2002. Magnetic resonance imaging of induration in the irradiated breast. Radiother Oncol 64:157-162

Pan L, Zan L, Foster FS, 1998. Ultrasonic and viscoelastic properties of skin under transverse mechanical stress *in vitro*. Ultrasound Med Biol 24:995-1007

Pathak AP, Silver-Thorn MB, Thierfelder CA, Prieto TE, 1998. A rate-controlled indentor for *in vivo* analysis of residual limb tissues. IEEE Trans Rehabil Eng 6:12-20

Pedersen D, Bentzen SM, Overgard J. 1994. Early and late radiotherapeutic morbidity in 442 consecutive patients with locally advanced carcinoma of the uterine cervix. Int J Radiat Oncol Biol Phys 29:941-952

Pellacani G, Seidenari S, 1999. Variations in facial skin thickness and echogenicity with site and age. Acta Derm Venereol 79:366-369

Perez JE, Miller JG, 1991. Ultrasonic backscatter tissue characterization in cardiac diagnosis. Clin Cardiol 14:S4-9

Pinto JG, Patitucci PJ, 1980. Visco-elasticity of passive cardiac muscle. J Biomech Eng-Trans ASME 102:57-61

Polgar C, Forrai G, Szabo E, Riedl E, Fodor J, Fornet B, Nemeth G, 1999. Radiologic follow-up after breast-conserving surgery: value of MRI examination of the breast. Orv Hetil 140:2619-2625

Quaglino D Jr, Bergamini G, Boraldi F, Pasquali Ronchetti I, 1996. Ultrastructural and morphometrical evaluations on normal human dermal connective tissue – the influence of age, sex and body region. Br J Dermatol 134:1013-1022

Raju BI, Srinivasan MA, 2001. High-frequency ultrasonic attenuation and backscatter coefficients of *in vivo* normal human dermis and subcutaneous fat. Ultrasound Med Biol 27:1543-1556

Raju BI, Srinivasan MA, 2002. Statistics of envelope of high-frequency ultrasonic backscatter from human skin *in vivo*. IEEE Trans Ultrason Ferroelect Freq Contr 49:871-882

Raju BI, Swindells KJ, Gonzalez S, Srinivasan MA, 2003. Quantitative ultrasonic methods for characterization of skin lesions *in vivo*. Ultrasound Med Biol 29:825-838

Rallan D, Harland CC, 2003. Ultrasound in dermatology - basic principles and applications. Clin Exp Dermatol 28:632-638

Rankin G, Stokes M, 1998. Reliability of assessment tools in rehabilitation: an illustration of appropriate statistical analyses. Clin Rehabil 12:187-199

Remy J, Wegrowski J, Crechet F, Martin M, Daburon F, 1991. Long-term overproduction of collagen in radiation-induced fibrosis. Radiat Res 125:14-19

Reynolds DP, Lord M, 1992. Interface load analysis for computer-aided design of below knee prosthetic sockets. Med Biol Eng Comput 30:419-426

Riederer-Henderson MA, Olerud JE, O'Brien WD Jr, Forster FK, Steiger DL, Ketterer DJ, Odland GF, 1988. Biochemical and acoustical parameters of normal canine skin. IEEE Trans Biomed Eng 35:967-972

Riekki R, Jukkola A, Sassi ML, Hoyhtya M, Kallioinen M, Risteli J, Oikarinen A, 2000. Modulation of skin collagen metabolism by irradiation: collagen synthesis is increased in irradiated human skin. Br J Dermatol 142:874-880

Roberjot V, Bridal SL, Laugier P, Berger G, 1996. Absolute backscatter coefficient over a wide range of frequencies in a tissue-mimicking phantom containing two populations of scatterers. IEEE Trans Ultrason Ferroelect Freq Contr 43:970-978

Roberjot V, Laugier P, Berger G, 1994. Anisotropy in bovine skeletal muscle *in vitro*: frequency dependent attenuation and backscatter coefficient over a wide range of frequencies. IEEE Ultrason Symp Proc, pp.1467-1470

Robinson MH, Spruce L, Eeles R, Fryatt I, Harmer CL, Thomas JM, Westbury G, 1991. Limb function following conservation treatment of adult soft tissue sarcoma. Eur J Cancer 27:1567-1574

Rodemann HP, Bamberg M, 1995. Cellular basis of radiation-induced fibrosis. Radiother Oncol 35:83-90

Rodnan GP, Lipinski E, Luksick J, 1979. Skin thickness and collagen content in progressive systemic sclerosis and localized scleroderma. Arthritis Rheum 22:130-140

Rome K, Webb P, 2000. Development of a clinical instrument to measure heel pad indentation. Clin Biomech 15:298-300

Rome K, Webb P, Unsworth A, Haslock I, 2001. Heel pad stiffness in runners with plantar heel pain. Clin Biomech 16:901-905

Ryan LK, Foster FS, 1997. Tissue equivalent vessel phantoms for intravascular ultrasound. Ultrasound Med Biol 23:261-273

Saijo Y, Sasaki H, Okawai H, Nitta SI, Tanaka M, 1998. Acoustic properties of atherosclerosis of human aorta obtained with high-frequency ultrasound. Ultrasound Med Biol 24:1061-1064

Seidenari S, Belletti B, Conti A, 1996. A quantitative description of echographic images of sclerotic skin in patients with systemic sclerosis, as assessed by computerized image analysis on 20 MHz B-scan recordings. Acta Dermatol Venereol 76:361-364

Seidenari S, Di Nardo A, Pepe P, Giannetti A, 1991. Ultrasound B scanning with image analysis for assessment of allergic patch test reactions. Contact Dermatitis 24:216-222

Seidenari S, Pagnoni A, Di Nardo A, Giannetti A, 1994. Echographic evaluation with image analysis of normal skin: variations according to age and sex. Skin Pharmacol 7:201-209

Serup J, 1984. Localized scleroderma (morphoea): thickness of sclerotic plaques as measured by 15 MHz pulsed ultrasound. Acta Dermatol Venereol 64:214-219

Serup J, 1992. Ten years' experience with high-frequency ultrasound examination of the skin: development and refinement of technique and equipments. In "*Ultrasound in Dermatology*", (eds) Altmeyer P, El-Gammal S, Hoffmann K, Spring-Verlag, Berlin Heidelberg, pp.41-54

Shioya S, Tsuji C, Kurita D, Katoh H, Tsuda M, Haida M, Kawana A, Ohta Y, 1997. Early damage to lung tissue after irradiation detected by the magnetic resonance T2 relaxation time. Radiat Res 148:359-364

Shuster S, Black MM, McVitie E, 1975. The influence of age and sex on skin thickness, skin collagen and density. Br J Dermatol 93:639-643

Silver-Thorn, MB, 1999. *In vivo* indentation of lower extremity limb soft tissues. IEEE Trans Rehabil Eng 7:268-277

Smith SK, Karst NS, 2000. General histology. In "*Head & Neck Histology & Anatomy, A Self-Instructional Program"*, (eds) Smith SK, Karst NS, Appleton & Lange, Stamford, Connecticut, pp.1-32

Steiger DL, O'Brien WD, Jr, Olerud JE, Riederer-Henderson MA, Odland GF, 1988. Measurement uncertainty assessment of the scanning laser acoustic microscope and application to canine skin and wound. IEEE Trans Ultrason Ferroelect Freq Contr 35:741-748

Steinert M, Weiss M, Gottlober P, Belyi D, Gergel O, Bebeshko V, Nadejina N, Galstian I, Wagemaker G, Fliedner TM, Peter RU, 2003. Delayed effects of accidental cutaneous radiation exposure: fifteen years of follow-up after the Chernobyl accident. J Am Acad Dermatol 49:417-423

Stiller MJ, Driller J, Shupack JL, Gropper CG, Rorke MC, Lizzi FL, 1993. Three-dimensional imaging for diagnostic ultrasound in dermatology. J Am Acad Dermatol 29:171-175

Stinson SF, DeLaney TF, Greenberg J, Yang JC, Lampert MH, Hicks JE, Venzon D, White DE, Rosenberg SA, Glatstein EJ, 1991. Acute and long-term effects on limb function of combined modality limb sparing therapy for extremity soft tissue sarcoma. Int J Radiat Oncol Biol Phys 21:1943-1949

Tan CY, Marks R, Payne P, 1981. Comparison of xeroradiographic and ultrasound detection of corticosteroid induced dermal thinning. J Invest Dermatol 76:126-128

Tan CY, Statham B, Marks R, Payne PA, 1982. Skin thickness measurement by pulsed ultrasound: it reproducibility, validation and variability. Br J Dermatol 106:657-667

Taylor KJW, Wells PNT, 1989. Tissue characterisation. Ultrasound Med Biol 15:421-428

Thijssen JM, 1989. Ultrasonic tissue characterisation and echographic imaging. Phys Med Biol 34:1667-1674

Tikjob G, Kassis V, Sondergaard J, 1984. Ultrasonic B-scanning of the human skin. An introduction of a new ultrasonic skin-scanner. Acta Dermatol Venereol 64:67-70

Tonuk E, Silver-Thorn MB, 2003. Nonlinear elastic material property estimation of lower extremity residual limb tissues. IEEE Trans Neural Sys Rehabil Eng 11:43-53

Torres-Moreno R, 1991. Biomechanical analysis of the interaction between the above-knee residual limb and the prosthetic socket. PhD dissertation, University of Strathclyde, Glasgow, UK

Urmacher C, 1990. Histology of human skin. Am J Surg Pathol 14:671-686

Vannah WM, Childress DS, 1993. Modelling the mechanics of narrowly contained soft tissues: the effects of specification of Poisson's ratio. J Rehabil Res Dev 30:205-209

Vannah WM, Childress DS, 1996. Indentor tests and finite element modeling of bulk muscular tissue *in vivo*. J Rehabil Res Dev 33:239-252

Vitellaro-Zuccarello L, Cappelletti S, Dal Pozzo Rossi V, Sari-Gorla M, 1994. Stereological analysis of collagen and elastic fibers in the normal human dermis: variability with age, sex, and body region. Anat Rec 238: 153-162

Wagner RF, Insana MF, Brown DG, 1987. Statistical properties of radio-frequency and envelope-detected signals with applications to medical ultrasound. J Opt Soc Am A 4:910-922

Warszawski A, Rottinger EM, Vogel R, Warszawski N, 1997. 20 MHz ultrasonic imaging for quantitative assessment and documentation of early and late postradiation skin reactions in breast cancer patients. Radiother Oncol 47:241-247

Wegrowski J, Lafuma C, Lefaix JL, Daburon F, Robert L, 1988. Modification of collagen and noncollagenous proteins in radiation-induced muscular fibrosis. Exp Mol Pathol 48:273-285

Woo SLY, Simon BR, Kuei SC, Akeson WH, 1980. Quasi-linear viscoelastic properties of normal articular cartilage. J Biomech Eng-Trans ASME 102:85-90

Yeh WC, Huang SW, Li PC, 2003. Liver fibrosis grade classification with B-mode ultrasound. Ultrasound Med Biol 29:1229-1235

Yeh WC, Li PC, Jeng YM, Hsu HC, Kuo PL, Li ML, Yang PM, Lee PH, 2002. Elastic modulus measurements of human liver and correlation with pathology. Ultrasound Med Biol 28:467-474

Zhang M, Zheng YP, Mak AFT, 1997. Estimating the effective Young's modulus of soft tissues from indentation tests - nonlinear finite element analysis of effects of friction and large deformation. Med Eng Phys 19:512-517

Zheng YP, Bridal SL, Shi J, Saied A, Lu MH, Jaffre B, Mak AF, Laugier P, 2004. High resolution ultrasound elastomicroscopy imaging of soft tissues: system development and feasibility. Phys Med Biol 49:3925-3938

Zheng YP, Choi YKC, Wong K, Chan S, Mak AFT, 2000a. Biomechanical assessment of plantar foot tissue in diabetic patients using an ultrasound indentation system. Ultrasound Med Biol 26:451-456

Zheng YP, Leung SF, Mak AFT, 2000b. Assessment of neck tissue fibrosis using an ultrasound palpation system: a feasibility study. Med Biol Eng Comput 38:497-502

Zheng YP, Mak AFT, 1996. An ultrasound indentation system for biomechanical properties assessment of soft tissues *in-vivo*. IEEE Trans Biomed Eng 43:912-918

Zheng YP, Mak AFT, 1999a. Extraction of quasi-linear viscoelastic parameters for lower limb soft tissues from manual indentation experiment. J Biomech Eng-Trans ASME 121:330-339

Zheng YP, Mak AFT, 1999b. Effective elastic properties for lower limb soft tissues from manual indentation experiment. IEEE Trans Rehabil Eng 7:257-267

Zheng YP, Mak AFT, Leung AKL, 2001. State-of-the-art methods for geometric and biomechanical assessments of residual limbs: a review. J Rehabil Res Dev 38:487-504

Zheng YP, Mak AFT, Lue BL, 1999. Objective assessment of limb tissue elasticity: development of a manual indentation procedure. J Rehabil Res Dev 36:71-85

Ziegert JC, Lewis JL, 1978. *In-vivo* mechanical properties of soft tissue covering bony prominences. J Biomech Eng-Trans ASME 100:194-201